

**DRIVE SIGNAL SIMULATION
THROUGH VEHICLE SUSPENSION MODELING**

MOHAMMAD ARIF NURHADIYANTO

**MECHANICAL ENGINEERING DEPARTMENT
UNIVERSITI TEKNOLOGI PETRONAS**

MAY 2005

Title of thesis

Drive Signal Simulation through Vehicle Suspension Modeling

I, MOHAMMAD ARIF NURHADIYANTO

hereby allow my thesis to be placed at the Information Resource Center (IRC) of Universiti Teknologi PETRONAS (UTP) with the following conditions:

1. The thesis becomes the property of UTP.
2. The IRC of UTP may make copies of the thesis for academic purposes only.
3. This thesis is classified as

Confidential

Non-confidential

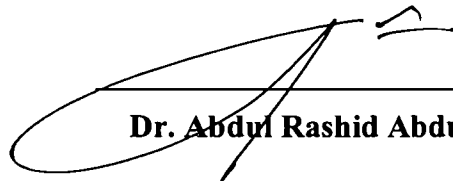
Endorsed by



Mohammad Arif Nurhadiyanto

Sidoarum I, Flamboyan 3
Godean, Sleman
Yogyakarta 55564
Indonesia

Date : 19 July 2005



Dr. Abdul Rashid Abdul Aziz

Mechanical Engineering Department
Universiti Teknologi Petronas
31750 Tronoh, Perak Darul Ridzuan
Malaysia

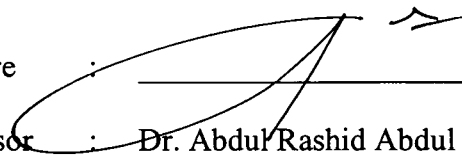
Date : 19 July 2005

UNIVERSITI TEKNOLOGI PETRONAS

Approval by Supervisor

The undersigned certify that they have read, and recommend to The Postgraduate Studies Programme for acceptance, a thesis entitled “**Drive Signal Simulation through Vehicle Suspension Modeling**” submitted by **Mohammad Arif Nurhadiyanto** for the fulfillment of the requirements for the degree of Master of Science in Mechanical Engineering

Date : 19 July 2005

Signature : 
Supervisor : Dr. Abdul Rashid Abdul Aziz
Date : 20/7/2005

UNIVERSITI TEKNOLOGI PETRONAS

Drive Signal Simulation through Vehicle Suspension Modeling

By

Mohammad Arif Nurhadiyanto

A THESIS

SUBMITTED TO THE POSTGRADUATE STUDIES PROGRAMME

AS A REQUIREMENT FOR THE

DEGREE OF MASTER OF SCIENCE


IN MECHANICAL ENGINEERING

BANDAR SERI ISKANDAR,

PERAK

JULY 2005

I hereby declare that the thesis is based on my original work except for quotations and citations which have been duly acknowledged. I also declare that it has not been previously or concurrently submitted for any other degree at UTP or other institutions.

Signature : 

Name : Mohammad Arif Nurhadiyanto

Date : 19 July 2005

DEDICATION

To my mother and father

who waited so long for this

ACKNOWLEDGEMENT

I would like to gratefully acknowledge the enthusiastic supervision of Dr. Abdul Rashid Abdul Aziz during this work. I thank Pn Haslina and Rosle Yaakub for opening a golden opportunity to me. Staffs of the Proton Berhad are thanked for numerous stimulating discussions, help with experimental setup, and general advice; in particular I would like to acknowledge the help of Azmihan Arifin, Syammim, Wahab Lung, Zuliana Kamaruzaman, and Jayakanthan for their support. Dr. Ing. Yul Y. Nazaruddin, is thanked for his assistance with all types of technical problems.

I am grateful to all my friends from Universiti Teknologi Petronas, for being the surrogate family during the many years I stayed there and for their continued moral support there after. From the staff, Pn. Norma, Ir. Idris, En. Azhar, En. Sani, Hazlin, Suhaily, Ustaz Cahyono, are especially thanked for their care and attention.

Finally, I am forever indebted to my parents and my family for their understanding, endless patience, and encouragement when it was most required. I am also grateful to Fadli and Arief for their support.

Arif

July 2005

ABSTRACT

Road simulation testing of vehicles is often performed using a four posters road simulator. Four hydraulic actuators are used to replicate motions recorded during a previous test-drive using a drive signal. Typically, recordings are made of the vehicle sprung and unsprung accelerations at each of the four corners of the vehicle during an actual field-test. The hydraulic actuators are then driven and iterative tuning is performed such that the vehicle sprung and unsprung accelerations track those measured in the field. Thus realistic suspension movements can be reproduced with the drive signal obtained from the iterative approach.

The overall goal of this research is to replace this iterative tuning which is specific for certain model of a car with a suspension system model. Acceleration data obtained from driving two test vehicles over selected well-defined sections of a test-track at constant speed were used for conducting this research. In modeling of the car suspension, the model of the system is assumed to be a quarter vehicle model and a rigid body system. Inputs to the system are the sprung and unsprung mass vertical accelerations. The output of the model is the drive signal estimation.

Two approaches of modeling have been applied for characterizing the dynamics of vehicle suspension. In the first approach, a linear model is derived from the equation of motion of vehicle suspension and a transfer function model is produced. In the second approach, a nonlinear modeling is used which treats the suspension as a black box model and considers only on the input and output of the suspension system.

Comparison of the results obtained from the two modeling approaches was then made and the errors were quantified. RMS error produced from the nonlinear modeling is found to be 2.4 % as compared to the linear modeling which produced a 14.5 % RMS error. This modeling result agreed with prior prediction that the simulated drive signal produced from the nonlinear modeling could better track the iterated drive signal rather than the linear modeling.

ABSTRAK

Ujian simulasi jalan raya untuk kenderaan dilakukan dengan menggunakan “four posters road simulator”. Empat pendorong hidraulik digunakan untuk mengimbas pergerakan yang direkod semasa pandu uji dengan menggunakan signal pengendalian. Kebiasaannya pecutan jisim terpegas dan jisim tak-terpegas pada empat penjuru kenderaan akan direkodkan semasa ujian praktikal dijalankan. Pendorong hidraulik akan digerakkan dan penalaan iteratif dijalankan sebagaimana pecutan jisim terpegas dan jisim tak-terpegas dianalisis semasa ujian praktikal. Oleh itu, pergerakan sebenar suspensi boleh dihasilkan daripada signal pengendali melalui penalaan iteratif yang telah dibuat.

Objektif keseluruhan projek ini adalah untuk menggantikan penalaan iteratif yang khas untuk sebuah model kereta dengan model sistem suspensi. Analisis data pecutan yang diperolehi daripada ujian keatas kedua-dua jenis kereta pada halaju malar telah digunakan di dalam kajian ini. Kereta tersebut diuji pada jarak yang sama di atas sebuah litar. Suspensi ini hanya dimodelkan daripada suku bahagian kenderaan dan adalah sistem yang tegar. Nilai yang bertindak pada sistem adalah pecutan menegak daripada jisim terpegas dan jisim tak-terpegas. Hasil daripada model ini adalah anggaran signal pengendali.

Untuk memodelkan suspensi kenderaan, dua pendekatan telah digunakan untuk mengklasifikasikan pergerakan suspensi. Pendekatan pertama, persamaan pergerakan suspensi kenderaan melalui model linear dibuat dan perubahan fungsi model diperolehi. Sementara itu, untuk pendekatan kedua, model tidak-linear dibina berdasarkan suspensi yang berfungsi sebagai model “kotak hitam”. Hanya data yang dimasukkan dan dikeluarkan diambilkira untuk pendekatan kedua.

Kedua-dua keputusan daripada pendekatan diatas diperolehi dan dibandingkan. Daripada keputusan tersebut, peratus ketidak tepatan telah dikira. Ketidak tepatan untuk RMS hasil daripada model tidak-linear adalah 2.4% dibandingkan dengan 14.5% apabila model linear digunakan. Keputusan daripada simulasi ini telah membuktikan bahawa model tidak-linear memberi keputusan yang lebih baik jika di bandingkan dengan model linear.

TABLE OF CONTENTS

Status of thesis	i
Approval Page.....	ii
Title Page	iii
Declaration.....	iv
Dedication	v
Acknowledgement	vi
Abstract	vii
Abstrak	viii
Table of Contents.....	ix
List of Tables	xii
List of Figures.....	xiii
CHAPTER 1 : INTRODUCTION.....	1
1.1 Research Background	1
1.2 Research Objective	2
1.3 Research Scope	3
1.4 Research Methodology	3
1.5 Thesis Outline	7
CHAPTER 2 : LITERATURE REVIEW.....	8
2.1 Vehicle Suspension Modeling	8
2.2 Road Profiling	9
2.3 Nonlinear Modeling of Vehicle Suspension	10
2.4 Conclusion	10
CHAPTER 3 : MODELING OF VEHICLE SUSPENSION SYSTEM.....	12
3.1 Vehicle Suspension System	12
3.2 Mathematical Modeling of Vehicle Suspension Systems	16

3.2.1	Description of the System	16
3.2.2	State Space Model and Transfer Function Model	17
3.3	Artificial Neural Network	18
3.4	Neural Network Modeling of Vehicle Suspension System	24
CHAPTER 4 : TESTING AND DATA ANALYSIS		29
4.1	Test Procedure	29
4.1.1	General Test Design	29
4.1.2	Test Preparation	33
4.1.3	Instrumented Ride Vibration Measurement	36
4.1.4	Test Rig Description	37
4.2	Data Processing	38
4.2.1	China Road Data	38
4.2.1.1	Signal Filtering	42
4.2.1.2	Signal Integration	45
4.2.1.3	Signal Differentiation	48
4.2.2	Proton Test Track Data	50
4.2.2.1	Signal Filtering	52
4.2.2.2	Signal Integration	55
4.2.2.3	Signal Differentiation	57
CHAPTER 5 : RESULTS		59
5.1	Mathematical Modeling Results	59
5.2	Artificial Neural Network Modeling Results	67
CHAPTER 6 : DISCUSSION		69
6.1	Linear Modeling	69
6.2	Artificial Neural Network Modeling	71
CHAPTER 7 : CONCLUSION		73

REFERENCES76

APPENDICES78

LIST OF TABLES

Table 4.1	Tire parameters of test vehicles	33
Table 4.2	Suspension parameters of Proton X.....	34
Table 4.3	Suspension parameters of Proton Y	35
Table 6.1	RMS error for China road drive signal modeling	70
Table 6.2	RMS error for Proton test-track drive signal modeling	70
Table 6.3	RMS error for China road drive signal modeling using ANN.....	72

LIST OF FIGURES

Figure 1.1	China road modeling steps.....	4
Figure 1.2	Proton test-track modeling steps.....	5
Figure 1.3	Artificial neural network modeling steps.....	6
Figure 3.1	SAE vehicle axis systems	13
Figure 3.2	Ride dynamic system	13
Figure 3.3	Quarter-car model	14
Figure 3.4	Tire spring rate	15
Figure 3.5	Characteristics of neuron	19
Figure 3.6	Common activation functions	20
Figure 3.7	A single layer neural net	21
Figure 3.8	A multilayer neural net	21
Figure 3.9	Backpropagation neural network with one hidden layer	22
Figure 3.10	Algorithm of backpropagation neural net	23-24
Figure 3.11	ANN model structure for vehicle suspension	28
Figure 4.1	Comparison between industrial practice and current approach	30
Figure 4.2	FRF calculation.....	32
Figure 4.3	Iterative process	32
Figure 4.4	Proton simulation test track	36
Figure 4.5	Sensor placement	37
Figure 4.6	Laboratory testing set up.....	38
Figure 4.7	Acceleration signal (unsprung-front left-Proton X).....	39
Figure 4.8	Acceleration signal (sprung-front left-Proton X).....	39
Figure 4.9	Iterated drive signal (front left-Proton X).....	40
Figure 4.10	FFT acceleration signal (unsprung-front left-Proton X).....	40
Figure 4.11	FFT acceleration signal (sprung-front left-Proton X).....	41
Figure 4.12	FFT iterated drive signal (front left-Proton X)	41

Figure 4.13	Filtered acceleration signal (unsprung-front left-Proton X)	42
Figure 4.14	Filtered acceleration signal (sprung-front left-Proton X)	43
Figure 4.15	Filtered iterated drive signal (front left-Proton X).....	43
Figure 4.16	FFT – Filtered acceleration signal (unsprung-front left-Proton X)	44
Figure 4.17	FFT – Filtered acceleration signal (sprung-front left-Proton X)	44
Figure 4.18	FFT – Filtered iterated drive signal (front left-Proton X).....	45
Figure 4.19	Velocity signal (unsprung-front left-Proton X)	46
Figure 4.20	Detrend velocity signal to remove DC offset (unsprung-front left-Proton X).....	46
Figure 4.21	Detrend velocity signal to remove DC offset (sprung-front left-Proton X).....	47
Figure 4.22	Displacement signal (unsprung-front left-Proton X)	47
Figure 4.23	Displacement signal (sprung-front left-Proton X)	48
Figure 4.24	Acceleration data comparison (unsprung-front left-Proton X).....	49
Figure 4.25	Acceleration data comparison (sprung-front left-Proton X).....	49
Figure 4.26	Acceleration signal (unsprung-front left-Proton X).....	50
Figure 4.27	Acceleration signal (sprung-front left-Proton X).....	51
Figure 4.28	FFT acceleration signal (unsprung-front left-Proton X).....	51
Figure 4.29	FFT acceleration signal (sprung-front left-Proton X).....	52
Figure 4.30	Filtered acceleration signal (unsprung-front left-Proton X)	53
Figure 4.31	Filtered acceleration signal (sprung-front left-Proton X)	53
Figure 4.32	FFT – Filtered acceleration signal (unsprung-front left-Proton X)	54
Figure 4.33	FFT – Filtered acceleration signal (sprung-front left-Proton X)	54
Figure 4.34	Velocity signal (unsprung-front left-Proton X)	55
Figure 4.35	Velocity signal (sprung-front left-Proton X)	55
Figure 4.36	Displacement signal (unsprung-front left-Proton X)	55
Figure 4.37	Displacement signal (sprung-front left-Proton X)	57
Figure 4.38	Acceleration data comparison (unsprung-front left-Proton X).....	57
Figure 4.39	Acceleration data comparison (sprung-front left-Proton X).....	58

Figure 5.1	Comparison: simulated and iterated drive signal (front left-Proton X).....	61
Figure 5.2	Comparison: simulated and iterated drive signal (front right-Proton X).....	61
Figure 5.3	Comparison: simulated and iterated drive signal (rear left-Proton X)	62
Figure 5.4	Comparison: simulated and iterated drive signal (rear right-Proton X)	62
Figure 5.5	Unfiltered simulated drive signal (front left-Proton X)	63
Figure 5.6	FFT – unfiltered simulated drive signal (front left-Proton X)	64
Figure 5.7	Filtered simulated drive signal (front left-Proton X)	65
Figure 5.8	FFT – filtered simulated drive signal (front left-Proton X)	65
Figure 5.9	Simulated drive signal comparison at front left (Proton X - Proton Y)	66
Figure 5.10	Simulated drive signal comparison at rear left (Proton X - Proton Y)	66
Figure 5.11	Validation result of ANN model.....	67
Figure 5.12	Simulation result of ANN model	68
Figure 7.1	Drive signal comparison (front left-Proton X).....	74
Figure 7.2	Drive signal comparison (rear left-Proton X)	74

CHAPTER 1

INTRODUCTION

This chapter describes a general overview of this research. Background information related to the topic of vehicle suspension system and the objective of the research are introduced. The scope of the research and the research methodology are also presented here. Finally an outline of the thesis and a brief description on the contents of each chapter are also presented.

1.1 Research Background

Research in vehicle suspension system has been an on-going study for decades, ever since the invention of automobiles. Engineers and researchers have been trying to fully understand the dynamic behavior of vehicle suspension as it is subjected to different road conditions and different driving conditions, such as moderate daily driving and extreme emergency maneuvers. They want to apply this finding to improve issues such as ride comfort and safety factor, and develop innovative design that will improve vehicle operations. With the aid of fast computers to perform complicated design simulations and high speed electronics that can be used as controllers, new and innovative concepts have been tested and implemented into vehicles. This type of research is mainly conducted by automotive companies and academic institutions.

Automotive companies, together with academic institutions, are constantly improving on the chassis design and development by re-engineering the suspension systems with new technology. For example, the recent developments of vehicle suspension system show that a marriage of vehicle suspension dynamics and electronics can improve both ride comfort and safety factor. Examples of such systems are semi-active and fully-active suspension. It enables damping characteristics of the suspension system to be set by a feedback controller in real time, thus improving the ride quality of the vehicle on different types of road conditions.

The interaction between vehicles and road has been studied for several decades. An example of such research is indirect testing of whole vehicles. The concept is to perform a simple laboratory test on each axle of the vehicle, to measure its dynamic characteristics. This information is then used to generate a numerical model of the response of the whole vehicle to a typical road type input. More detail information about this technique will be explained in the following section.

1.2 Research Objective

Fatigue and vibration testing of vehicles are often performed using a four posters road simulator, where the test vehicle sits on four hydraulic actuators which are used to replicate motions recorded during a previous road test. Typically, recordings are made of the body and chassis accelerations at each of the four corners of the vehicle. The hydraulic actuators are then driven with appropriate input signals so-called drive signal such that the body and chassis accelerations follow those measured in the field. Thus realistic suspension movements can be reproduced and the drive signal is obtained.

The current solution to this 'mission reproduction' involves an iterative, off-line procedure (Westwick et al., 1999). First, an identification experiment is performed by exciting the system with a relatively broad-band noise input. A linear Frequency Response Function (FRF) is estimated from the test data. The target outputs are then filtered using the inverse of the FRF, producing an initial input sequence. If, as is often the case, the initial input sequence does not cause the system to track the target outputs adequately, the inputs are refined. The inverse FRF is applied to track the error, and the result is added to the test input. This off-line refinement process iterates until sufficient tracking accuracy is obtained.

The overall goal of this research is to replace this iterative tuning which is specific for certain model of car with a deterministic method. Transfer function and state space model will be derived from vehicle suspension system to recreate the movement of suspension. It is then compared with nonlinear modeling results using Artificial Neural Network. It should be pointed out that the result of the modeling is not the road profile. This research is trying to find the drive signal that accurately reproduces response the same as road simulator excitation using unsprung and sprung acceleration data.

1.3 Research Scope

Two models of Proton passenger cars with conventional suspension system were used for this research. Two kinds of input (random and deterministic) were excited on each of the vehicle wheel. The acceleration sensors were mounted on the sprung and unsprung mass of the vehicle to measure its vertical acceleration. The lateral and longitudinal forces to the vehicle are assumed to be negligible. Two modeling approaches, i.e. mathematical and artificial neural network modeling, were used to model the system to get the drive signal. This simulated drive signal was then compared with the iterated drive signal which was reproduced from the road simulator.

Some assumptions are made in modeling the vehicle suspension system. The major assumptions for this research are:

1. The vehicle body is considered as a rigid body. Therefore in deriving the vehicle equation of motion, the vehicle body is treated as a rigid body system.
2. The system is viewed as a quarter car system.
3. The car parameters used in modeling the system are obtained from a certain car model. The car model used in this work cannot be revealed due to confidentiality agreement with Proton

1.4 Research Methodology

This research attempted to compare transfer function (linear) model against neural network (nonlinear) model. The following steps describe the above two approaches:

1. Transfer function model.

Figure 1.1 shows the transfer function model approach using Proton X car model with random signal input (China public road). Acceleration data was measured at sprung and unsprung mass of the car at front left, front right, rear left, and rear right position. Iterated drive signal was determined by 'mission reproduction' using road measured data (acceleration data) and road simulator.

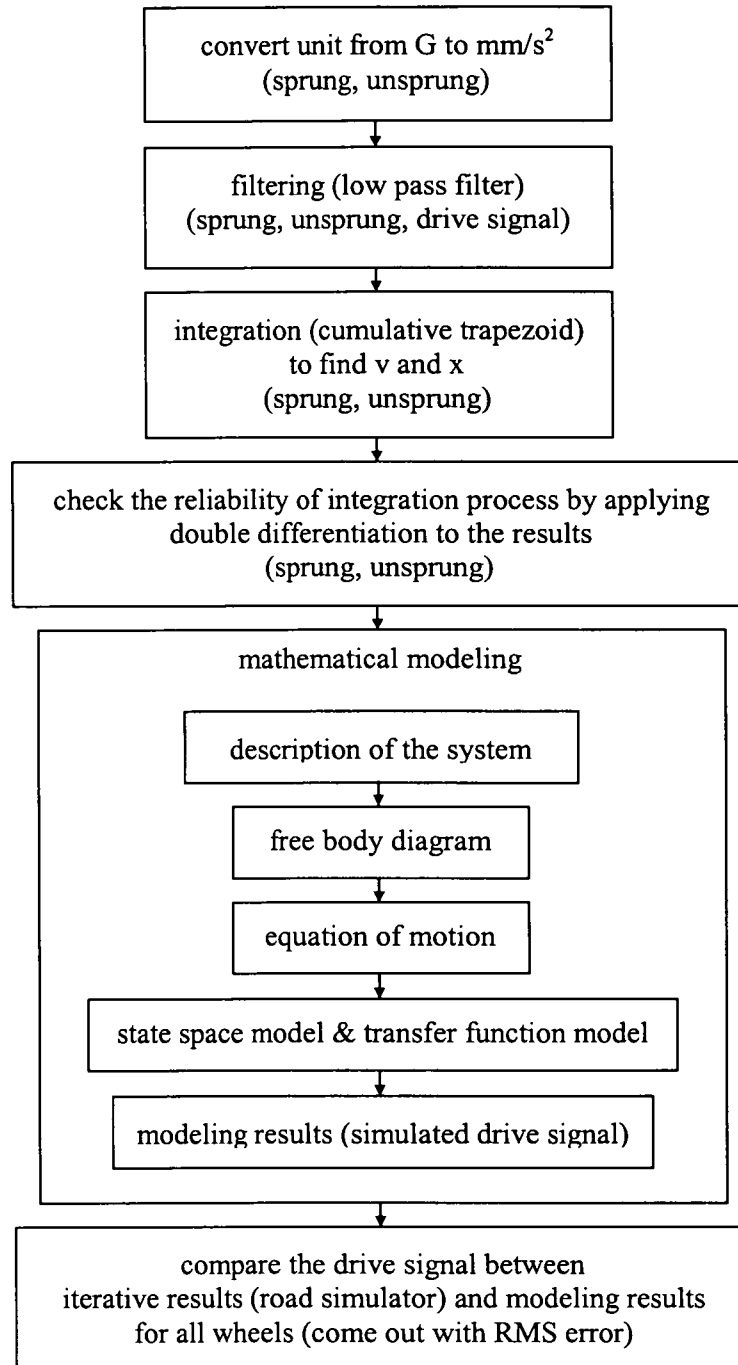


Figure 1.1 China road modeling steps.

Figure 1.2 uses two car models, i.e. Proton X and Proton Y, using Proton test-track as deterministic signal input. Acceleration data was measured at sprung and unsprung mass of the car at front left and rear left positions. Drive signal was not provided.

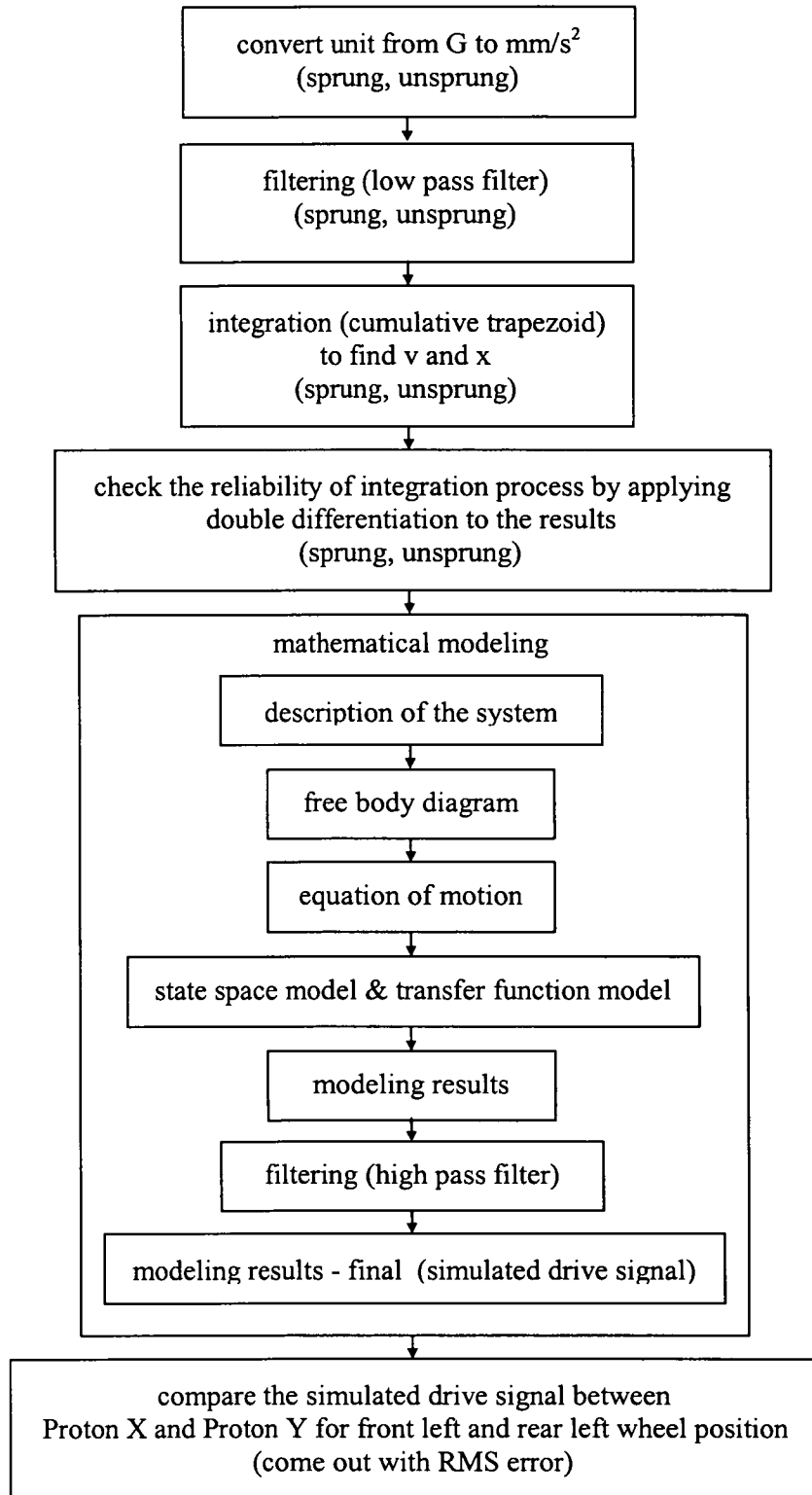


Figure 1.2 Proton test-track modeling steps.

2. Artificial Neural Network (ANN) model.

In the ANN modeling, the Proton test-track data was used for training process, whilst the China road data was used for simulation. Figure 1.3 shows the steps of the ANN modeling using Proton X car model.

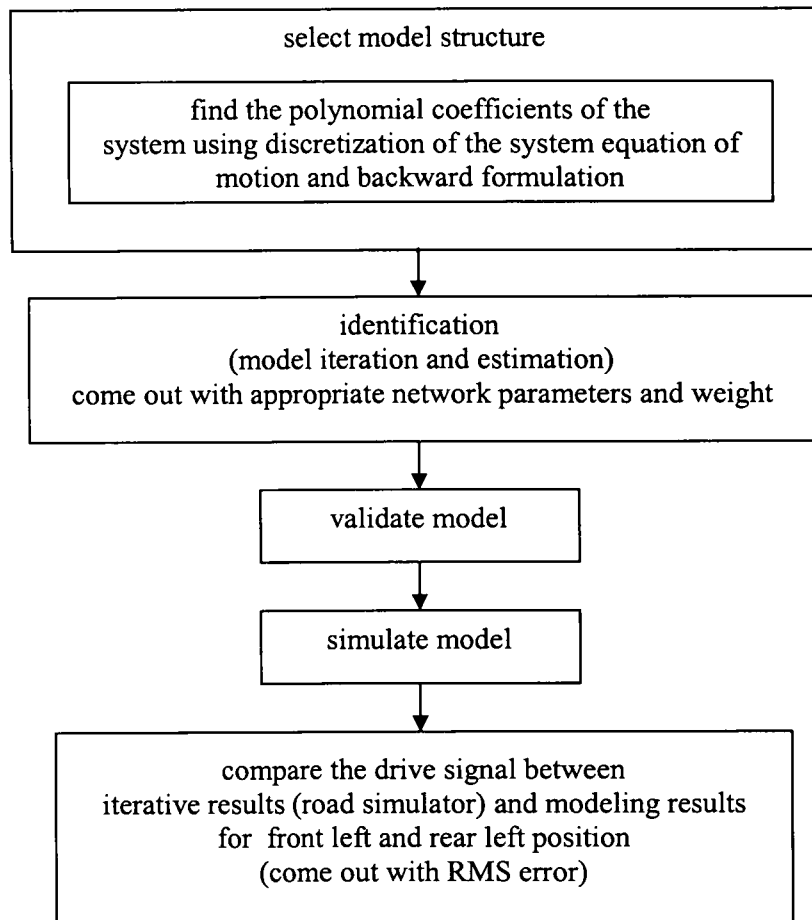


Figure 1.3 Artificial neural network modeling steps.

Comparison was then made between the transfer function model and neural network model.

1.5 Thesis Outline

Chapter 1 describes general overview of this research. Background information related to the topic of vehicle suspension system and objective of this research are introduced. The scope of the research and the research methodology are also presented here.

Chapter 2 briefly describes the published papers, journals, proceedings, that were found most relevant and complimentary to this research.

Chapter 3 explains the dynamic modeling of vehicle suspension system. The concept of vehicle suspension system and the derivation of linear and nonlinear modeling of vehicle suspension are presented in this chapter.

Test procedure and data analysis methodology for obtaining the best data are provided in chapter 4. There are two kinds of data that were obtained, i.e. road data from China and track data from Proton test-track.

Chapter 5 describes the modeling results of vehicle suspension systems. In the first section of this chapter, the results of mathematical modeling for both China road and Proton test-track will be presented. It is then followed by nonlinear modeling results using artificial neural network.

Chapter 6 briefly discusses the main issue in this research. The results of vehicle suspension modeling for both linear and nonlinear modeling are the main topics briefed in this chapter.

Finally, the conclusion of the research is provided in chapter 7.

CHAPTER 2

LITERATURE REVIEW

This chapter provides information on past research on vehicle suspension modeling to recreate the drive signal using analytic and nonlinear algorithms. An extensive literature search was conducted with the most relevant results presented in this chapter. Although the nonlinear modeling of vehicle suspension has been addressed in a number of articles, none of the previous studies tried to compare the modeling results between linear and nonlinear modeling with the same input-output. This research has also succeeded on producing the drive signal for both random and deterministic road profile input.

2.1 Vehicle Suspension Modeling

Modeling of vehicle suspension and its components have been studied for several decades. Vast assortments of models have been proposed and are used for many different circumstances. A study by Tao (2000), addressed a modeling suspension damper modules using LS-Dyna. It describes a finite element model of a suspension damper and accurately represents component interactions and force distributions within the module. The study conducted by Ruihong and Runhua (1999), has successfully reduced the variation of velocity characteristic of the shock absorber in a car using modern robust optimal design method, applied to its structural parameter design. They tried to analyze the influences of the parameters on velocity characteristics and the robust values which can improve velocity characteristic. The study by Rao and Gruenberg (1997) described a new testing and analysis methodology for obtaining equivalent linear stiffness and damping of automotive shock absorbers for use in system-level chassis and vehicle computer aided engineering models for noise and vibration prediction.

A study by Lacombe (2000) addressed the tire model for simulations of vehicle motion on high and low friction road surfaces. He developed an on-road analytical tire model to predict tire forces and moments at the tire/road interface. Takahashi et al. (2000) presented a new tire model of the overturning moment (OTM) characteristics and the

influence of OTM on the vehicle behavior based on the magic formula by adding the new term of the residual pneumatic scrub. The concept of the new model is to identify the difference between the simple model and the measurements to the newly defined functions. They investigated the influence of tire OTM on the vehicle rollover. The study conducted by Hankook Tire Co., Ltd. (2001) describes the role of tire modeling on the design process of a tire and vehicle system.

Renner (2000) proposed an Empirical Dynamic Models (EDM) for nonlinear suspension components. The models addressed in this study are faster to be created rather than analytical models, more accurate than other black box methods, and faster model execution. Automotive testing company, MTS, has proposed EDM to accelerate new suspension development. ElBeheiry and Karnopp (1996) investigated five types of suspensions: fully active, the limited active, the optimal passive, the actively damped, and the variable damper systems. Comparisons were made among these systems in terms of RMS response, frequency domain predictions, and eigen-frequency behavior as functions of disturbance intensity. They tried to optimize the variable parameter suspension to use the available suspension deflection to provide maximum isolation.

2.2 Road Profiling

The measurement method of road profile have been studied and conducted a great deal by many researchers and companies. Sayers and Karamihas (1998) released the Little Book of Profiling, the most popular reference related with this area of research. It gives a basic information about measuring and interpreting road profiles. The study conducted by Katech (2000) describes the construction of Dynamic Road Profiling Devices (DRPD) and the signal processing for advanced double integration and road profiling for AEIPR (an Accelerometer Established Inertial Profiling Reference) method.

Some studies related with the process of simulation 'from the field to the laboratory' have also been conducted by many researchers. Westwick et al. (1999) models the dynamic of a car attached to a vibration test rig and presented a realistic simulation of a nonlinear automobile suspension. The overall goal of their research is to replace the mission reproduction which is involves an iterative, off-line procedure with an online controller. Storer et al. (1998) characterized the transfer of road surface excited

vibrations through vehicle suspension system. They applied a technique called Transfer Path Analysis, originally developed to study the aspect of powertrain-induced vibrations of the vehicle body, to the suspensions of the complete vehicle being tested on the road or in the laboratory on a road simulator.

2.3 Nonlinear Modeling of Vehicle Suspension

The nonlinear modeling of vehicle suspension has been such an important issue in the automotive research activities that many studies have addressed different aspects and method of these modeling. Felicia and Ioan (2000) applied neural networks to vehicle suspension system. They focused on exploring the possibility of deriving the (semi)active suspension system controllers based on the artificial intelligence strategy, and verifying the proposed procedure of derivation by simulation results. Lin and Kanellakopoulos (1995) proposed a nonlinear backstepping design for active suspension system which aims to improve the trade-off between ride quality and suspension travel. They showed that the intentional introduction of nonlinearity through the controller into an otherwise linear system can be beneficial in cases where the desired closed-loop response is different operating regions. Yul and Yamakita (1999) presented an alternative approach to identify suspension system model using neuro-fuzzy technique. By using this approach, the nonlinear characteristics of the suspension system have accommodated. Westwick et al. (1999) addressed a nonlinear identification of automobile vibration dynamic. They developed a technique for identifying a restricted class of nonlinear state space systems, a structure which can be used to model a wide variety of systems.

2.4 Conclusion

The nonlinear modeling of vehicle suspension to recreate the drive signal is of great importance to the automotive industry and has therefore been the subject of many studies. Previous studies have addressed many aspects and methods of the modeling and have attempted to develop models based on the actual measurement from a running test vehicle. Modeling of suspension component, such as shock absorber, and tire modeling, especially in dynamic condition, has also been studied a great deal by many researchers. With the aim of improving the ride comfort behavior of vehicles for road-surface

excitation, a great deal of researchers and companies have been trying to understand in detail the dynamic characteristics of the suspension systems and the transfer of vibration through the vehicle suspension.

Most of the previous studies have been limited in the modeling technique and experimental data for verification. The previous research applied only one type of modeling and one type of input. This research tried to compare the modeling results between linear and nonlinear modeling with the same input-output. This research has also attempted to reproduce the vehicle suspension movement by determining the drive signal for both random and deterministic road profile input.

CHAPTER 3

MODELING OF VEHICLE SUSPENSION SYSTEM

This chapter briefly describes the dynamic modeling of vehicle suspension system. The concept of vehicle suspension system, includes a quarter-car system is first presented in this chapter. It then describes the derivation of linear and nonlinear modeling approaches for identifying the characteristic of vehicle suspension.

3.1 Vehicle Suspension System

The excitation source (i.e. vertical forces exerted by the road on a tire) is transmitted to the vehicle body through the vehicle suspension system. This system allows its components to absorb the energy of the road roughness so passengers can have a smooth ride. In other words, it provides vertical compliance so the wheels can follow the uneven road, isolating the body from roughness in the road. The others primary functions of a suspension system are to (Gillespie, 1992):

- Maintain the wheels in the proper steer and camber attitudes to the road surface.
- Resist roll of the chassis.
- React to the control forces produced by the tires – longitudinal (acceleration and braking) forces, lateral (cornering) forces, braking and driving torques.
- Keep the tires in contact with the road with minimal load variation.

To study the fundamental behavior and characteristics of vehicle suspension system, it is necessary to understand the basic concepts of vehicle dynamics, ride, and quarter car model. This section presents the necessary information on those subjects. The vibration-absorber-components of vehicle are also described in this section.

Vehicle Dynamics

The subject of ‘vehicle dynamics’ is concerned with the movements of vehicles on a road surface. The forces imposed on the vehicle from the tires, gravity, and aerodynamics determine dynamic behavior of the vehicle. The vehicle and its

components are studied to determine what forces will be produced by each of these sources at a particular maneuver and trim condition, and how the vehicle will respond to these forces. Understanding vehicle dynamics can be accomplished at two levels—the empirical and the analytical. The empirical understanding derives from trial and error from which one learns about the factors that influence the vehicle performance. The empirical method, however, can often lead to failure. Without a mechanistic understanding of how changes in vehicle design or properties affect performance, extrapolating past experience to new conditions may involve unknown factors which may produce a new result, defying the prevailing rules of thumb. For this reason, engineers favor the analytical approach. The analytical approach attempts to describe the mechanics of interest based on the known laws of physics so that an analytical model can be established and represented by differential equations that relate forces or motions of interest to control inputs and vehicle or tire properties.

Ride

Vehicles travel at high speed, and as a consequence experience a broad spectrum of vibrations. These are transmitted to the passengers either by tactile, visual, or aural paths. The term ‘ride’ is commonly used in reference to tactile and visual vibrations, while the aural vibrations are categorized as noise. Alternatively, the spectrum of vibrations may be divided up according to frequency and classified as ride i.e. 0-25 Hz, and noise i.e. 25-20000 Hz (Gillespie, 1992). The lower-frequency ride vibrations are manifestations of dynamic behavior common to all rubber-tired motor vehicles. Thus, the study of these modes is an important area of vehicle dynamics. As an aid in developing a systematic picture of ride behavior, it is helpful to think of the overall dynamic system as shown in Figure 3.2.

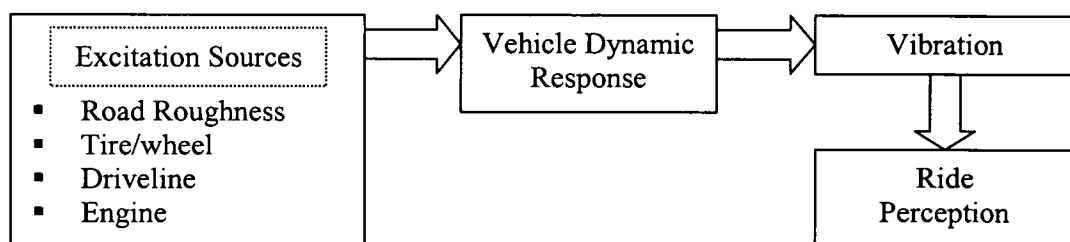


Figure 3.2 Ride dynamic system.

(adopted from: Gillespie, Fundamentals of Vehicle Dynamics, 1992).

Quarter-car Model

At the most basic level, all vehicles share the ‘ride isolation’ properties common to a sprung mass supported by primary suspension systems at each wheel. The dynamic behavior of this system is the first level of isolation from the roughness of the road. The essential dynamics of the vehicle suspension system can be simplified and represented by a quarter-car model as shown in Figure 3.3.

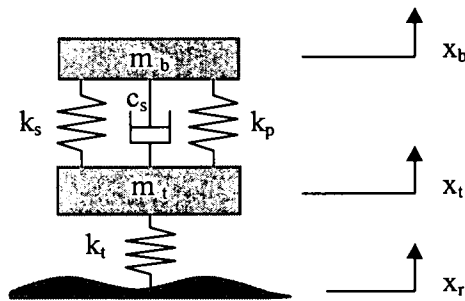


Figure 3.3 Quarter-car model.

It consists of a sprung mass (m_b) supported on a primary suspension, which in turn is connected to the unsprung mass (m_t). The suspension has stiffness (k_s , k_p) and damping (c_s) properties. Tire, which interacts between the road and the car, has a spring rate (k_t) to cushion the car against road irregularities.

A quarter-car model is the simplest model that includes a proper representation of the problem of controlling wheel load variation. It contains no representation of geometric effects of having four wheels or the use of front suspension state information to improve the performance at the rear. However, it does appear to contain the most basic features of the real problem and gives rise to design thinking. Thus, to demonstrate the application of identification algorithm on a manageable, nonetheless realistic, this research uses a continuous-time simulation of a quarter-car model.

The Tire

Motion of the vehicle is controlled almost entirely through the forces exerted on the tire by the road. The tire characteristics therefore have a major effect on handling problems.

The tire serves essentially three basic functions (Gillespie, 1992):

- It supports the vertical load, while cushioning against road irregularity
- It develops longitudinal forces for acceleration and braking
- It develops lateral forces for cornering

The tire can be simply represented as a simple spring (k_t), although a damper is often included to represent the small amount of damping inherent to the visco-elastic nature of the tire. The tire spring rate can be illustrated as Figure 3.4.

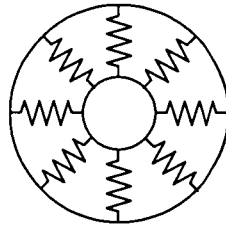


Figure 3.4 Tire spring rate.

Spring

Spring can be defined as a component that is designed to have a relatively low stiffness compared with normal rigid members, thus making it possible to exert a force that varies in a controlled way with the length of the member. Springs are generally classified according to the material used and the way that the forces and corresponding stresses occur. In a quarter-car model, spring is represented as k_s .

Damper

It is one of the most important parts on vehicle suspension. The damper is commonly known as the shock absorber, although the implication that shocks are absorbed is misleading. Contrary to their name, they do not absorb the shock from road bumps. Rather the suspension absorbs the shock and the shock absorber's function then is to dissipate the energy put into the system by the bump (Dixon, 1996). The primary purposes of a damper are (Dixon, 1996):

- To dissipate any energy in the vertical motion of body or wheels.
- To optimize vehicle control behavior by preventing response overshoots.
- To minimize the influence of unavoidable resonance.

In a quarter-car model, damper is represented as c_s .

Parasitic Coefficient

Apart from the deliberately introduced suspension spring and tire spring rate, there are other sources of springing material inherent in the system. One is rubber bushes. In a quarter-car model, parasitic coefficient is represented as k_p .

Mass

The total mass of the vehicle may be considered to be divided into sprung mass (m_b) and unsprung mass (m_t). These terms refer to the component motion relative to the road. Basically the sprung mass is the body and the unsprung mass is mass of the wheels and axles. The term “wheel” may be used in a wide sense to include the whole of the rotating element including the tire, or in a narrow sense to mean the part that connects the tire to the hub.

3.2 Mathematical Modeling of Vehicle Suspension System

3.2.1 Description of the System

As previously mentioned, the essential dynamics of vehicles can be expressed by a two-mass model as shown in Figure 3.3. It contains two vertical degrees of freedom: the displacement of the unsprung mass, x_t , and displacement of the sprung mass, x_b . The road displacement input is denoted by x_r . K_s , k_p , and k_t are the spring coefficient of suspension, parasitic, and tyre, respectively, and c_s is the damper coefficient.

By applying Newton's second law of motion to the quarter-car system as showed in Figure 3.3, the equation of motion of the system can be written as

$$\ddot{x}_t + \frac{c_s}{m_t} \dot{x}_t - \frac{c_s}{m_t} \dot{x}_b + \frac{(k_p + k_s + k_t)}{m_t} x_t - \frac{(k_p + k_s)}{m_t} x_b = \frac{k_t}{m_t} x_r \quad (3.1)$$

$$\ddot{x}_b - \frac{c_s}{m_b} \dot{x}_t + \frac{c_s}{m_b} \dot{x}_b - \frac{(k_p + k_s)}{m_b} x_t + \frac{(k_p + k_s)}{m_b} x_b = 0 \quad (3.2)$$

3.2.2 State Space Model and Transfer Function Model

- **State Space Model**

Following Ihsan (2002), by using the state variables:

$$x_1 = x_t$$

$$x_2 = x_b$$

$$x_3 = \dot{x}_t$$

$$x_4 = \dot{x}_b$$

Eq. (3.1) and (3.2) can be rewritten as

$$\begin{bmatrix} \dot{x}_1 \\ \dot{x}_2 \\ \dot{x}_3 \\ \dot{x}_4 \end{bmatrix} = \begin{bmatrix} 0 & 0 & 1 & 0 \\ 0 & 0 & 0 & 1 \\ -\frac{(k_p + k_s + k_t)}{m_t} & \frac{(k_p + k_s)}{m_t} & -\frac{c_s}{m_t} & \frac{c_s}{m_t} \\ \frac{(k_p + k_s)}{m_b} & -\frac{(k_p + k_s)}{m_b} & \frac{c_s}{m_b} & -\frac{c_s}{m_b} \end{bmatrix} \begin{bmatrix} x_1 \\ x_2 \\ x_3 \\ x_4 \end{bmatrix} + \begin{bmatrix} 0 \\ 0 \\ \frac{k_t}{m_t} \\ 0 \end{bmatrix} x_r \quad (3.3)$$

Equation (3.3) is the state space model representation of vehicle suspension system.

- **Transfer Function Model**

Another way of representing the mathematical model of vehicle suspension system is the transfer function model of its system. The model can be obtained by applying Laplace transform and Cramer law to Eq. (3.1) and (3.2).

First, Eq. (3.1) and (3.2) can be written in a matrix form,

$$\begin{bmatrix} m_t & 0 \\ 0 & m_b \end{bmatrix} \begin{bmatrix} \ddot{x}_t \\ \ddot{x}_b \end{bmatrix} + \begin{bmatrix} c_s & -c_s \\ -c_s & c_s \end{bmatrix} \begin{bmatrix} \dot{x}_t \\ \dot{x}_b \end{bmatrix} + \begin{bmatrix} (k_p + k_s + k_t) & -(k_p + k_s) \\ -(k_p + k_s) & (k_p + k_s) \end{bmatrix} \begin{bmatrix} x_t \\ x_b \end{bmatrix} = \begin{bmatrix} k_t x_r \\ 0 \end{bmatrix} \quad (3.4)$$

The Laplace transform of Eq. (3.4) is

$$\begin{bmatrix} m_t s^2 + c_s s + k_p + k_s + k_t & -(c_s s + k_s + k_p) \\ -(c_s s + k_s + k_p) & m_b s^2 + c_s s + k_p + k_s \end{bmatrix} \begin{bmatrix} X_t(s) \\ X_b(s) \end{bmatrix} = \begin{bmatrix} k_t X_r(s) \\ 0 \end{bmatrix}$$

Next, using Cramer law,

$$X_b(s) = \frac{\begin{vmatrix} m_t s^2 + c_s s + k_p + k_s + k_t & k_t X_r(s) \\ -(c_s s + k_s + k_p) & 0 \end{vmatrix}}{\begin{vmatrix} m_t s^2 + c_s s + k_p + k_s + k_t & -(c_s s + k_s + k_p) \\ -(c_s s + k_s + k_p) & m_b s^2 + c_s s + k_p + k_s \end{vmatrix}}$$

$$X_b(s) = \frac{(c_s s + k_s + k_p) k_t X_r(s)}{(m_t s^2 + c_s s + k_p + k_s + k_t)(m_b s^2 + c_s s + k_p + k_s) - (c_s s + k_p + k_s)^2}$$

$$TF(s) = \frac{X_b(s)}{X_r(s)} = \frac{(c_s s + k_s + k_p) k_t}{(m_t s^2 + c_s s + k_p + k_s + k_t)(m_b s^2 + c_s s + k_p + k_s) - (c_s s + k_p + k_s)^2} \quad (3.5)$$

$$X_b(s) = \frac{\begin{vmatrix} k_t X_r(s) & -(c_s s + k_s + k_p) \\ 0 & m_b s^2 + c_s s + k_p + k_s \end{vmatrix}}{\begin{vmatrix} m_t s^2 + c_s s + k_p + k_s + k_t & -(c_s s + k_s + k_p) \\ -(c_s s + k_s + k_p) & m_b s^2 + c_s s + k_p + k_s \end{vmatrix}}$$

$$X_t(s) = \frac{(m_b s^2 + c_s s + k_s + k_p) k_t X_r(s)}{(m_t s^2 + c_s s + k_p + k_s + k_t)(m_b s^2 + c_s s + k_p + k_s) - (c_s s + k_p + k_s)^2}$$

$$TF(s) = \frac{X_t(s)}{X_r(s)} = \frac{(m_b s^2 + c_s s + k_s + k_p) k_t}{(m_t s^2 + c_s s + k_p + k_s + k_t)(m_b s^2 + c_s s + k_p + k_s) - (c_s s + k_p + k_s)^2} \quad (3.6)$$

Eq. (3.5) is the sprung mass-road transfer function model, while Eq. (3.6) is the unsprung mass-road transfer function model.

3.3 Artificial Neural Network

Artificial Neural Network (ANN) is one of nonlinear modeling method of dynamics systems. It has capability to control a system with uncertainty relationships between input and output. It works as biological neural networks therefore ANN has an ability to imitate the function and characteristics of human neural networks. In other words, the main strength of ANN is its ability for learning and training, as human characteristics.

It is obvious that vehicle suspension components, such as damper, bushing, even spring has a nonlinear characteristic. Due to this nonlinearity, ANN with its nonlinear characteristic capability, was applied to model the vehicle suspension system.

Architectures/ Structures of Neural Network

Artificial neural networks have been developed as generalizations of mathematical models of human cognition or neural biology, based on the assumptions that (Fausett, 1994):

- Information processing occurs at many simple elements called neurons.
- Signals are passed between neurons over connection links.
- Each connection link has an associated weight, which, in a typical neural net, multiplies the signal transmitted.
- Each neuron applies an activation function (usually nonlinear) to its net input (sum of weighted input signals) to determine its output signal.

A neural network is characterized by (1) its pattern of connection between the neurons (called its architecture), (2) its method of determining the weights on the connections (called its training, or learning, algorithm), and (3) its activation function.

Figure 3.5 shows a simple processing element called neuron, unit, cell, or node. A neuron can send only one signal at a time, although that signal is broadcast to several other neurons. It is illustrated in Figure 3.5 that the neuron has input vector $\mathbf{x} = (x_1, \dots, x_i, \dots, x_n)$.

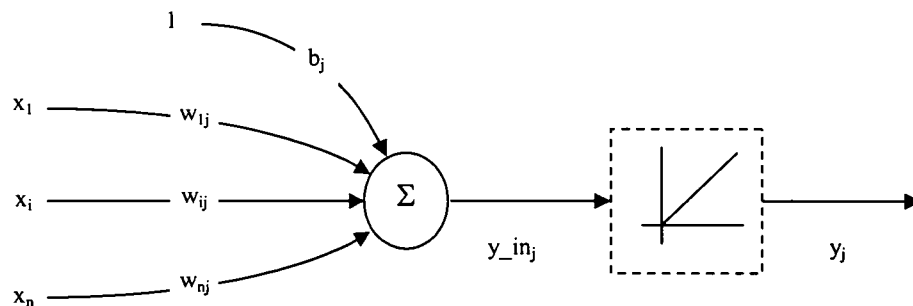


Figure 3.5 Characteristics of neuron.

Each neuron is connected to other neurons by means of directed communication links, each with an associated weight. The weights represent information being used by

the net to solve the problem. A bias can be included by adding a component $x_0 = 1$ to the vector \mathbf{x} , i.e., $\mathbf{x} = (1, x_1, \dots, x_i, \dots, x_n)$. The bias is treated exactly like any other weight, i.e., $w_{0j} = b_j$.

Each neuron has an internal state, called its activation or activity level, which is a function of the inputs it has received. Typically, a neuron sends its activation as a signal to several other neurons. As we can see from Fig 3.5, the output of the neuron is y_j .

$$\begin{aligned} y_{in_j} &= \sum_{i=0}^n x_i w_{ij} \\ &= w_{0j} + \sum_{i=1}^n x_i w_{ij} \\ &= b_j + \sum_{i=1}^n x_i w_{ij} \\ y_j &= f(y_{in_j}) \end{aligned}$$

As mentioned before, the basic operation of an artificial neuron involves summing its weighted input signal and applying an output, or activation function. There are several functions that can be used for activation function as illustrated in Figure 3.6.

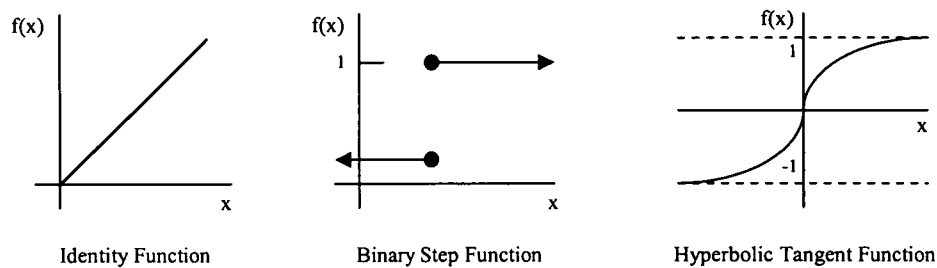


Figure 3.6 Common activation functions.

(adopted from: Hines, Fuzzy and Neural Approaches in Engineering, 1994).

From those three functions, hyperbolic tangent function is the most widely used in application from these following reasons:

- Nonlinear characteristics
- Continuous function

- Simple relationship between the value of the function at a point and the value of the derivative at that point (reduces the computational burden during training).

The hyperbolic tangent is

$$h(x) = \frac{\exp(x) - \exp(-x)}{\exp(x) + \exp(-x)}$$

The derivative of the hyperbolic tangent is

$$h'(x) = [1 + h(x)][1 - h(x)]$$

The arrangement of neurons into layers and the connection patterns within and between layers is called the net architecture. The net illustrated in Figure 3.7 consist of input units and output units.

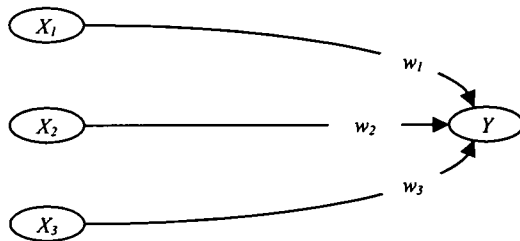


Fig 3.7 A single layer neural net.

Neural nets are often classified as single layer or multilayer. In determining the number of layers, the input units are not counted as a layer, because they perform no computation. The net illustrated in Figure 3.7 is single layer net, while the net shown in Figure 3.8 has two layers, consist of input units, output units, and one hidden unit.

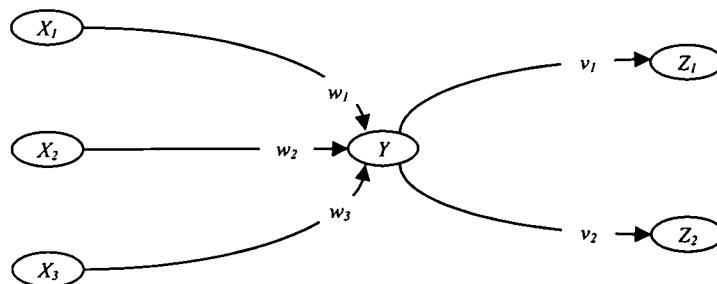


Fig 3.8 A multilayer neural net.

Backpropagation Neural Net

A multilayer neural network with one layer of hidden units (the Z units) is shown in Figure 3.9. The output units (the Y units) and the hidden units also may have biases. The bias on a typical output unit Y_k is denoted by w_{0k} ; the bias on a typical output unit Z_j is denoted by v_{0j} . Only the direction of information flow for the feedforward phase of operation is shown. During the backpropagation phase of learning, signals are sent in the reverse direction.

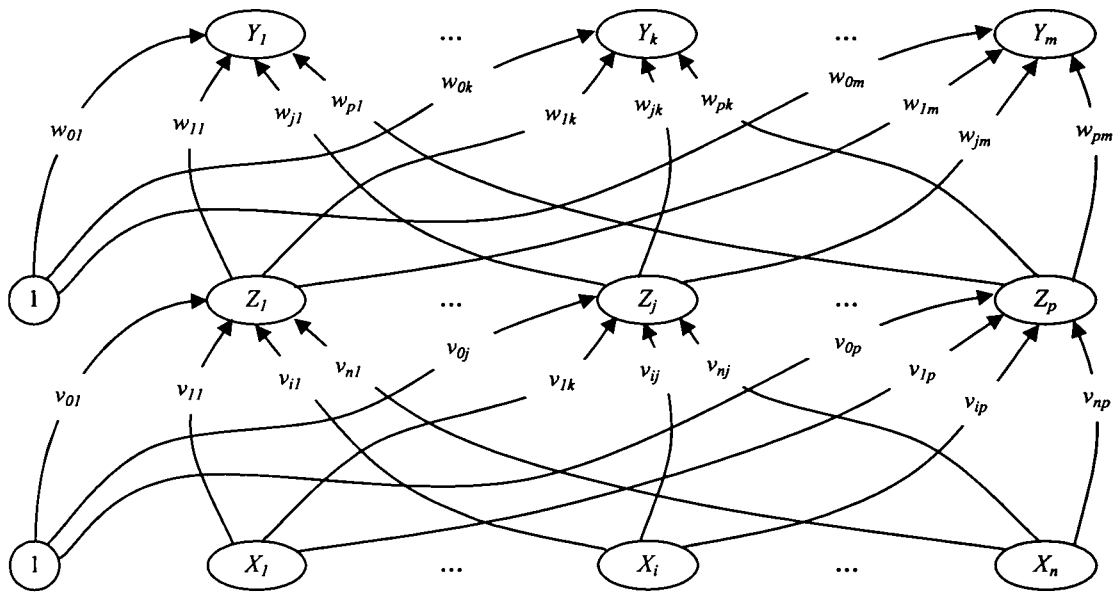


Fig 3.9 Backpropagation neural network with one hidden layer.

(adopted from: Fausett, *Fundamentals of Neural Networks*, 1994).

The training of a network by backpropagation involves three stages: the feedforward of the input training pattern, the calculation and backpropagation of the associated error, and the adjustment of the weights. The algorithm of backpropagation neural net is illustrated in Figure 3.10

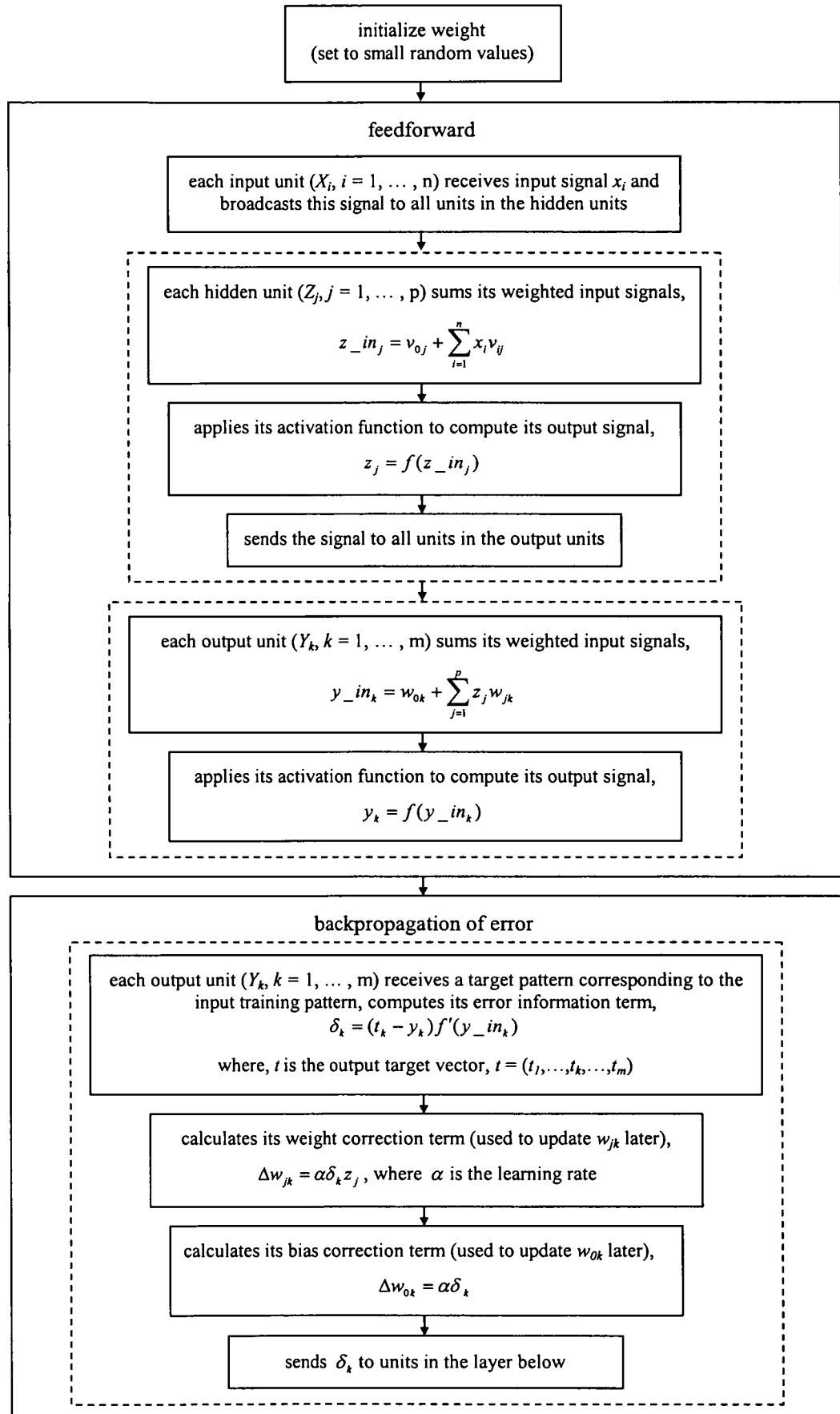


Fig 3.10 Algorithm of backpropagation neural net (continued to next page)

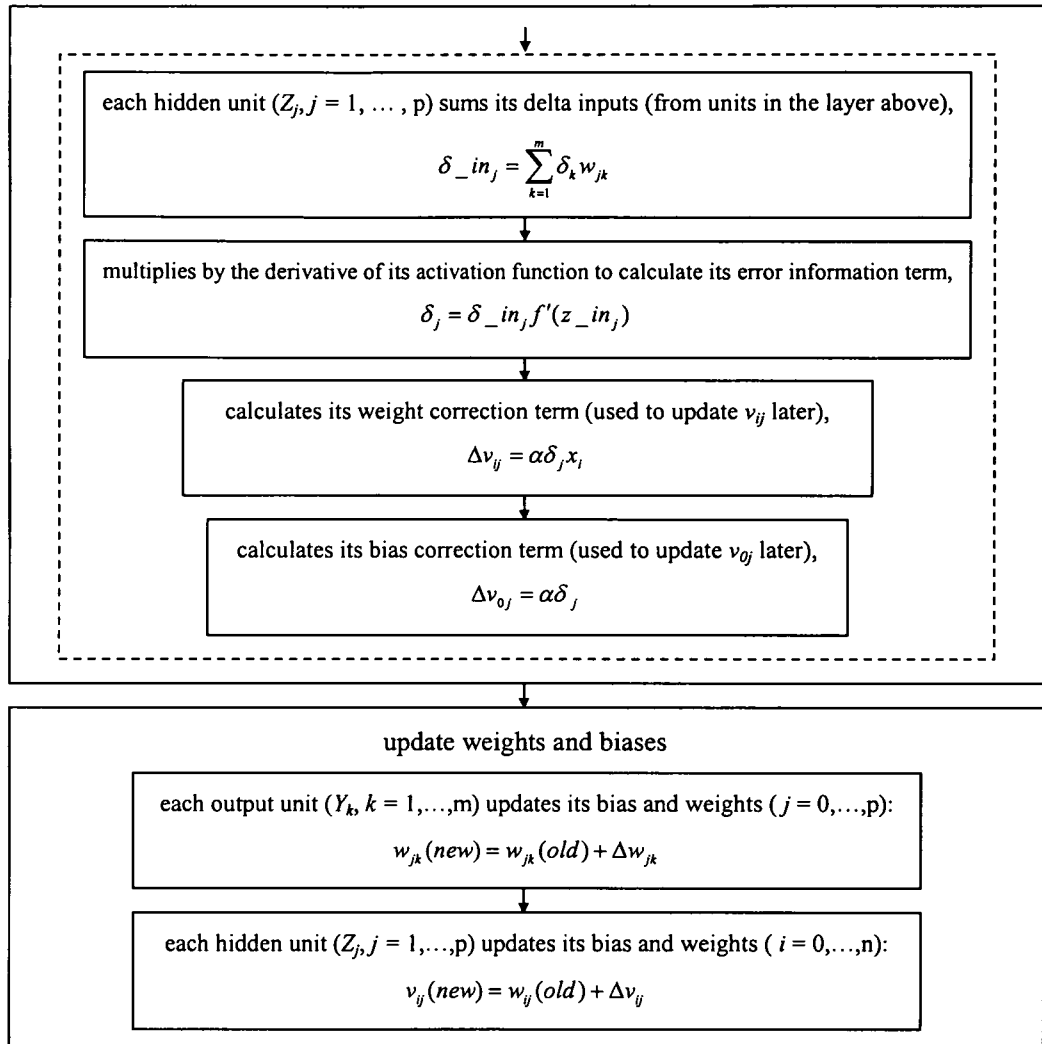


Fig 3.10 Algorithm of backpropagation neural net.

3.4 Neural Network Modeling of Vehicle Suspension System

Determination of Model Structure

The structure of ANN model is constructed by its composed parameters. Those parameters are number of layers, number of nodes in input, hidden, and output layer, activation function for each node in hidden layer and output layer, and the weights. The weakness of this modeling is no definite method to establish the network parameters. Therefore, the only way to define the variables for getting the best model structure is iteration. Iteration can be performed by varying the network parameters.

One of the network variables, that is the number of layers, can be first determined. Santosa (1998) stated that performance of network with one hidden layer compared with two hidden layers is not different for simple model such as quarter-car system. Therefore, two network layers were applied for constructing the model, consist of input layer, output layer, and one hidden layer.

The number of nodes in input layer can be determined by deriving the sprung and unsprung transfer function model to find its polynomial coefficient. Structure of ANN input layer can be written as

$$[y(t-1) \dots y(t-na) \quad u(t-nk) \dots u(t-nb-nk+1)]^T \quad (3.7)$$

where,

u = input signal

y = output signal

na = number of past outputs used for determining the prediction

nb = number of past inputs used for determining the prediction

nk = time delay (usually 1)

then, by using coefficients na , nb , and nk , the number of input layer nodes can be determined.

Firstly, the vehicle suspension transfer function is rewritten,

$$TF(s) = \frac{X_b(s)}{X_r(s)} = \frac{(c_s s + k_s + k_p)k_t}{(m_t s^2 + c_s s + k_p + k_s + k_t)(m_b s^2 + c_s s + k_p + k_s) - (c_s s + k_p + k_s)^2}$$

$$TF(s) = \frac{X_t(s)}{X_r(s)} = \frac{(m_b s^2 + b_s s + k_s + k_p)k_t}{(m_t s^2 + c_s s + k_p + k_s + k_t)(m_b s^2 + c_s s + k_p + k_s) - (c_s s + k_p + k_s)^2}$$

By defining constants

$$a_1 = \frac{c_s}{m_b} \quad a_2 = \frac{k_s + k_p}{m_b}$$

$$a_3 = \frac{c_s}{m_t} \quad a_4 = \frac{k_s + k_p}{m_t}$$

$$\omega_0^2 = \frac{k_t}{m_t} \quad (\omega_0 \text{ is the natural frequency of the unsprung subsystem})$$

then from Eq. (3.5) and (3.6) the following equation is obtained

$$TF(s) = \frac{X_b(s)}{X_r(s)} = \frac{\omega_0^2(a_1s + a_2)}{s^4 + (a_1 + a_3)s^3 + (a_2 + a_4 + \omega_0^2)s^2 + a_1\omega_0^2s + a_2\omega_0^2} \quad (3.8)$$

$$TF(s) = \frac{X_t(s)}{X_r(s)} = \frac{\omega_0^2(s^2 + a_1s + a_2)}{s^4 + (a_1 + a_3)s^3 + (a_2 + a_4 + \omega_0^2)s^2 + a_1\omega_0^2s + a_2\omega_0^2} \quad (3.9)$$

By letting X_b, X_t as input and X_r as output variable, Eq. (3.8) and (3.9) can be rewritten

$$\overset{\dots}{X}_b + (a_1 + a_3)\overset{\dots}{X}_b + (a_2 + a_4 + \omega_0^2)\overset{\dots}{X}_b + a_1\omega_0^2\overset{\cdot}{X}_b + a_2\omega_0^2X_b = \omega_0^2(a_1\overset{\cdot}{X}_r + a_2X_r) \quad (3.10)$$

$$\overset{\dots}{X}_t + (a_1 + a_3)\overset{\dots}{X}_t + (a_2 + a_4 + \omega_0^2)\overset{\dots}{X}_t + a_1\omega_0^2\overset{\cdot}{X}_t + a_2\omega_0^2X_t = \omega_0^2(\overset{\cdot}{X}_r + a_1\overset{\cdot}{X}_r + a_2X_r) \quad (3.11)$$

By defining $\overset{n}{X}_b = y(t-n)$, $\overset{n}{X}_t = z(t-n)$, and $\overset{n}{X}_r = u(t-n)$, Eq. (3.10) and (3.11) can be written in discrete time equation,

$$\begin{aligned} y(t-4) + (a_1 + a_3)y(t-3) + (a_2 + a_4 + \omega_0^2)y(t-2) + a_1\omega_0^2y(t-1) + a_2\omega_0^2y(t) \\ = a_1\omega_0^2u(t-1) + a_2\omega_0^2u(t) \end{aligned} \quad (3.12)$$

$$\begin{aligned} z(t-4) + (a_1 + a_3)z(t-3) + (a_2 + a_4 + \omega_0^2)z(t-2) + a_1\omega_0^2z(t-1) + a_2\omega_0^2z(t) \\ = \omega_0^2u(t-2) + a_1\omega_0^2u(t-1) + a_2\omega_0^2u(t) \end{aligned} \quad (3.13)$$

By defining constants

$$A_1 = \frac{a_1\omega_0^2}{a_2\omega_0^2}, \quad A_2 = \frac{(a_2 + a_4 + \omega_0^2)}{a_2\omega_0^2}, \quad A_3 = \frac{(a_1 + a_3)}{a_2\omega_0^2}, \quad A_4 = \frac{1}{a_2\omega_0^2}$$

$$B_1 = \frac{a_1\omega_0^2}{a_2\omega_0^2}, \quad B_2 = \frac{\omega_0^2}{a_2\omega_0^2}$$

then Eq. (3.12) and (3.13) can be written in basic equation as follows

$$y(t) + A_1y(t-1) + A_2y(t-2) + A_3y(t-3) + A_4y(t-4) = u(t) + B_1u(t-1)$$

$$y(t) + A_1y(t-1) + A_2y(t-2) + A_3y(t-3) + A_4y(t-4) = u(t) + B_1u(t-1) + B_2u(t-2)$$

Consider $y(t - na) = q^{-na} y(t)$ and $u(t - nb) = q^{-nb} u(t)$, then constants A and B can be expressed in time delay operator q^{-1} with

$$A(q) = 1 + a_1 q^{-1} + a_2 q^{-2} + a_3 q^{-3} + a_4 q^{-4}$$

$$B(q) = b_1 q^{-1}$$

for sprung mass, and

$$A(q) = 1 + a_1 q^{-1} + a_2 q^{-2} + a_3 q^{-3} + a_4 q^{-4}$$

$$B(q) = b_1 q^{-1} + b_2 q^{-2}$$

for unsprung mass.

Therefore, the polynomial coefficients of the models can be determined.

For unsprung mass:

$$na = 4$$

$$nb = 3$$

$$nk = 1$$

For sprung mass:

$$na = 4$$

$$nb = 2$$

$$nk = 1$$

Using Eq. (3.7), the structure of input layer is

$$[y(t-1) \dots y(t-4) \quad u(t-1) \dots u(t-3)]^T \text{ for unsprung mass}$$

$$[y(t-1) \dots y(t-4) \quad u(t-1) \dots u(t-2)]^T \text{ for sprung mass}$$

The number of node in hidden layer along with its activation function can only be determined by iteration since there is no certain method for it. Whilst, for determining the output layer nodes, it is complied with the problem faced.

Iteration was performed using Matlab™ Neural Network Toolbox. The network structure which produces the best model is illustrated in Figure 3.11.

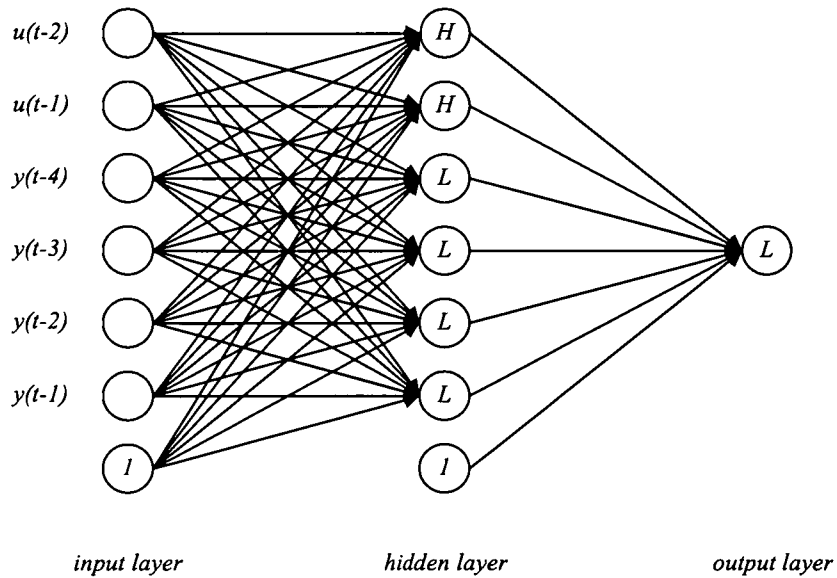


Figure 3.11 ANN model structure for vehicle suspension.

It is shown in Figure 3.11 that iteration was performed using input and output data at $(t-2)$ and $(t-1)$. $(t-2)$ means that two past values were used for determining the renewed value. Each data was then forward-propagated to each hidden layer nodes which has activation function [L L L L H H]. L stands for linear activation function, while H stands for hyperbolic tangent activation function. Output from hidden layer was forward-propagated again to output layer with activation function [L]. Output from output layer node was then back-propagated to renew the weights. The weight is always corrected until satisfactory modeling is obtained.

CHAPTER 4

TESTING AND DATA ANALYSIS

The roughness in a road is the deviation in elevation seen by a vehicle as it moves along the road. The roughness acts as a vertical displacement input to the wheels, thus exciting ride vibrations. Yet the most common and meaningful measure of ride vibration is the acceleration produced. Therefore, for the purpose of understanding the dynamics of ride, the roughness should be viewed as acceleration input at the wheels.

This chapter explains the testing of Proton's suspension system to measure its ride dynamic characteristic for further modeling analysis. The test procedure encompasses general test design, test preparation, instrumented ride vibration measurement, and test rig description. This chapter also describes the 'initial treatment' to the acceleration data obtained, i.e. filtering and numerical integration for mathematical modeling purpose.

4.1 Test Procedure

4.1.1 General Test Design

A typical ride test consists of running vehicle over selected well-defined sections of road at constant speed and certain type of road was performed. Accelerometers were mounted on the vehicle sprung and unsprung mass to measure its vertical acceleration. The field measured data was then brought to the laboratory for 'mission reproduction' using Remote Parameter Control (RPC) technique which is a built-in iteration software in the road simulator. Using the same car model, the actuators of the servo hydraulic four posters road simulator were then driven and iterative tuning were performed such that the sprung and unsprung acceleration match those measured in the field. This iteration process involves estimation of a linear FRF (Frequency Response Function) from the test data and refinement of the input sequence by using inverse of the FRF. Thus, realistic body motion and drive signal from the road simulator can be reproduced under controlled environment. A more detail explanation about this iteration technique will be described in the next section.

As previously mentioned, the overall goal of this research is to replace this iterative tuning which is specific for certain model of car with a car suspension system model. Once the model of the suspension has been determined, the drive signal can be recreated using acceleration data from the accelerometers and the car physical data. The comparison between industrial practice procedure and modeling approach is illustrated in Figure 4.1.

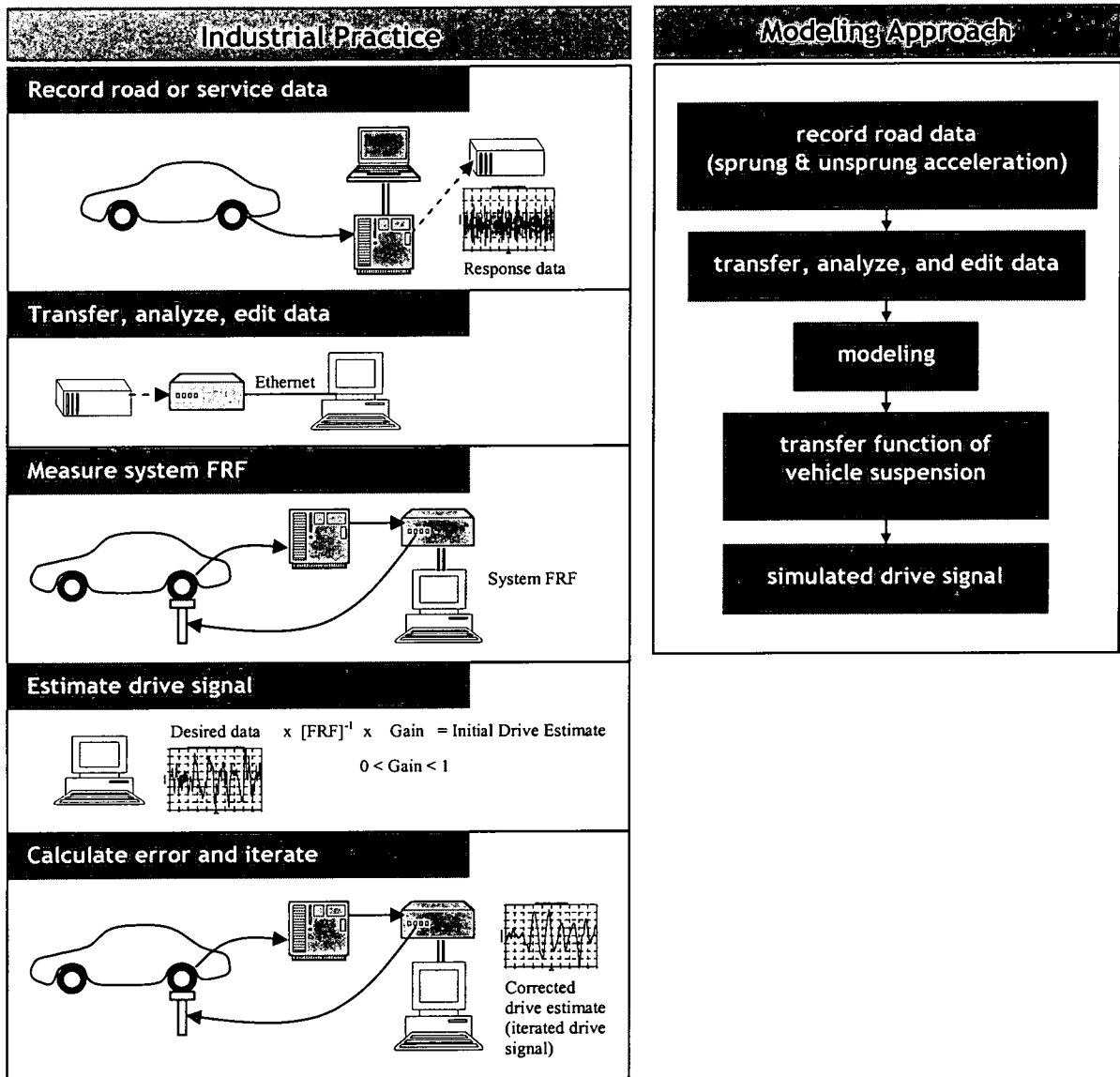


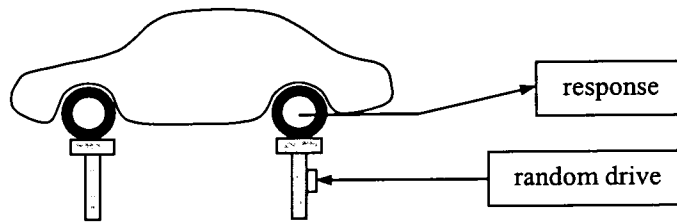
Figure 4.1 Comparison between industrial practice and current modeling approach. (adopted from: Arifin et al., Using Model Parameter to Monitor Vehicle Changes during a Durability Test, 2000)

Remote Parameter Control

Remote Parameter Control (RPC) is an advanced simulation technique that is used to replicate and analyze 'in service' vibrations and motions of a specimen using a dynamic mechanical system in a controlled laboratory environment. RPC was developed by MTS Systems Corporation which is then applied to their product, i.e. road simulator.

Refer to Figure 4.1, the RPC process can be explained as follows (Arifin et al., 2000):

1. Vehicle instrumentation and data collection.
 - The test vehicle is instrumented with accelerometers and data recorder.
2. Edit and reduce data.
 - The measured data is converted to RPC file format and analyzed using the RPC III TEDIT program.
 - Data is reduced to the required data length.
 - The acceleration data is run through the RPC III 'remove_trend' program. This program removes the slope in the data. The slope of the data is removed to remove any drift in the accelerometers during data collection.
 - A filter is constructed with a band-pass frequency of 0.6-50 Hz (typical for a servo-hydraulic four posters). The filter is applied to each of the time histories.
3. Measure system FRF (Frequency Response Function).
 - The purpose of measuring the FRF is to linearly approximate the laboratory system. The laboratory system consists of any mechanical and electrical components between the drive signal to each actuator and the response of each signal accelerometer. This includes the servo-controller, actuators, servo-valves, hydraulic power supply, hydraulic accumulators, test vehicle, transducer conditioner, and filters. The FRF is measured by creating random, white noise, playing this signal out to the test system, and then collecting the response from each accelerometer. Figure 4.2 illustrates the calculation of FRF.



$$FRF = [H] = \frac{G_{xy}(f)}{G_{xx}(f)} \quad (6.1)$$

where G_{xy} is the Cross Spectral Density and G_{xx} is the Auto Spectral Density.

Figure 4.2 FRF calculation.

As shown in Figure 4.2, the FRF is calculated by taking the Cross Spectral Density (CSD) between the drive signal and the acceleration response. The CSD is then divided by the Auto Spectral Density (ASD) of the drive signal. The output is a 4x4 matrix (4-wheels acceleration responses, 4-wheels drive signals) which provides the linear relationship between drive and response signal at all frequencies.

4. Estimate drive signal and iteration

- The estimation process is an iterative process as shown in Figure 4.3.

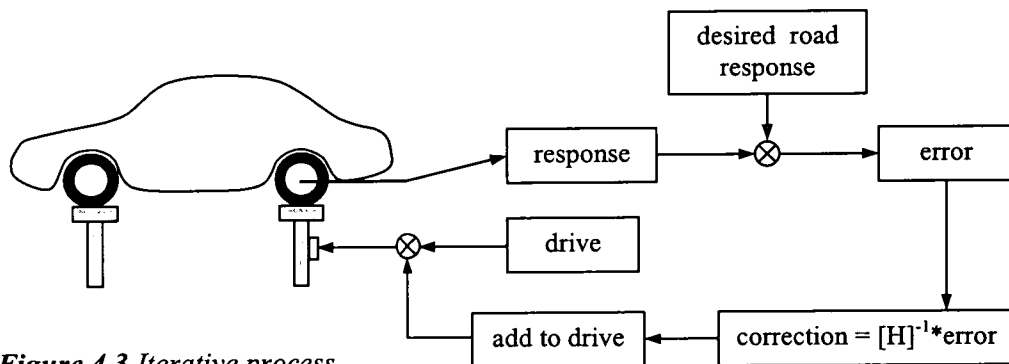


Figure 4.3 Iterative process

- At this point, the FRF needs to be inverted prior to performing the estimation.
- An initial drive is calculated by convolving the response with the inverse FRF ($[FRF]^{-1}$) and multiplying the result with a gain factor. The gain factor used

for the estimation is 0.5 for each of drive channel. The result of this process gives a four-channel initial drive file. This drive file is then played out to the test system to get the acceleration responses.

- As shown in Figure 4.3, the acceleration signal as a response from the drive signal excitation is then subtracted from the desired response (i.e. measured acceleration signal). This file is called an error file. The error file is then convolved with the inverse of FRF and multiplied by a gain factor to get the correction file. The correction is then added to the previous drive signal.
- The new drive signal is then played out to the test system. This process is repeated until the RMS of the error file becomes quite small.

4.1.2 Test Preparation

The test vehicles are two models of Proton cars, mid-sized sedan, powered by a 1.6 liter MPI engine. The front suspension is fitted with Mc Pherson struts and a coil with a stabilizer bar; the rear suspension is a multi-link system that also uses a stabilizer bar.

Tires

The tire characteristics play a fundamental role in the transmission of longitudinal, lateral, and vertical forces between the vehicle and road. The tire properties should be as constant as possible and hence predictable by the driver. All tires are standardized to guarantee interchangeability, i.e. to guarantee the possibility of using tires from different manufacturers but with the same designation on one vehicle. Table 4.1 shows some information contained in test-vehicle tire which are obtained from the manufacturer.

Table 4.1 Tire parameters of test vehicles.

Car Model	Proton X	Proton Y
Tire Specification	195/55 R15 84V	185/60 R14 82V
Tire Spring Rate	208.5 N/mm	194 N/mm
Tire Pressure	2.9 kg/cm ²	2.9 kg/cm ²

Suspension Specification

Suspension is a crucial functional element which determines vehicle quality. It comprises linkage mechanisms which permit an appropriately vertical motion of the vehicle body, controlled by the suspension spring and damper. For a normal road vehicle, the suspension links include rubber bushes, which are called parasitic spring components. The coefficients for these components together with the mass of the links are tabulated in Table 4.2 and 4.3 for Proton X and Y, respectively.

Table 4.2 Suspension parameters of Proton X.

No	Item	Unit	Proton X		
			Front	Rear	
1	tire spec	195 / 55 R 15 84 V			
2	tire spring rate (k_t)	N/mm	208.5	208.5	
3	suspension spring rate (k_s)	N/mm	23	18	
4	parasitic spring rate (k_p)	N/mm	6	6	
5	damping coefficient (c_s)	Ns/m	3959	2374	
6	mass				
	curb weight		kg	810.5	550.5
	tire mass with rim		kg	16.5	16.5
	left side				
	1	unsprung mass (m_t)	kg	35.19	41.88
	2	sprung mass (m_b)	kg	355.31	221.61
	right side				
	1	unsprung mass (m_t)	kg	35.19	41.88
	2	sprung mass (m_b)	kg	355.31	221.61

Table 4.3 Suspension parameters of Proton Y.

No	Item	Unit	Proton Y		
			Front	Rear	
1	tire spec	185 / 60 R 14 82 V			
2	tire spring rate (kt)	N/mm	194	194	
3	suspension spring rate (ks)	N/mm	24	18	
4	parasitic spring rate (kp)	N/mm	6	6	
5	damping coefficient (cs)	Ns/m	1313	1527	
6	mass				
	curb weight		kg	691.5	491.5
	tire mass with rim		kg	14	14
	left side				
	1	unsprung mass (mt)	kg	33.76	39.3
	2	sprung mass (mb)	kg	323.74	209.7
	right side				
	1	unsprung mass (mt)	kg	33.76	39.3
	2	sprung mass (mb)	kg	323.74	209.7

- **Test Site**

Road input data was measured from two locations which represent two types of input:

- China public road (random profile input)
- Proton simulation test-track (deterministic input), shown in Figure 4.4.

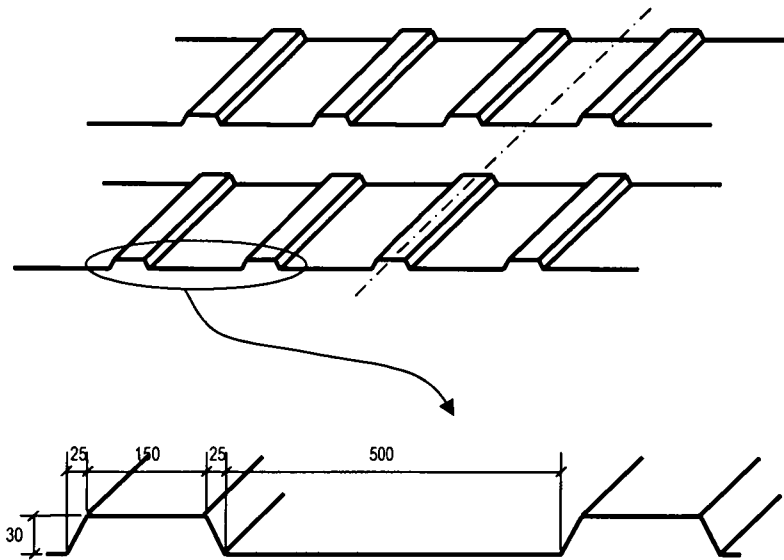


Figure 4.4 Proton simulation test-track (dimensions in mm units).

4.1.3 Instrumented Ride Vibration Measurement

Ride vibration measurements are obtained by measuring accelerations on the unsprung and sprung mass of the vehicle. The output of each acceleration transducer (accelerometer) was analyzed and the results will be utilized to produce numerical measures of ride vibration magnitude.

- **Accelerometer and Signal Conditioning**

To assure that engine and other high frequency vibrations will not be amplified, accelerometers with sufficiently high natural frequency and appropriate internal damping were used.

- *Accelerometer Location*

Accelerometers were mounted on the spindle (front) and lower arm (rear) to detect the vertical movement of the vehicle unsprung mass. While for measuring the sprung mass vertical acceleration, accelerometers were installed on strut mount (body). The sensor placement is illustrated in Figure 4.5.

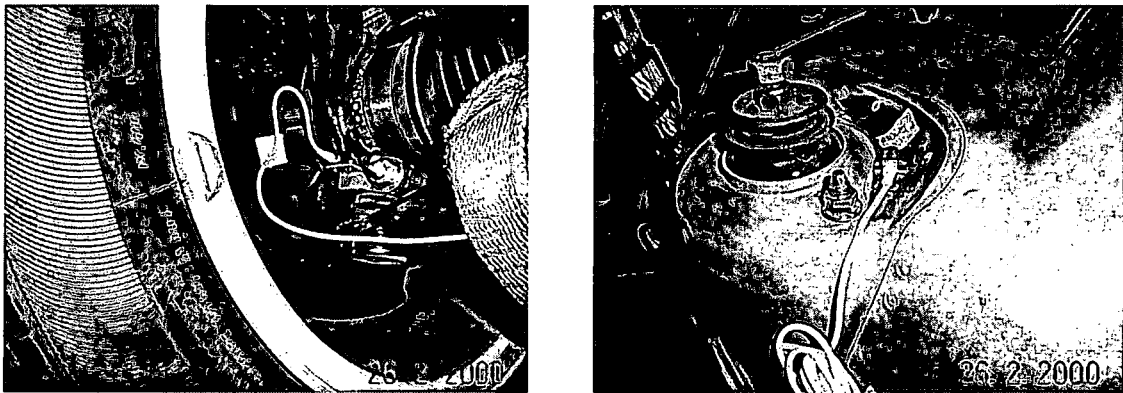


Figure 4.5 Sensor placements.

(adopted from: Proton documentation)

4.1.4 Test Rig Description

Inputs to the vehicle were provided via four MTS Series 248 double-ended actuators, each rated at 50 kN with 150 mm stroke. Each actuator has a built in Linear Variable Displacement Transducer (LVDT) for measuring the actuator displacement. The actuator was driven by a three-stage valve with a rated flow at 340 liters per minute.

The test vehicle was mounted on four 300 mm diameter wheel pans that were fixed to the ends of the actuators. To prevent the car from falling off the 4-poster, a wheel restraint was placed on the outer side of each wheel pan. The laboratory testing set up is illustrated in Figure 4.6.

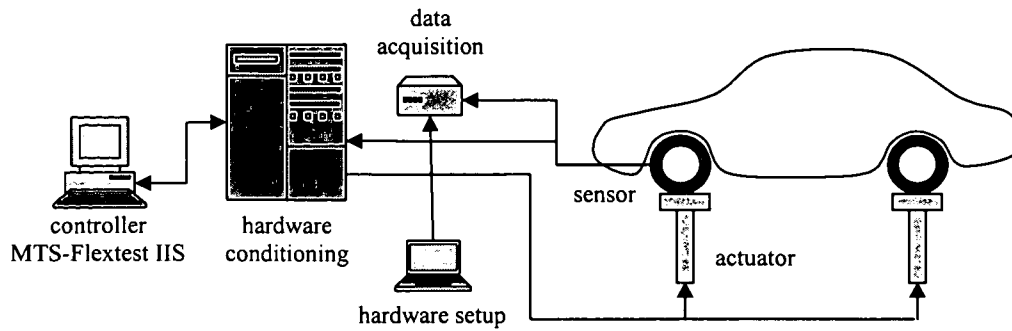


Figure 4.6 Laboratory testing set up.

4.2 Data Processing

Post processing analysis was performed on acceleration signals to get the other parameters of vehicle suspension model, i.e. velocity and displacement signal. It comprises several sequences of steps: filtering, integration, and checking the reliability of integration by applying double differentiation to displacement signal as integration result. These steps were applied for both China road data and Proton test-track data.

4.2.1 China Road Data

As one of their target market country, Proton sends car to China to get a specific public road input, by driving and testing a certain model of car over it. The testing operating conditions for China road testing are:

- Acceleration measures: G
- Data analysis parameters:
 - Data duration: 5 sec (vehicle speed = 30 m/s , distance travel = 41.7 m)
 - Sampling interval: 0.00488281 sec

Figures 4.7, 4.8, and 4.9 show the measured unsprung and sprung acceleration signal and iterated drive signal, respectively, for Proton X at front-left wheel position. The unsprung and sprung acceleration signal were obtained from the accelerometers mounted on the vehicle, while iterated drive signal was obtained as a result of iteration process using road simulator.

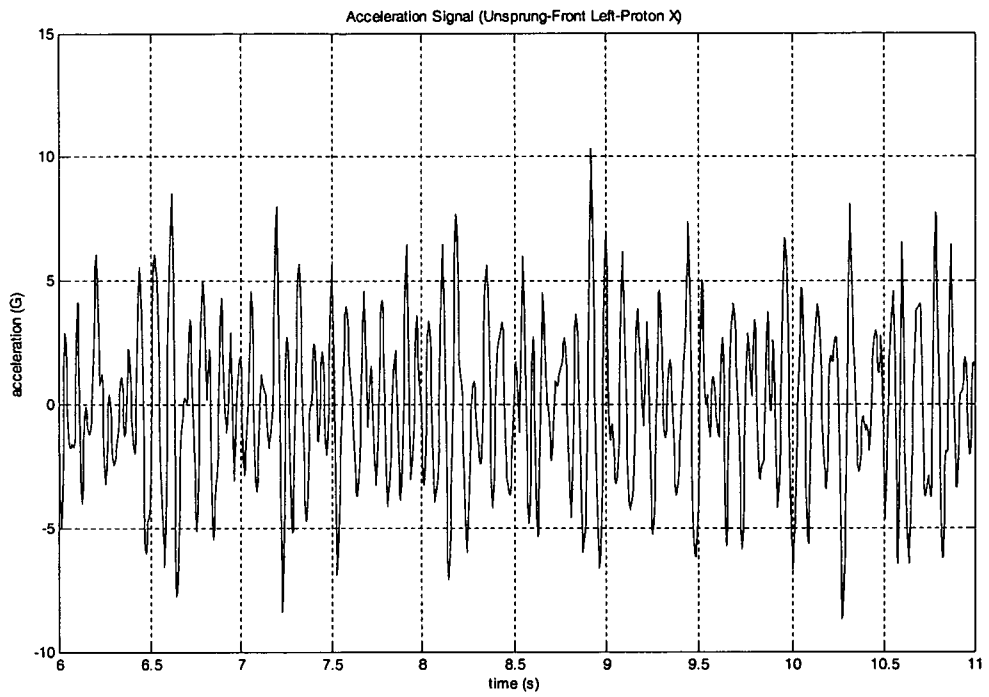


Figure 4.7 Acceleration signal (unsprung-front left-Proton X).

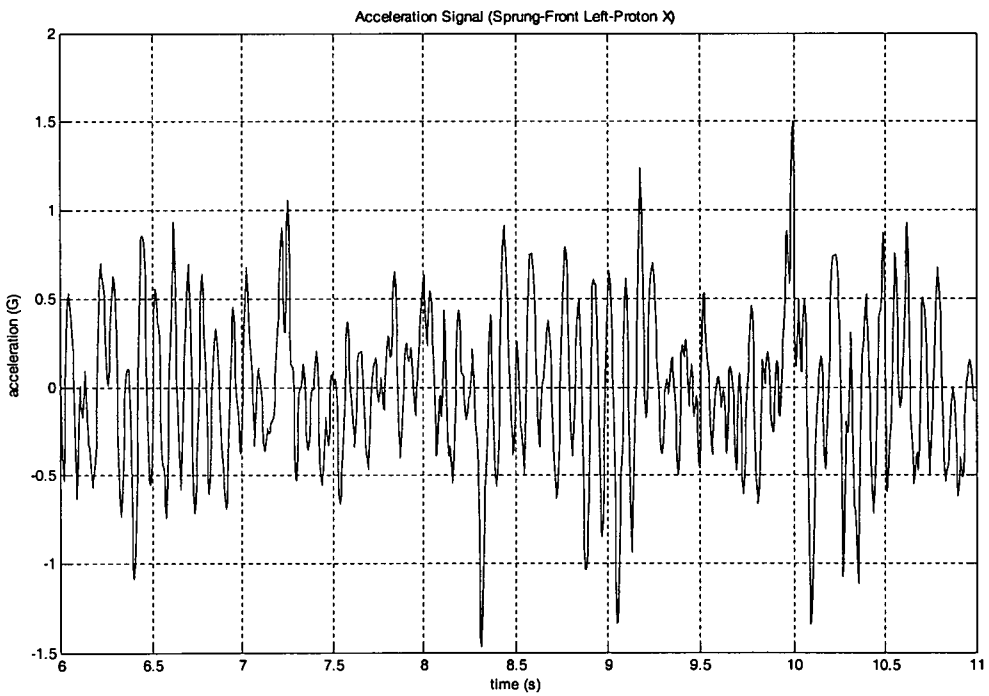


Figure 4.8 Acceleration signal (sprung-front left-Proton X).

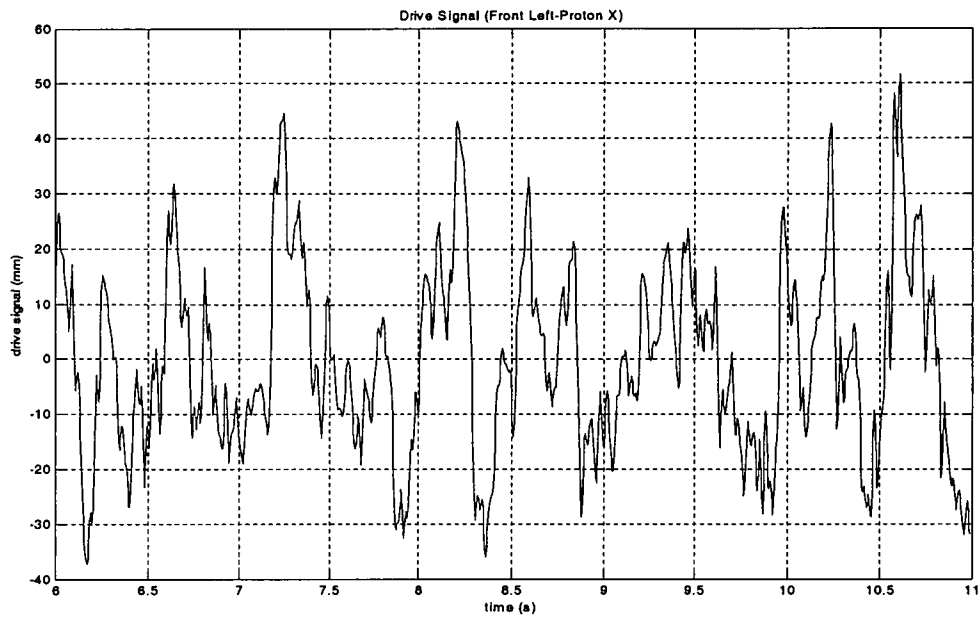


Figure 4.9 Iterated drive signal (front left-Proton X).

To see the pureness of the measured acceleration signals, whether it is contaminated with noise or not, Fast Fourier Transform (FFT) was applied to the signals. The FFT results for unsprung and sprung acceleration signal, and iterated drive signal are shown in Figure 4.10, 4.11, and 4.12, respectively.

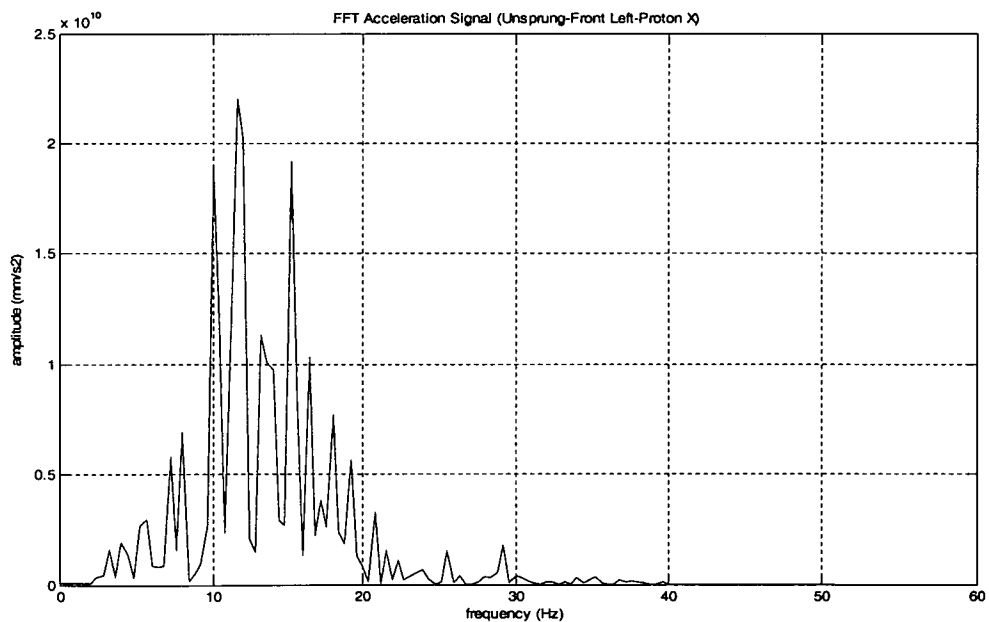


Figure 4.10 FFT acceleration signal (unsprung-front left-Proton X).

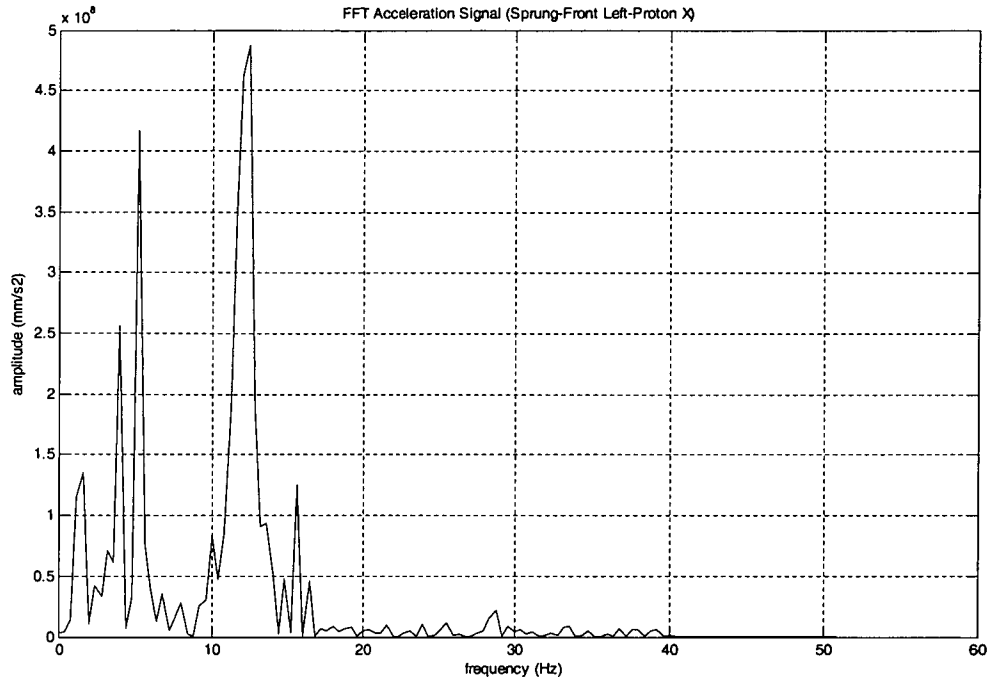


Figure 4.11 FFT acceleration signal (sprung-front left-Proton X).

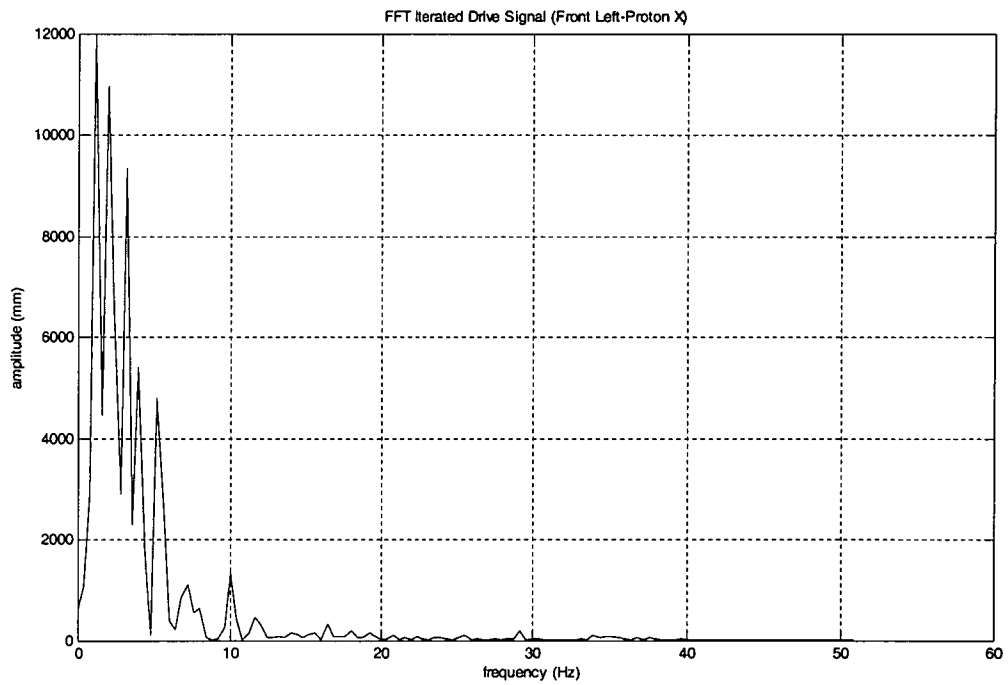


Figure 4.12 FFT iterated drive signal (front left-Proton X).

It is illustrated in Figure 4.10, 4.11, and 4.12 that the high frequency noise (above 15 Hz) appeared in the signal. The frequency above 15 Hz is unwanted noise frequency since the natural frequency for unsprung and sprung mass are below that frequency. Therefore, a low-pass filter must be constructed to eliminate the noise.

4.2.1.1 Signal Filtering

The purpose of filtering the time histories was to limit the band-width of the simulation to the filtered frequency range. It is used to eliminate unwanted component of signals.

A low-pass filter was constructed with a pass frequency of 15 Hz. This frequency was selected since the 50 Hz cut-off frequency of the RPC simulation (using road simulator) still produces a noisy signal. The sprung and unsprung mass natural frequency which is lying between 1-15 Hz remains unchanged. The filter was applied to each of the time histories (unsprung, sprung, and drive signal). The filtered raw data signals are shown in Figure 4.13, 4.14, and 4.15 for filtered unsprung and sprung acceleration signal and iterated drive signal, respectively. While, the FFT of the filtered signals are depicted in Figure 4.16, 4.17, and 4.18 for filtered unsprung acceleration signal, sprung acceleration signal, and iterated drive signal, respectively.

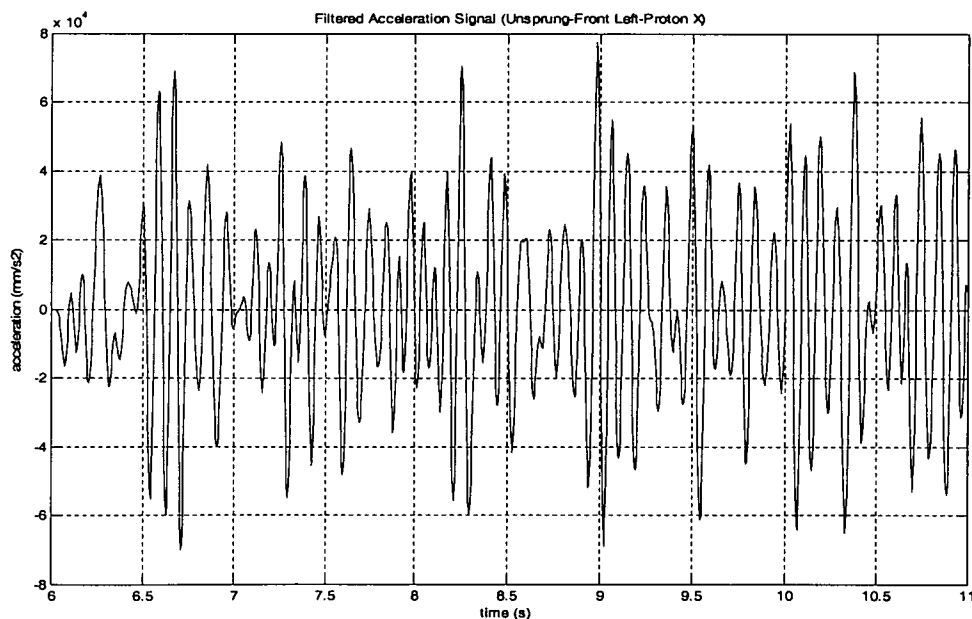


Figure 4.13 Filtered acceleration signal (unsprung-front left-Proton X).

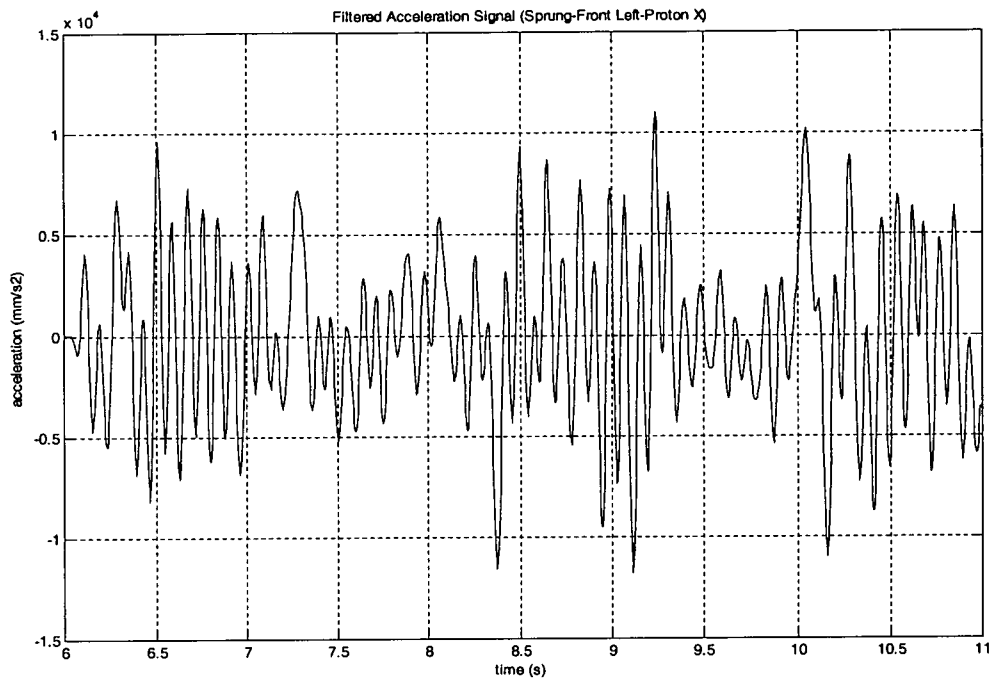


Figure 4.14 Filtered acceleration signal (sprung-front left-Proton X).

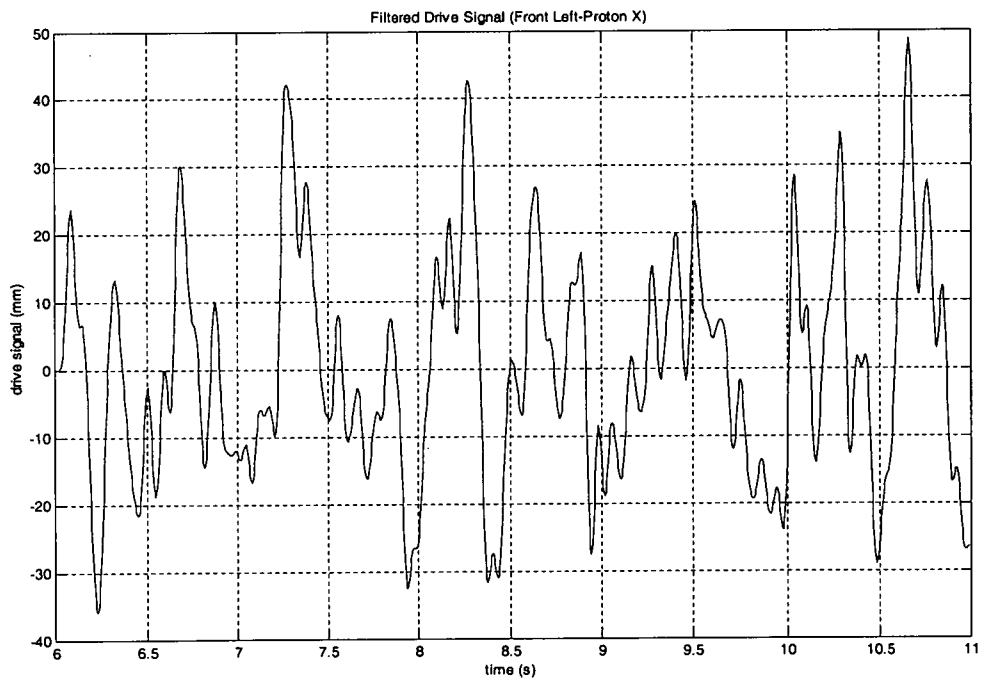


Figure 4.15 Filtered iterated drive signal (front left-Proton X).

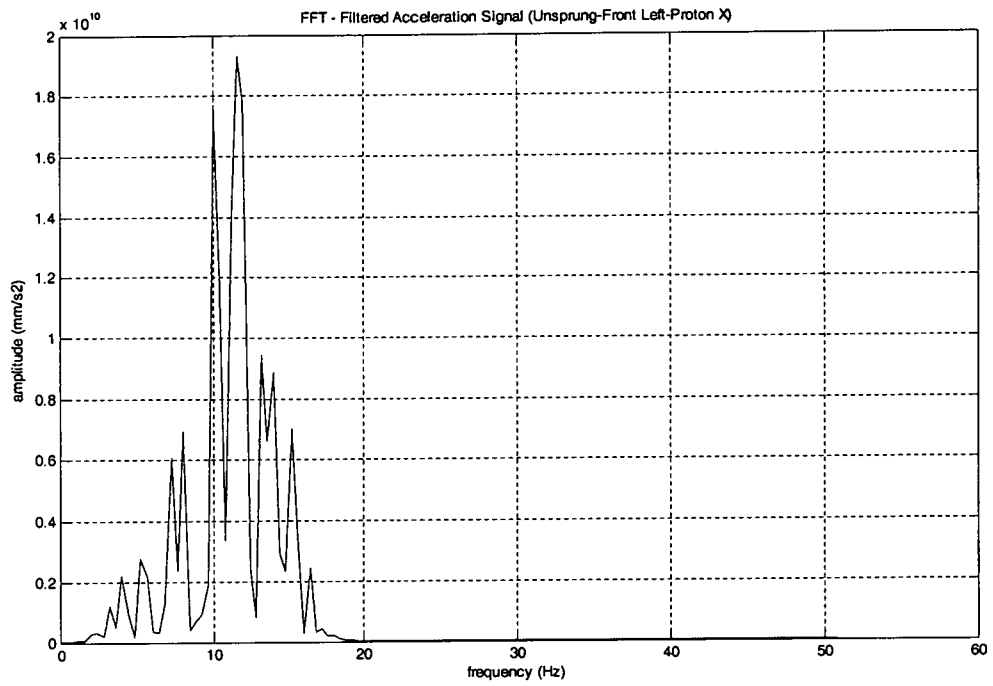


Figure 4.16 FFT - Filtered acceleration signal (unsprung-front left-Proton X).

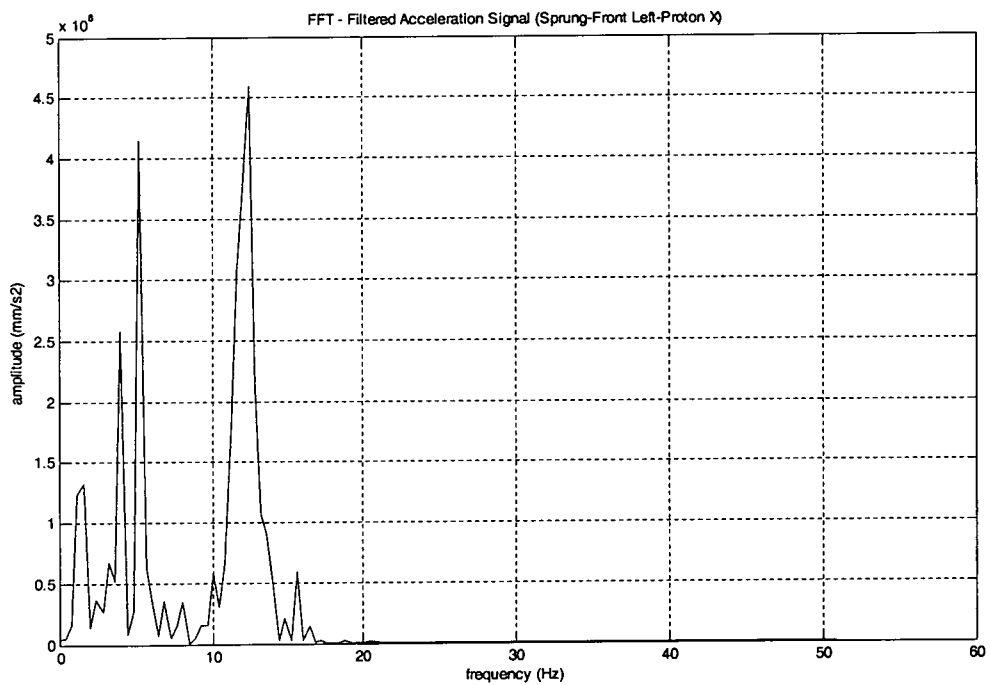


Figure 4.17 FFT - Filtered acceleration signal (sprung-front left-Proton X).

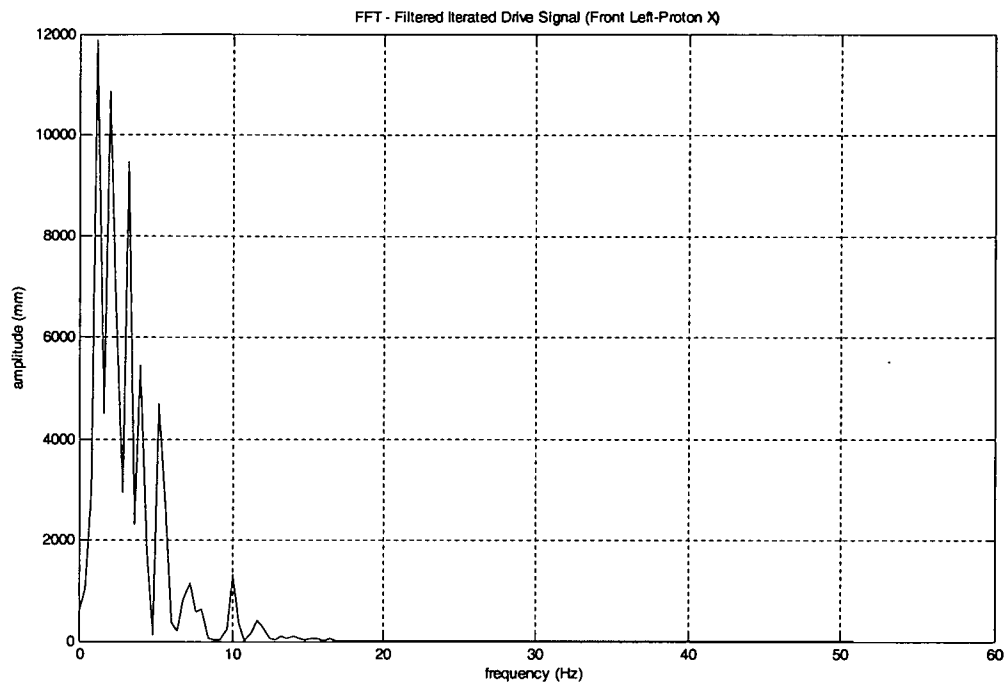


Figure 4.18 FFT - Filtered iterated drive signal (front left-Proton X).

Comparing between the unfiltered signals as shown in Figure 4.7, 4.8, 4.9 and the filtered signals as illustrated in Figure 4.13, 4.14, and 4.15 shows that the filtered signal is obviously smoother than unfiltered signal since the high frequency noise have been rejected. The filtered signal overall amplitude is also lower than the unfiltered one. It is clearly explained by comparing the FFT between unfiltered and filtered signal which is shown in Figure 4.10, 4.11, 4.12 for unfiltered signal and 4.16, 4.17, 4.18 for filtered signal.

4.2.1.2 Signal Integration

The unsprung and sprung acceleration signals were then numerically integrated to obtain velocity signal using cumulative trapezoidal numerical integration rule. The result of the integration must be multiplied by the sampling time to properly scale the velocity data. The velocity signal for “unsprung-front left-Proton X” is shown in Figure 4.19.

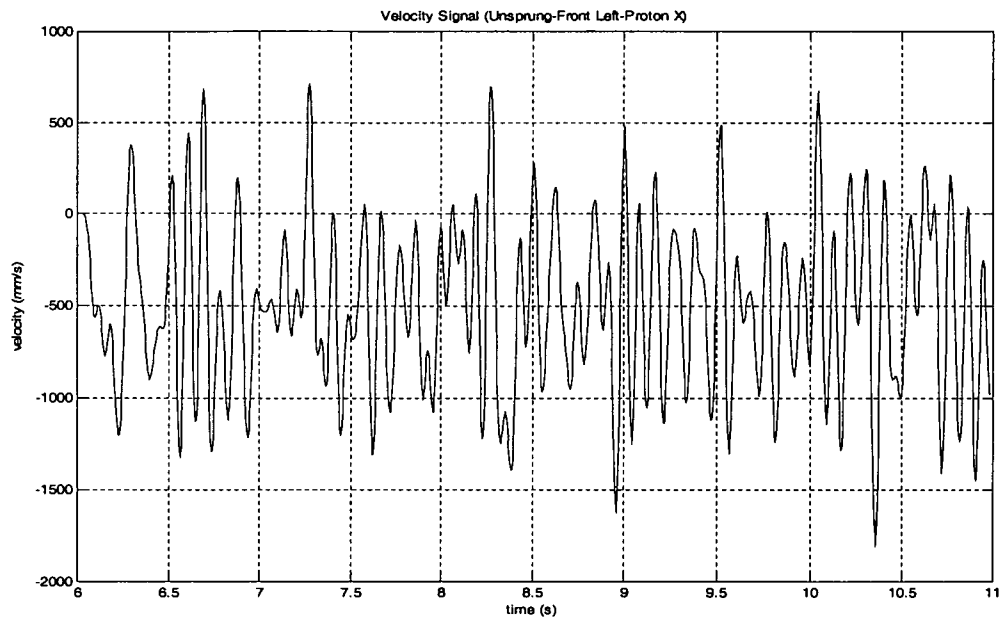


Figure 4.19 Velocity signal (unsprung-front left-Proton X).

It is clearly seen in Figure 4.19 that there is a vertical shift in the velocity graph. This is due to byproduct of DC offset in the acceleration data. The trend can be removed by detrend the signal. It eliminates the trend by removing the best straight-line fit linear trend from the data. Results of this treatment for unsprung and sprung velocity signal are shown in Figure 4.20 and 4.21.

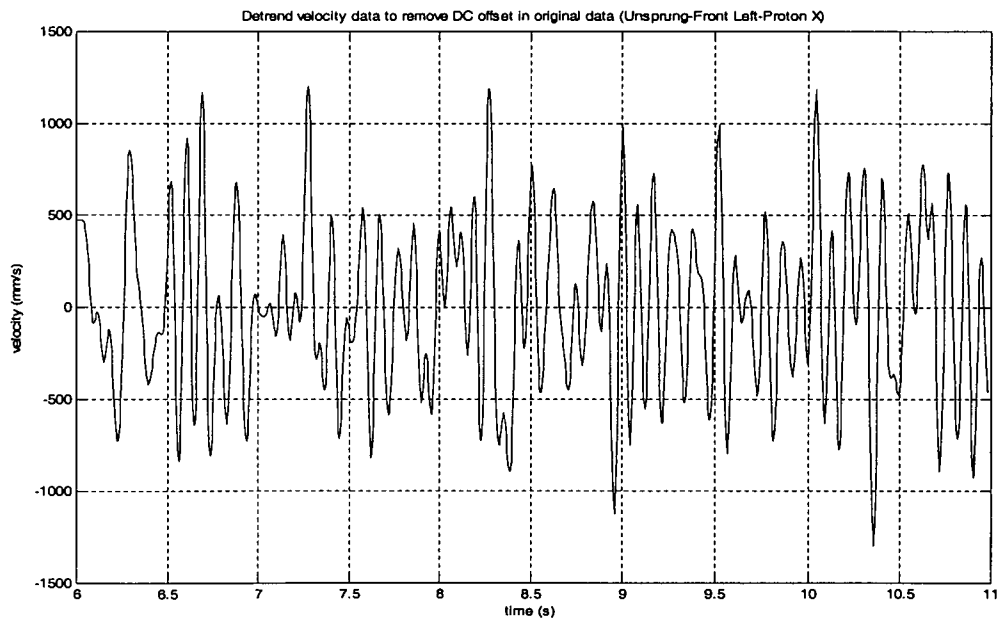


Figure 4.20 Detrend velocity signal to remove DC offset (unsprung-front left-Proton X).

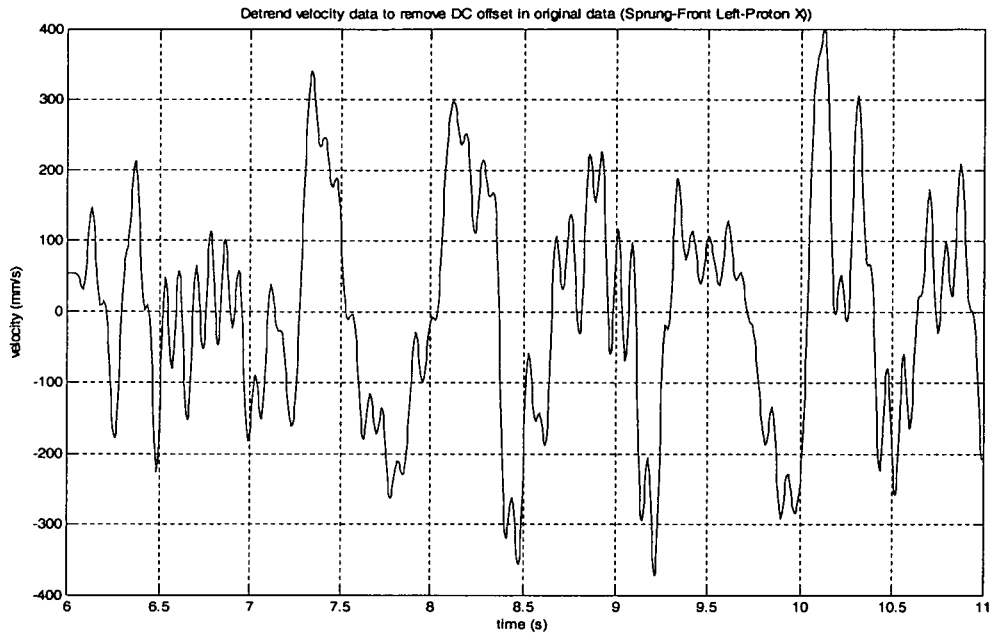


Figure 4.21 Detrend velocity signal to remove DC offset (sprung-front left-Proton X).

Using the same procedure, the velocity signal can then be numerically integrated to obtain displacement signal. Results of the integration process to unsprung and sprung velocity signal are shown in Figure 4.22 and 4.23.

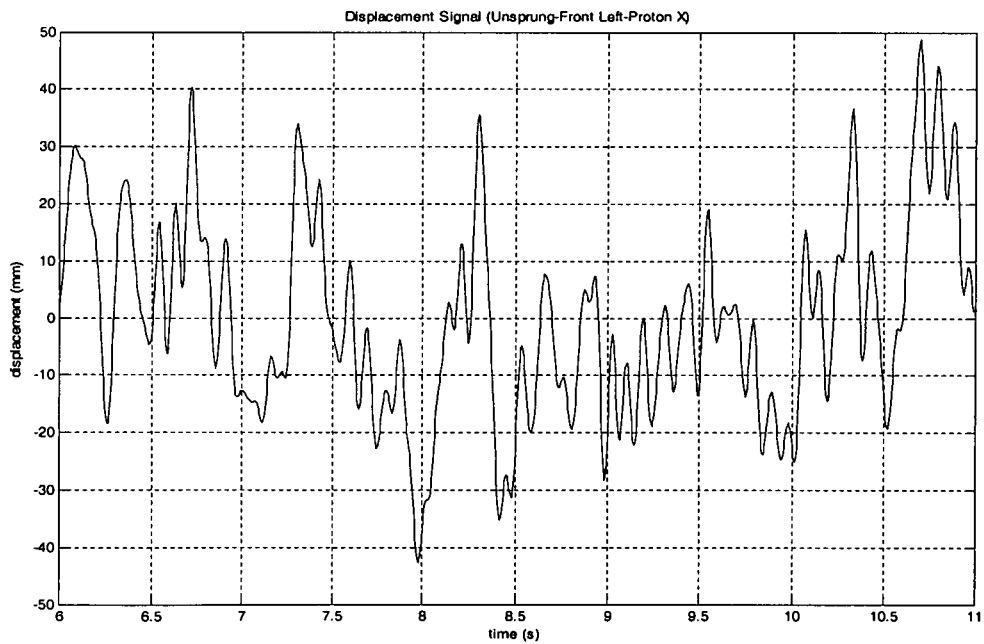


Figure 4.22 Displacement signal (unsprung-front left-Proton X).

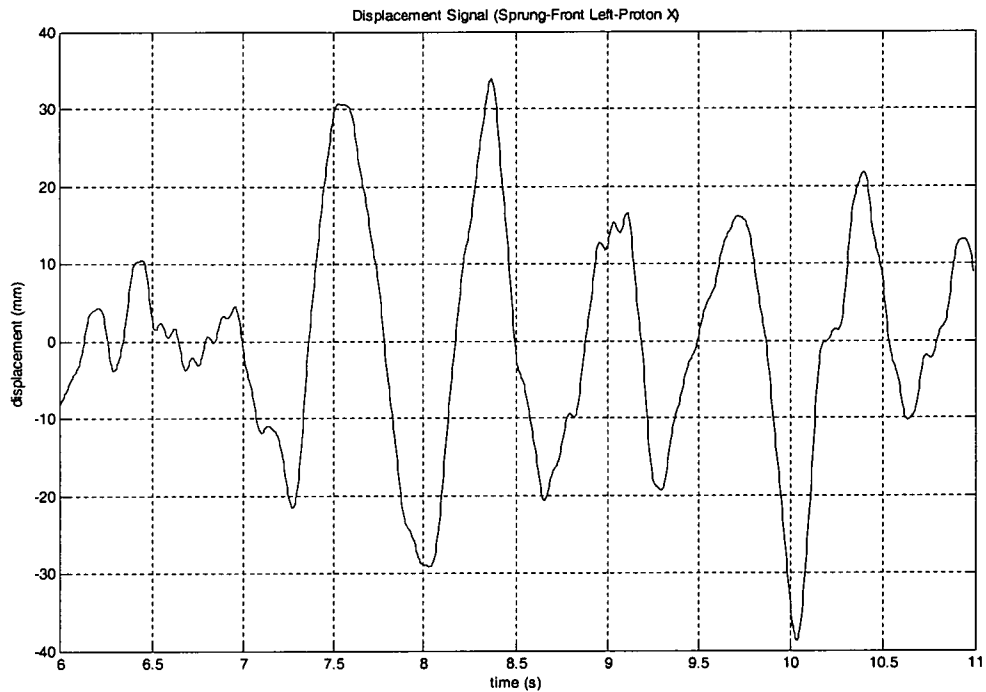


Figure 4.23 Displacement signal (sprung-front left-Proton X).

It is interesting to notice the match between Figure 4.15 and Figure 4.22. The trends of the two curves are similar, only the amplitudes on certain peaks are different. It can be concluded that the tire only gives a slight influence to the drive signal.

4.2.1.3 Signal Differentiation

To determine whether the integration process is valid or not, double differentiation was applied to unsprung and sprung displacement signal. Figure 4.24 and 4.25 shows the comparison between original acceleration signal and double-differentiated displacement signal.

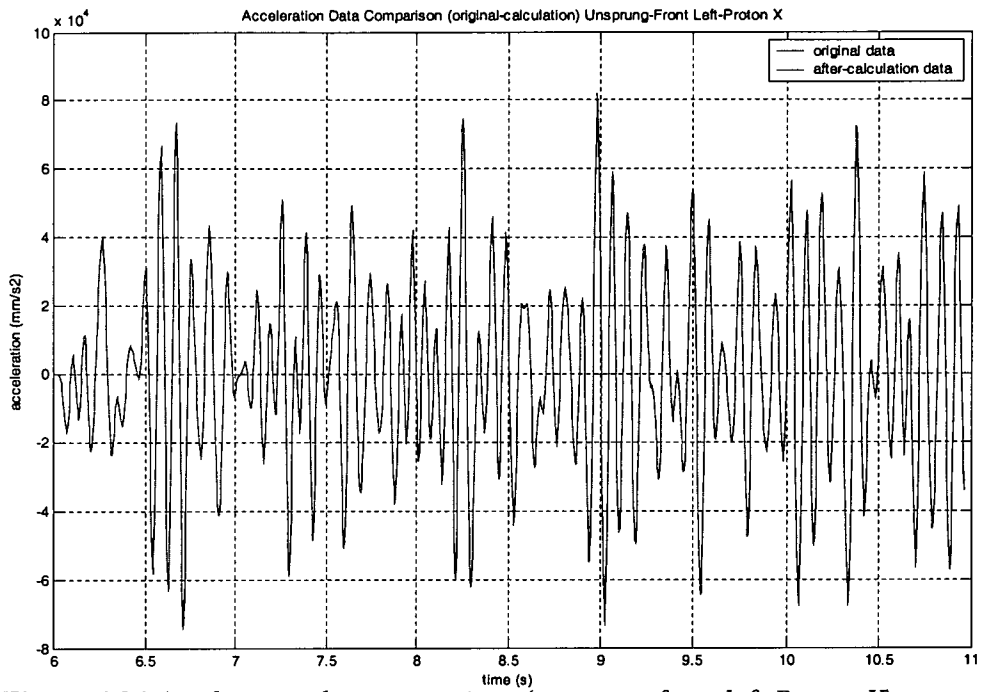


Figure 4.24 Acceleration data comparison (unsprung-front left-Proton X).

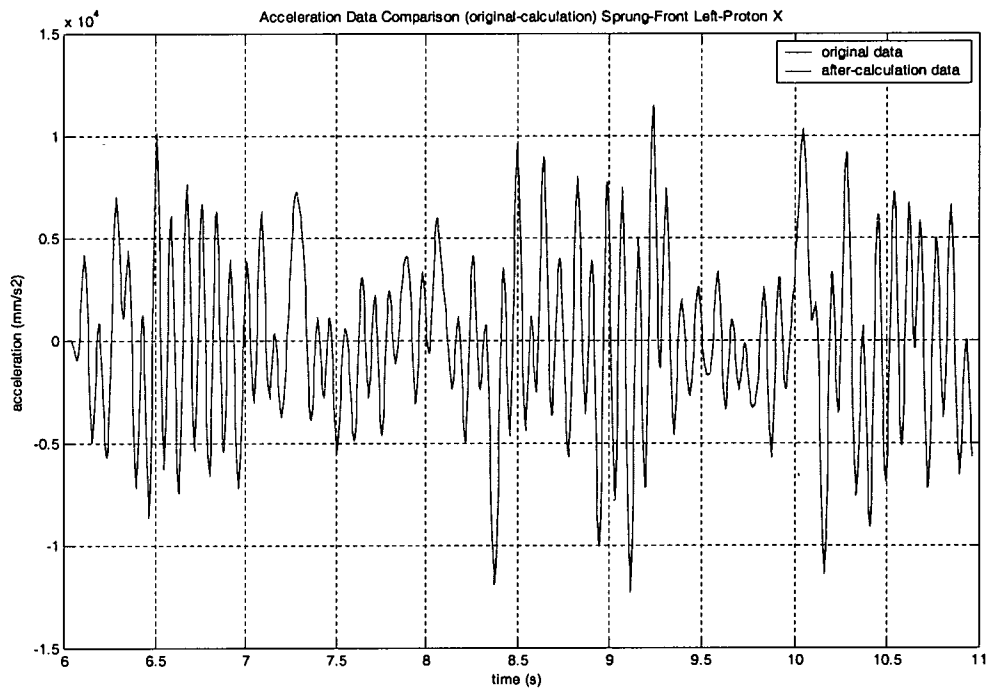


Figure 4.25 Acceleration data comparison (sprung-front left-Proton X).

4.2.2 Proton Test-Track Data

Proton test-track, which has deterministic trapezoid profile, was chosen as second excitation input to the car. It was selected as comparison to China road profile which has random characteristic profile. Two models of cars, that is Proton X and Y, were driven over the same track, and the simulated drive signal as modeling result, would be compared between the two. The testing operating conditions for test-track testing are:

- Acceleration measures: G
- Data analysis parameters:
 - Data duration: 4 sec (vehicle speed = 30 m/s , distance travel = 33.3 m)
 - Sampling interval: 0.00390625 sec

Figure 4.26 and 4.27 shows the measured unsprung and sprung acceleration signal for Proton X at front-left wheel position.

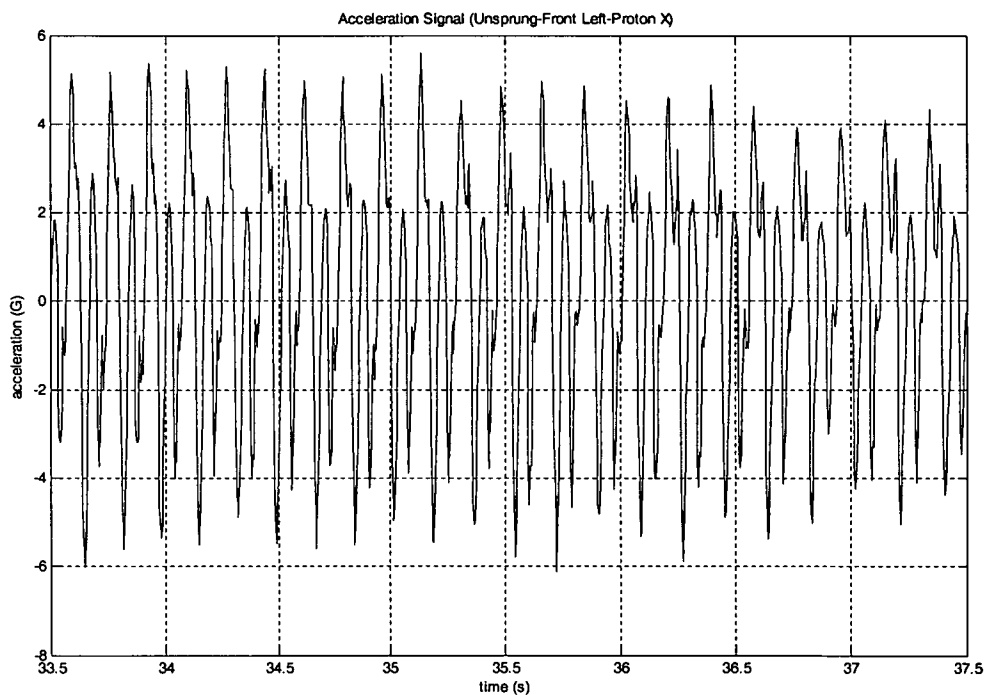


Figure 4.26 Acceleration signal (unsprung-front left-Proton X).

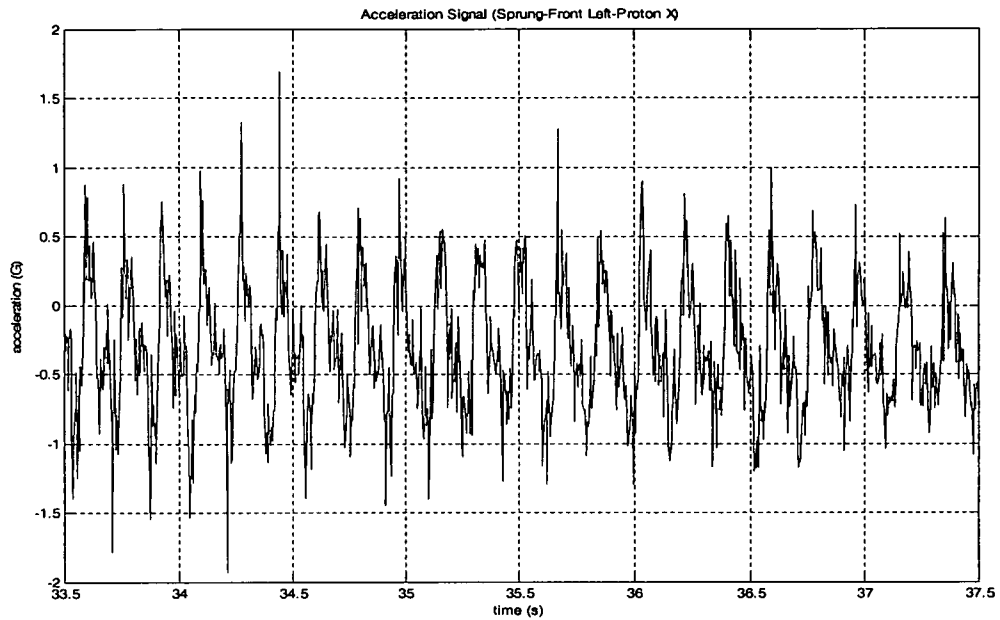


Figure 4.27 Acceleration signal (sprung-front left-Proton X).

To see the pureness of the measured acceleration signals, whether it is contaminated with noise or not, Fast Fourier Transform (FFT) was applied to the signals. The FFT results for unsprung and sprung acceleration signal are shown in Figure 4.28 and 4.29, respectively.

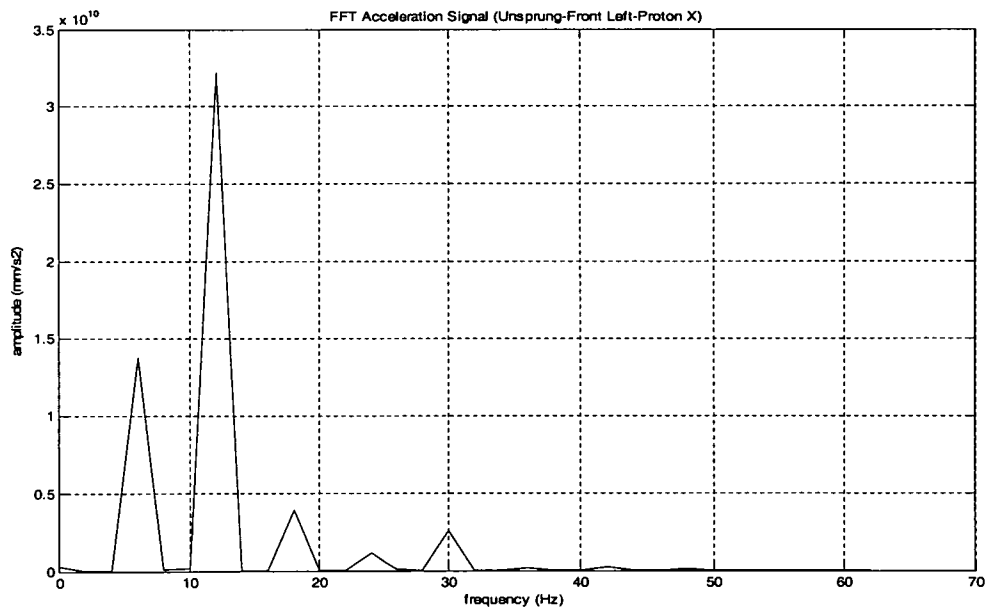


Figure 4.28 FFT acceleration signal (unsprung-front left-Proton X).

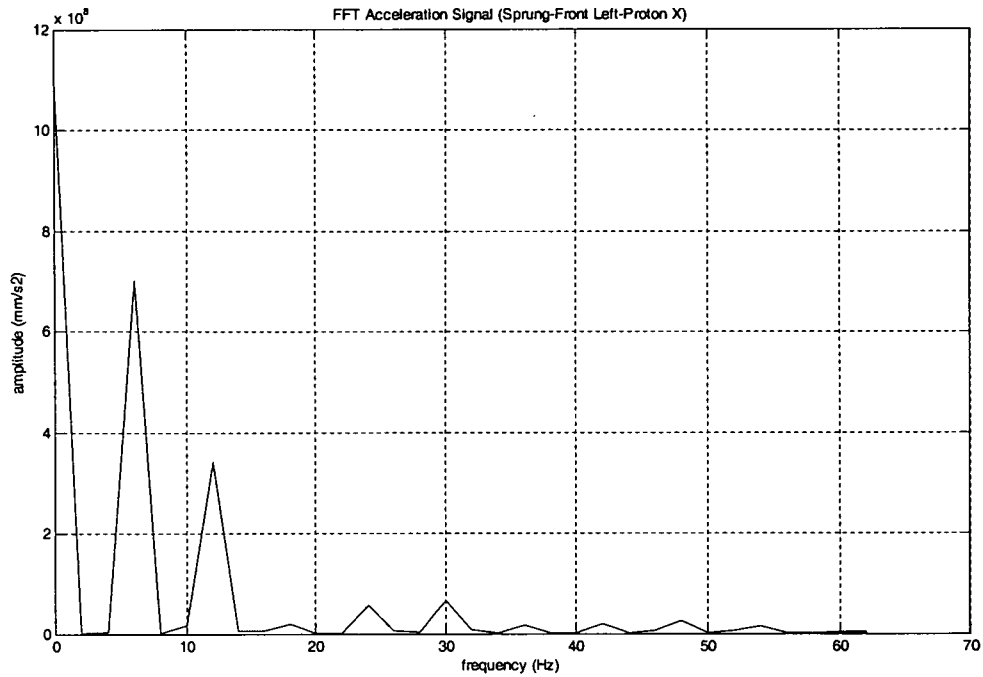


Figure 4.29 FFT acceleration signal (sprung-front left-Proton X).

It is illustrated in Figure 4.28 and 4.29 that the high frequency noise (above 15 Hz) appeared in the signal. The frequency above 15 Hz is unwanted noise frequency since the natural frequency for unsprung and sprung mass are below that frequency. Therefore, a low-pass filter must be constructed to eliminate the noise.

4.2.2.1 Signal Filtering

Using the same treatment as China road data, a low-pass filter was constructed with a pass frequency of 15 Hz. The filter was applied to each of the time histories (unsprung and sprung acceleration signal). The filtered raw data signals are shown in Figure 4.30 and 4.31. While, the FFT of the filtered signals are depicted in Figure 4.32 and 4.33 for filtered unsprung acceleration signal and sprung acceleration signal, respectively.

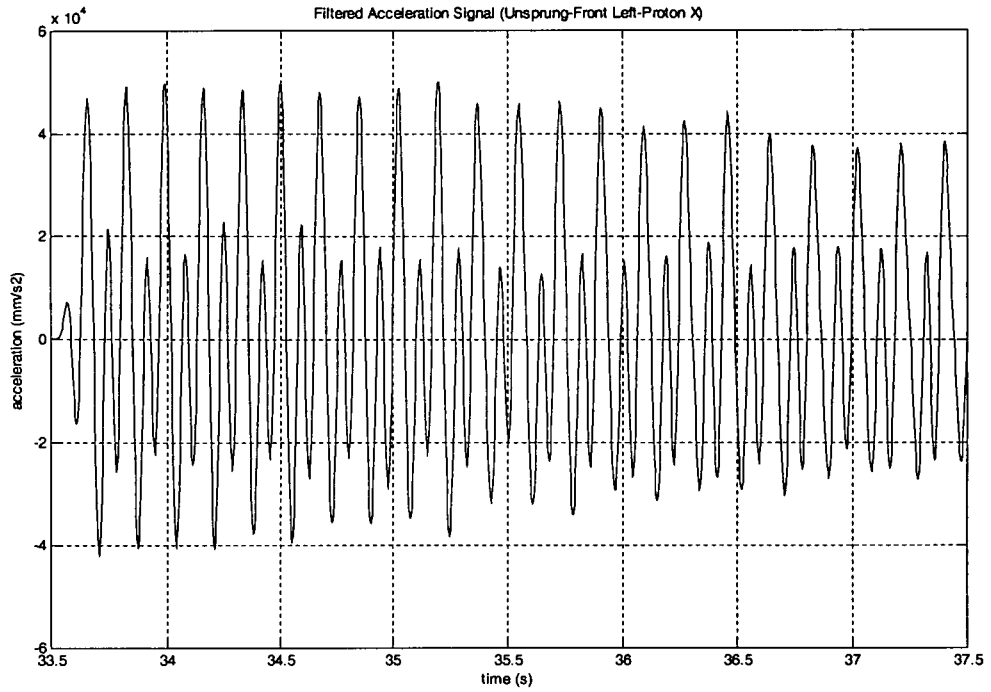


Figure 4.30 Filtered acceleration signal (unsprung-front left-Proton X).

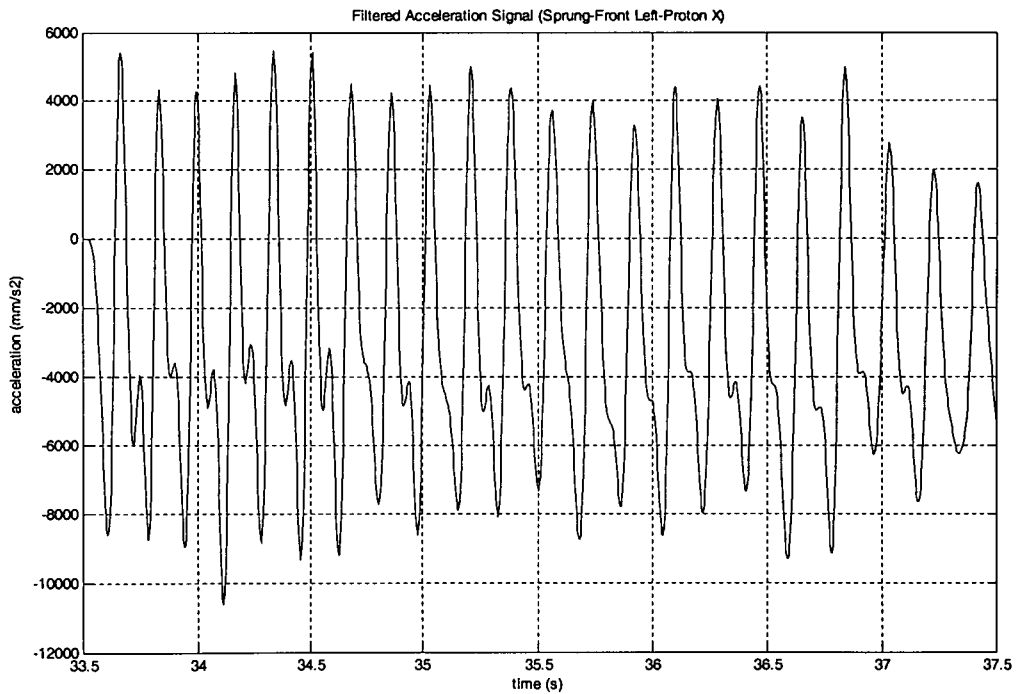


Figure 4.31 Filtered acceleration signal (sprung-front left-Proton X).

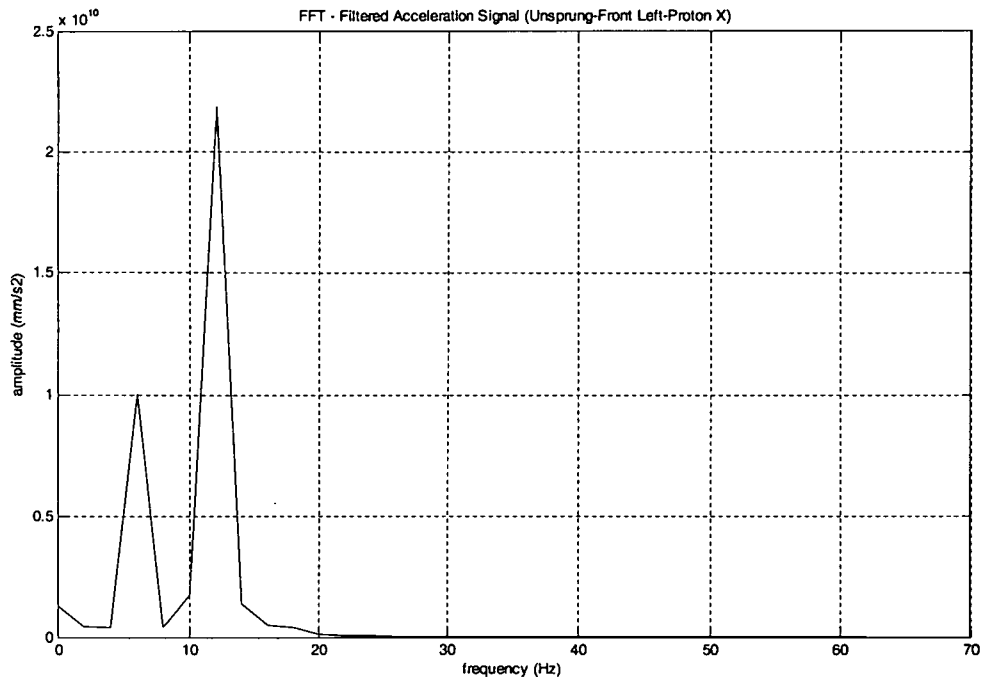


Figure 4.32 FFT - Filtered acceleration signal (unsprung-front left-Proton X).

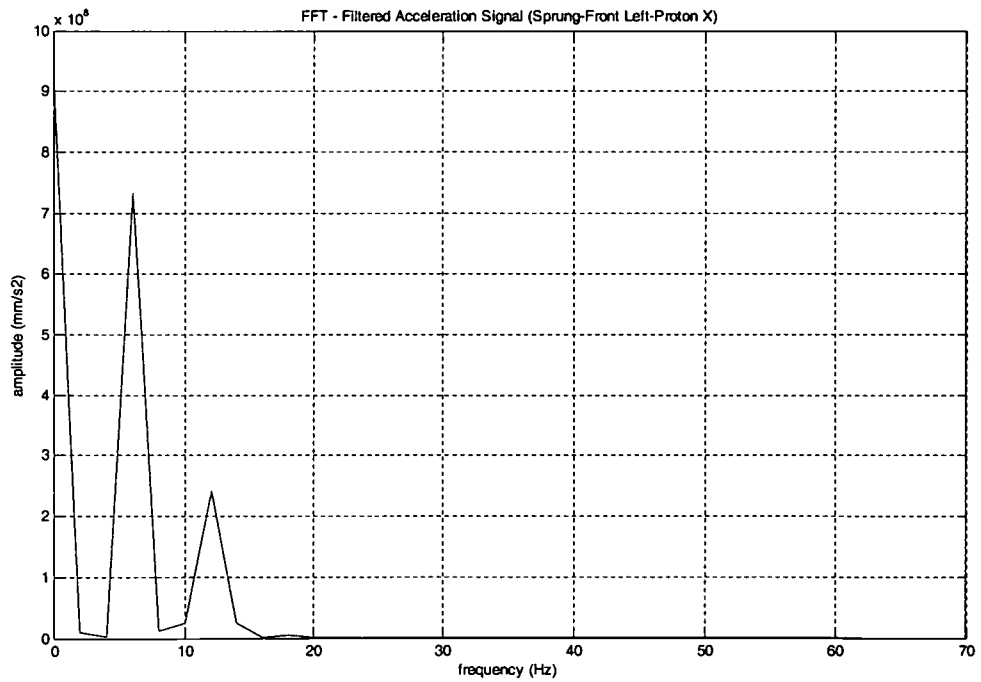


Figure 4.33 FFT - Filtered acceleration signal (sprung-front left-Proton X).

Comparing between the unfiltered signal as shown in Figure 4.26, 4.27 and the filtered signal as illustrated in Figure 4.30, 4.31 shows that the filtered signal is obviously smoother than unfiltered signal since the high frequency noise have been rejected. The filtered signal overall amplitude is also lower than the unfiltered one. It is clearly explained by comparing the FFT between unfiltered and filtered signal which is shown in Figure 4.28, 4.29 for unfiltered signal and 4.32, 4.33 for filtered signal.

4.2.2.2 Signal Integration

By using the same steps, the unsprung and sprung acceleration signals were then numerically integrated to obtain velocity signal using cumulative trapezoid rule. The result of the integration must be multiplied by the sampling time to properly scale the velocity data. Detrend was then applied to remove DC offset in the velocity data. The unsprung and sprung mass velocity signals are shown in Figure 4.34 and 4.35.

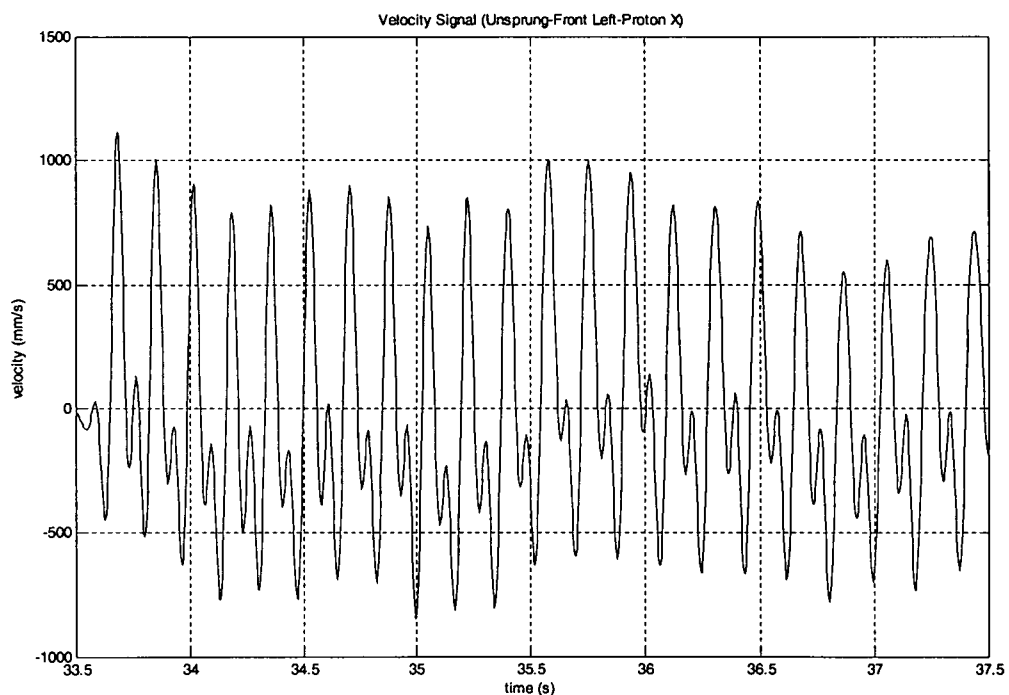


Figure 4.34 Velocity signal (unsprung-front left-Proton X).

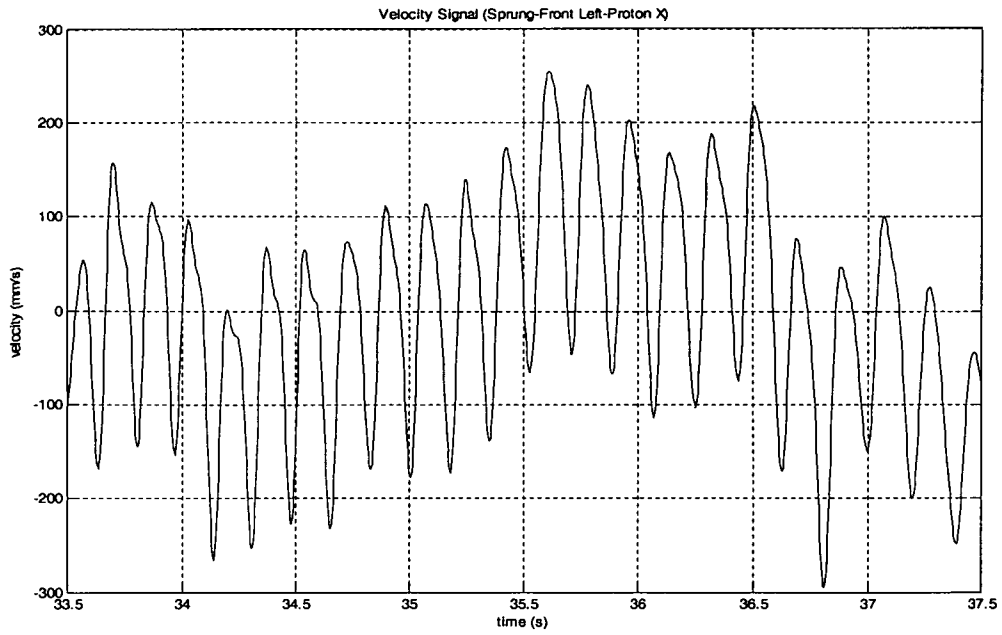


Figure 4.35 Velocity signal (sprung-front left-Proton X).

Using the same method, the velocity signal can then be numerically integrated to obtain displacement signal. Results of the integration process to unsprung and sprung velocity signal are shown in Figure 4.36 and 4.37.

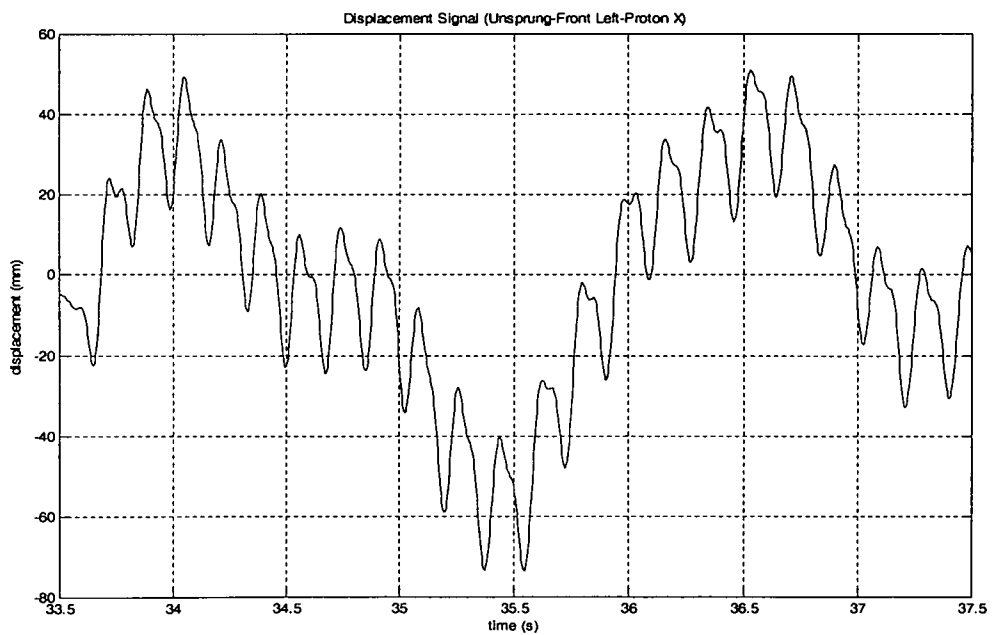


Figure 4.36 Displacement signal (unsprung-front left-Proton X).

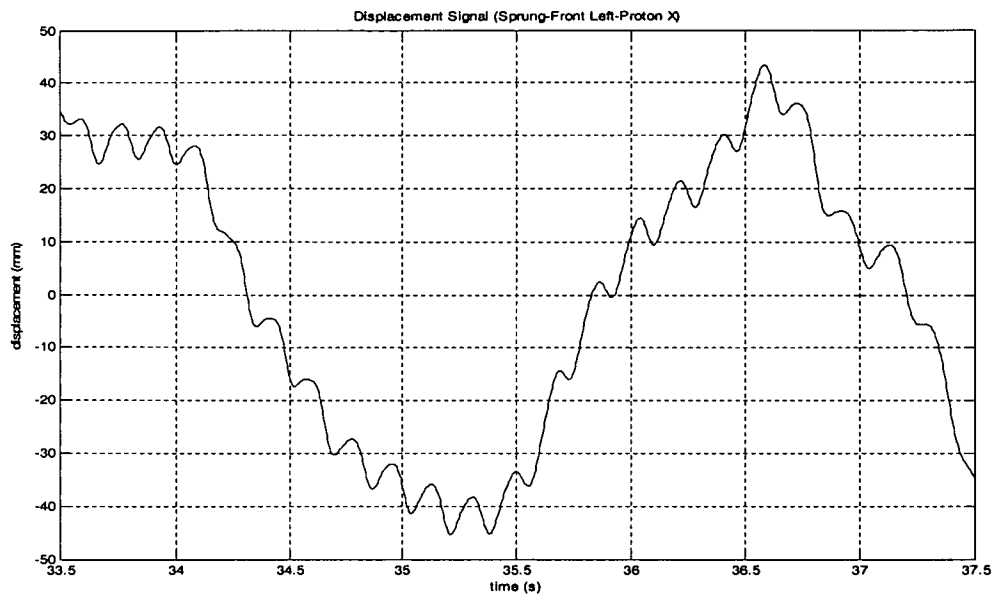


Figure 4.37 Displacement signal (sprung-front left-Proton X).

4.2.2.3 Signal Differentiation

The unsprung and sprung displacement signal were then double differentiated to determine whether the integration process is valid or not. Figure 4.38 and 4.39 shows the comparison between original acceleration signal and double-differentiated displacement signal.

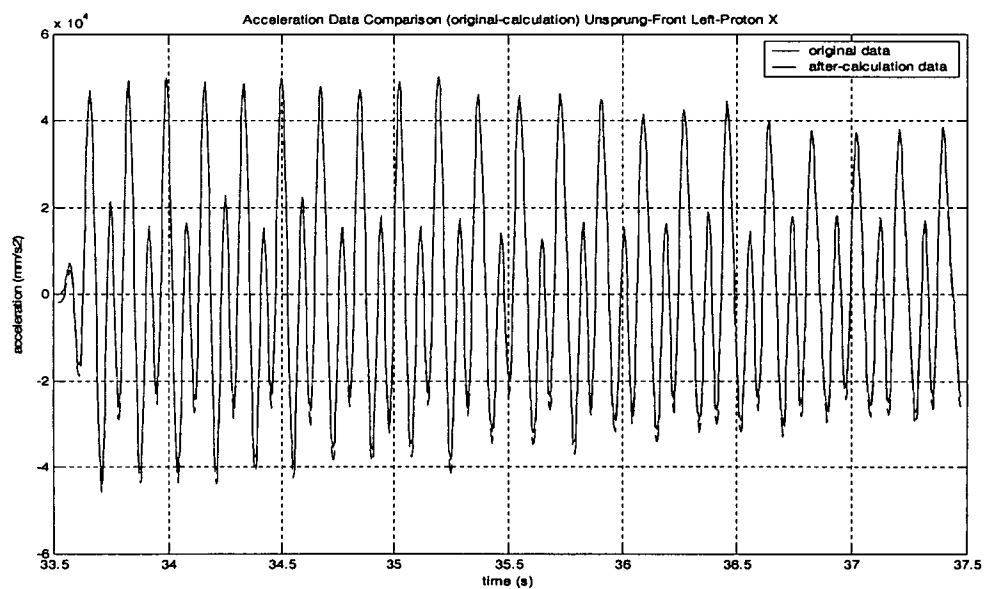


Figure 4.38 Acceleration data comparison (unsprung-front left-Proton X).

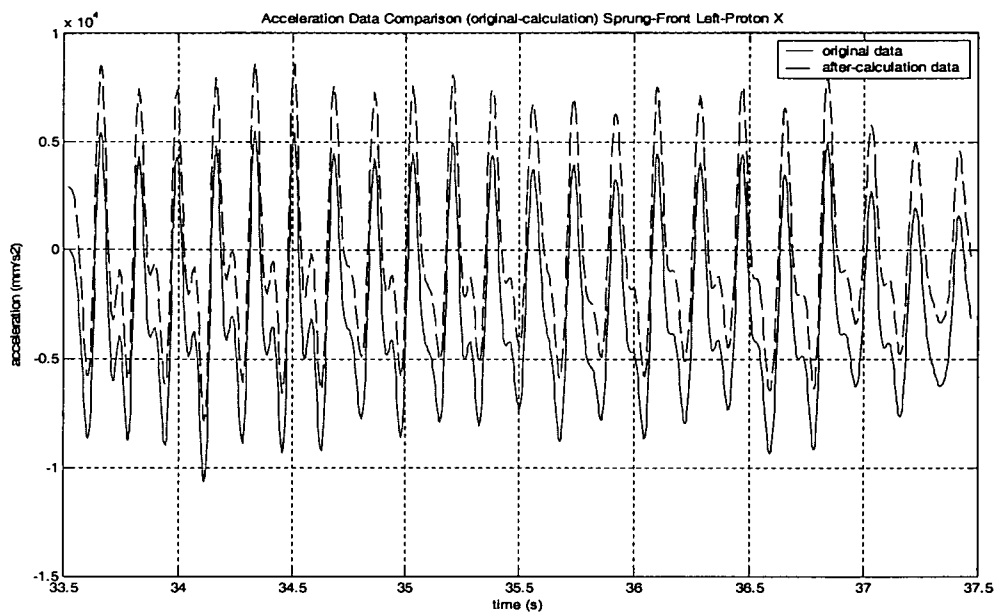


Figure 4.39 Acceleration data comparison (sprung-front left-Proton X).

Figure 4.38 shows that the two signals coincide. It means that the velocity and displacement signal which are integrated from acceleration signal are acceptable. Figure 4.39, on the other hand, shows that the sprung mass measured acceleration signal is not the same with the sprung mass differentiated acceleration signal, which means that the integration results is not acceptable. This unsatisfied integration results is also previously indicated by the sine trend on velocity and displacement signal. To overcome this unevenness, filtering should be applied again to the simulated drive signal to eliminate unwanted component in the signal. The filtering process will be explained on the next chapter.

CHAPTER 5

RESULTS

This chapter presents the modeling results of vehicle suspension system. Two modeling approaches have been reviewed in chapter 3. While, the model parameters have been derived in chapter 4. In the first section of this chapter, the results of mathematical modeling for both China road and Proton test-track will be presented. It is then followed by nonlinear modeling results using artificial neural network.

5.1 Mathematical Modeling Results

Mathematical (linear) modeling of vehicle suspension can be performed by deriving equation of motion of the suspension system model as shown in Equation 3.1 which is rewritten below

$$\ddot{x}_t + \frac{c_s}{m_t} \dot{x}_t - \frac{c_s}{m_t} \dot{x}_b + \frac{(k_p + k_s + k_t)}{m_t} x_t - \frac{(k_p + k_s)}{m_t} x_b = \frac{k_t}{m_t} x_r \quad (3.1)$$

The drive signal, i.e. x_r , can be determined by rearrangement Equation 3.1 above,

$$x_r = \frac{m_t}{k_t} \ddot{x}_t + \frac{c_s}{k_t} \dot{x}_t - \frac{c_s}{k_t} \dot{x}_b + \frac{(k_p + k_s + k_t)}{k_t} x_t - \frac{(k_p + k_s)}{k_t} x_b \quad (5.1)$$

It is shown in Equation 5.1 that to determine drive signal x_r , it needs car parameters data, measured acceleration signal, integrated velocity and displacement signals. The car parameters, i.e. tire spring rate (k_t), suspension spring rate (k_s), parasitic spring rate (k_p), damping coefficient (c_s), unsprung mass (m_t), and sprung mass (m_b) are provided in Table 4.2 and 4.3 for Proton X and Proton Y, respectively. The measured and integrated signals have been reviewed in sub chapter 4.2. By substituting car parameters, measured acceleration signal, integrated velocity and displacement signal into Equation 5.1, the simulated drive signal can be obtained.

- **Road Data from China**

The public road data represents random profile input to the vehicle suspension model. The drive signal can be simulated for each wheel of the vehicle. As mentioned earlier, the simulated drive signal can be determined using Equation 5.1. It needs car parameters data and measured and integrated signals. At front left wheel position for Proton X, the car parameters data can be seen in Table 4.2 which gives value:

- $k_t = 208.5 \text{ N/mm}$
- $k_s = 23 \text{ N/mm}$
- $k_p = 6 \text{ N/mm}$
- $c_s = 3959 \text{ Ns/m}$
- $m_t = 35.19 \text{ kg}$

By substituting car parameters data, measured unsprung acceleration signal \ddot{x}_t (shown in Figure 4.13), integrated unsprung velocity signal \dot{x}_t (shown in Figure 4.20), integrated sprung velocity signal \dot{x}_b (shown in Figure 4.21), integrated unsprung displacement signal x_t (shown in Figure 4.22), and integrated sprung displacement signal x_b (shown in Figure 4.23), simulated drive signal x_r can be determined. This process was carried out using matlab programming (see appendix N). Figure 5.1 shows drive signal comparison between simulated drive signal x_r (obtained from mathematical modeling) and iterated drive signal (shown in Figure 4.15, obtained from RPC process – road simulator) at front left wheel position for Proton X. Using the same way, drive signal comparison between simulated and iterated drive signal can be made at front right, rear left, and rear right wheel position for proton X, as shown in Figure 5.2, 5.3, and 5.4.

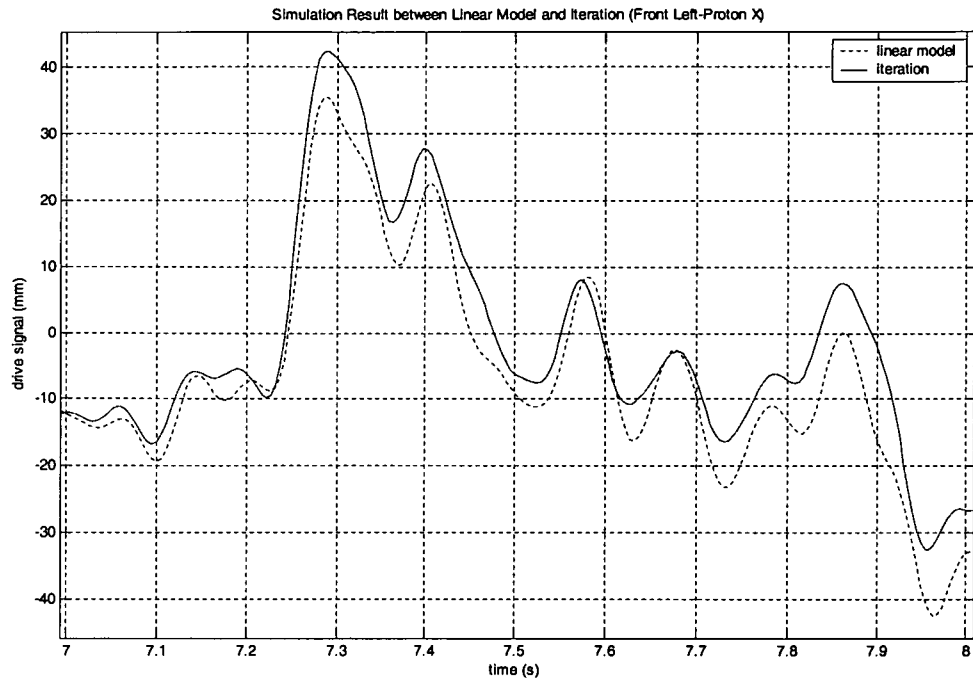


Figure 5.1 Comparison: simulated and iterated drive signal (front left-Proton X).

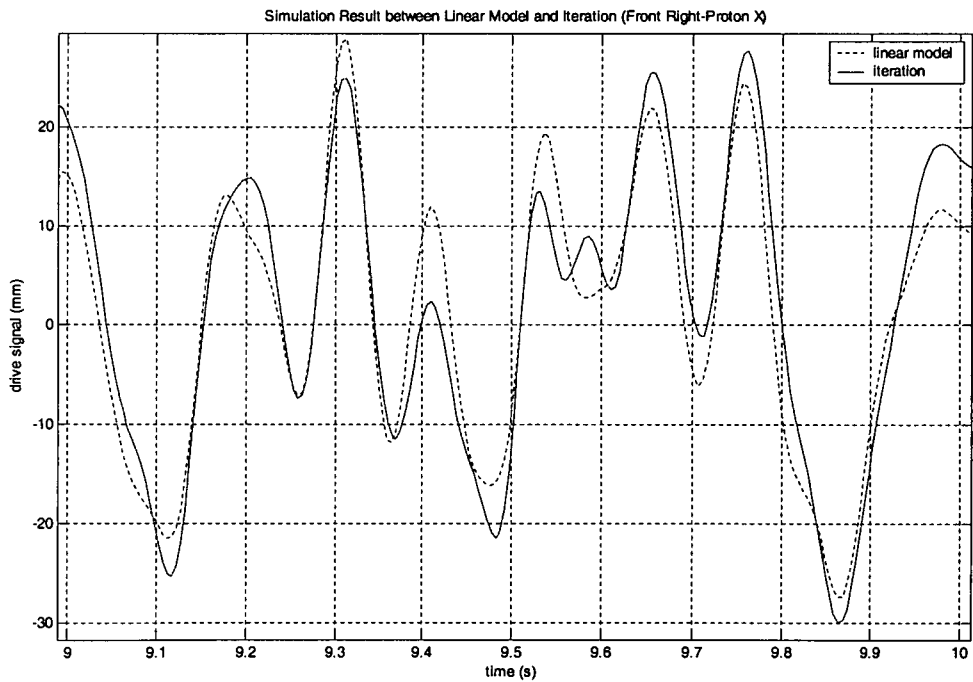


Figure 5.2 Comparison: simulated and iterated drive signal (front right-Proton X).

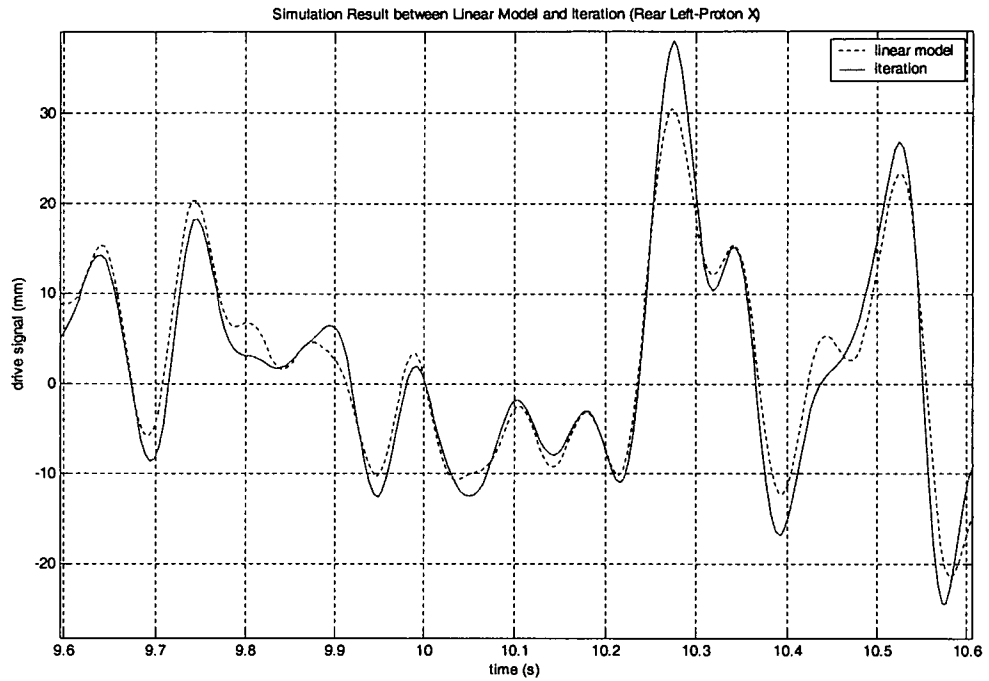


Figure 5.3 Comparison: simulated and iterated drive signal (rear left-Proton X).

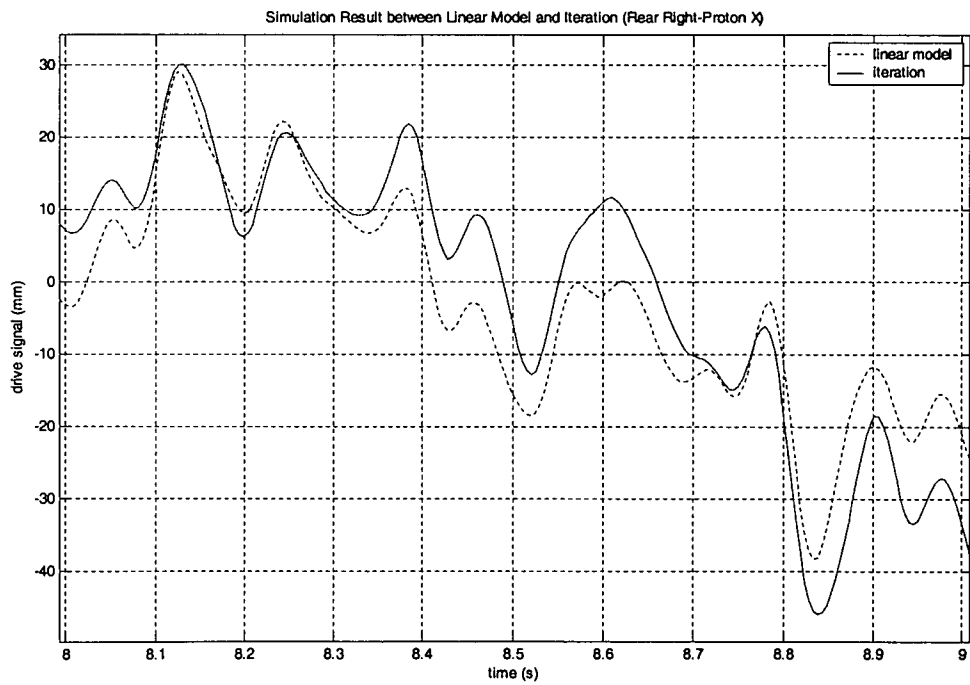


Figure 5.4 Comparison: simulated and iterated drive signal (rear right-Proton X).

- ***Proton Test-Track Data***

Proton test-track data represents deterministic profile input to the vehicle suspension model. As it was noted before, the simulated drive signal can be obtained by substituting car parameters data, measured acceleration signal, and integrated velocity and displacement signal into vehicle suspension model. Due to the poor quality of integrated signal which is indicated by the sine trend on velocity and displacement signal, therefore the simulated drive signal will have the same trend. Figure 5.5 shows the sine trend of simulated drive signal at front left wheel position for Proton X. While, Figure 5.6 illustrates the FFT of this drive signal.

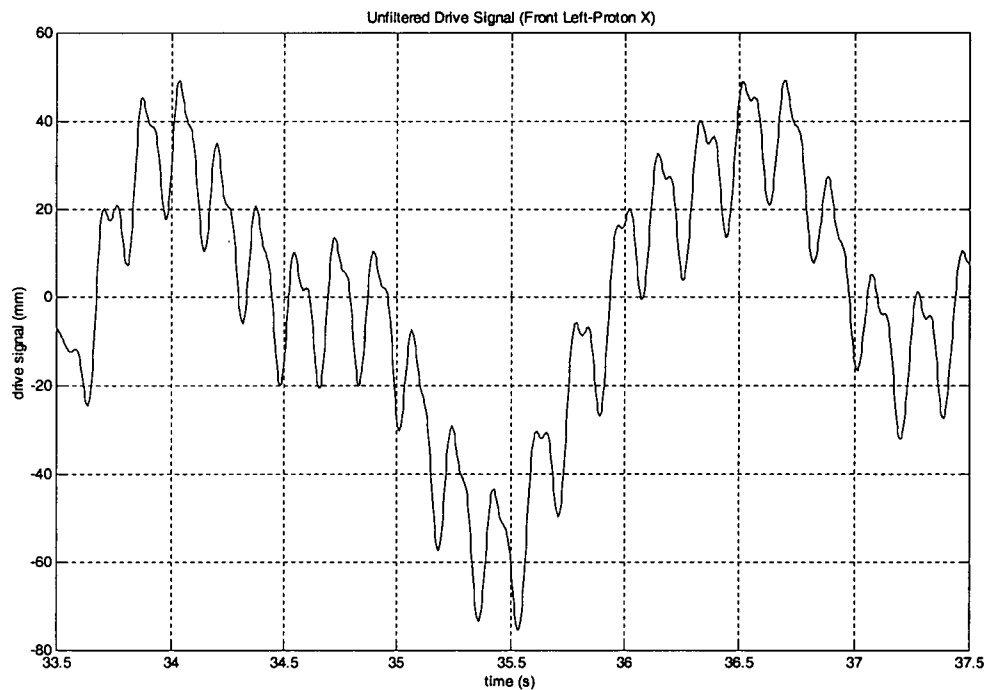


Figure 5.5 Unfiltered simulated drive signal (front left-Proton X).

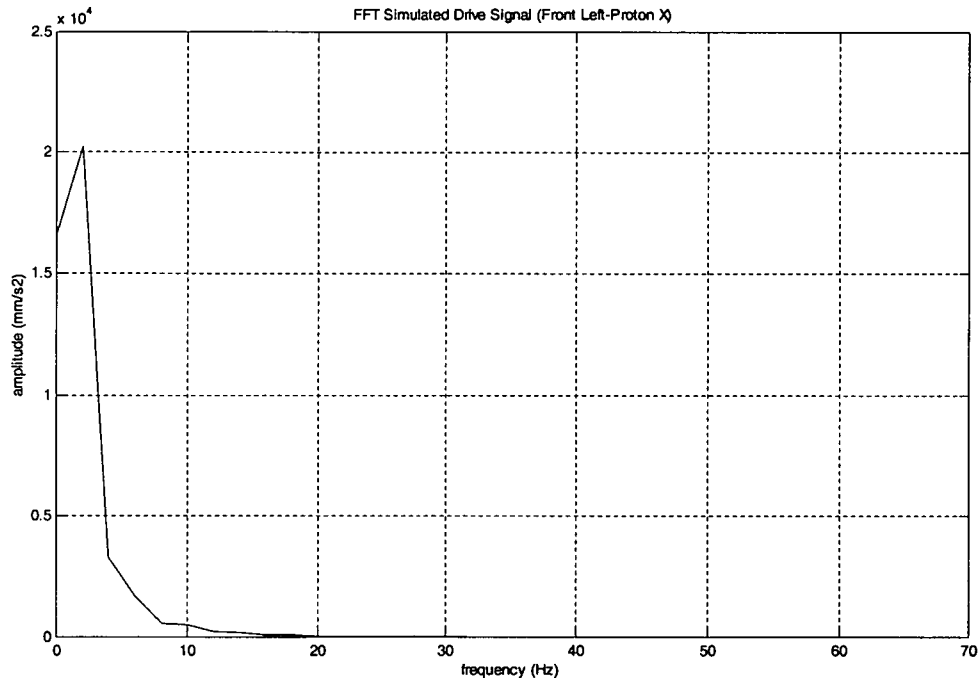


Figure 5.6 FFT- unfiltered simulated drive signal (front left-Proton X).

A high-pass filter was then constructed with a cut-off frequency of 5 Hz to reject the low frequency noise below 5 Hz, while the desired portion of the signal, i.e. above 5 Hz was passed unaltered by the filter. This low frequency noise is indicated by the sine trend on the simulated drive signal and the FFT of the signal, as shown in Figure 5.5 and 5.6. The result of the filtering, i.e. the filtered simulated drive signal at front left wheel position for Proton X, is shown in Figure 5.7, while the FFT of this signal is illustrated in Figure 5.8.

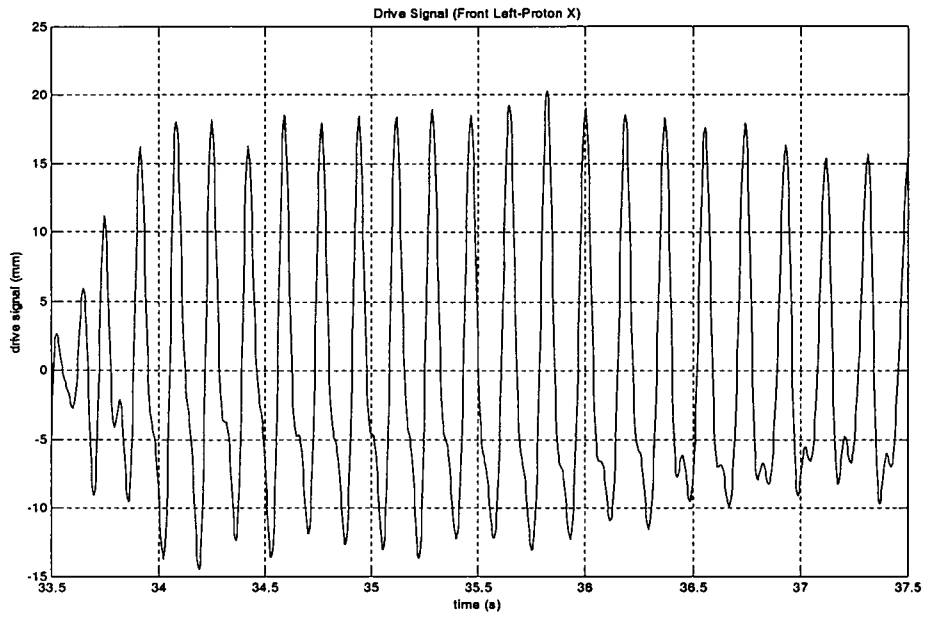


Figure 5.7 Filtered simulated drive signal (front left-Proton X).

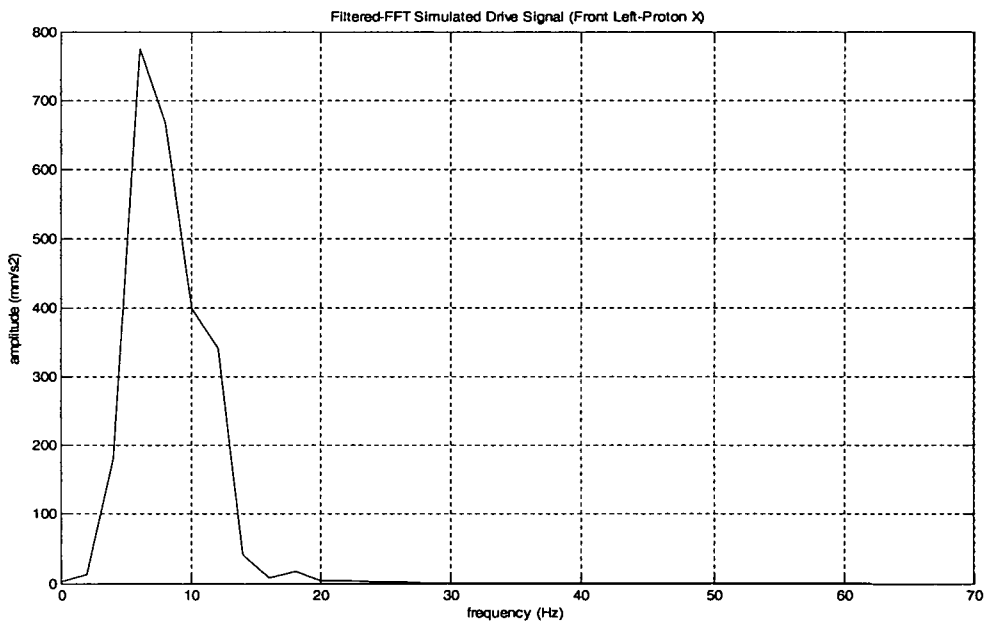


Figure 5.8 FFT - filtered simulated drive signal (front left-Proton X).

By using the same procedure, simulated drive signal was obtained for Proton Y. Since Proton Y was also driven over the same test-track and the same vehicle speed with

Proton X, the simulated drive signal comparison can be made between the two. Theoretically, since the test track is the same, the two simulated drive signals should coincide with each other. Figure 5.9 and 5.10 shows the simulated drive signal comparison between Proton X and Proton Y at front left and rear left wheel position, respectively.

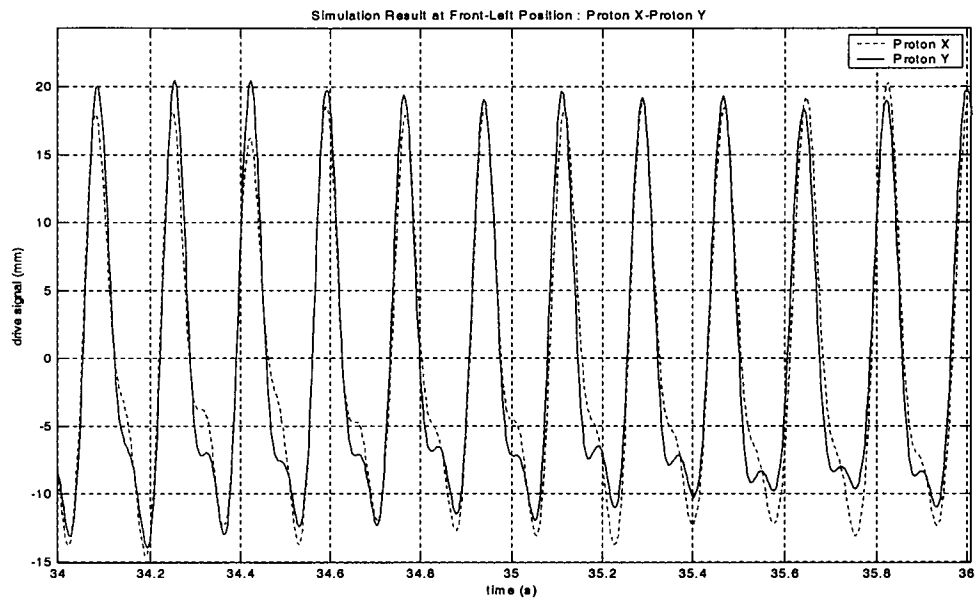


Figure 5.9 Simulated drive signal comparison at front left (Proton X - Proton Y).

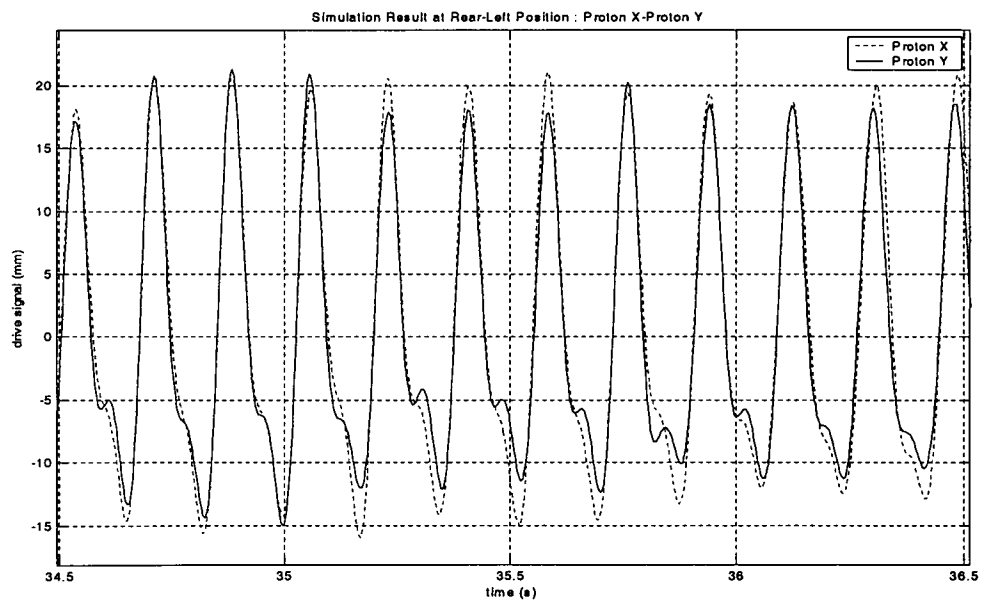


Figure 5.10 Simulated drive signal comparison at rear left (Proton X - Proton Y).

5.2 Artificial Neural Network Modeling Results

Model Identification and Validation using Proton Test-Track Data

Model identification and validation was performed using Proton test track data. For model identification, as an input to the model is the first half data of body acceleration data, while the output is the first half data of simulated drive signal. Result from this identification process is weight parameter for each connection link.

By using the weights from identification process, validation to the model can be performed afterwards. To validate the model, the second half data of body acceleration data is treated as an input, while the output is the second half data of simulated drive signal. Figure 5.11 shows validation results of the ANN model along with the error.

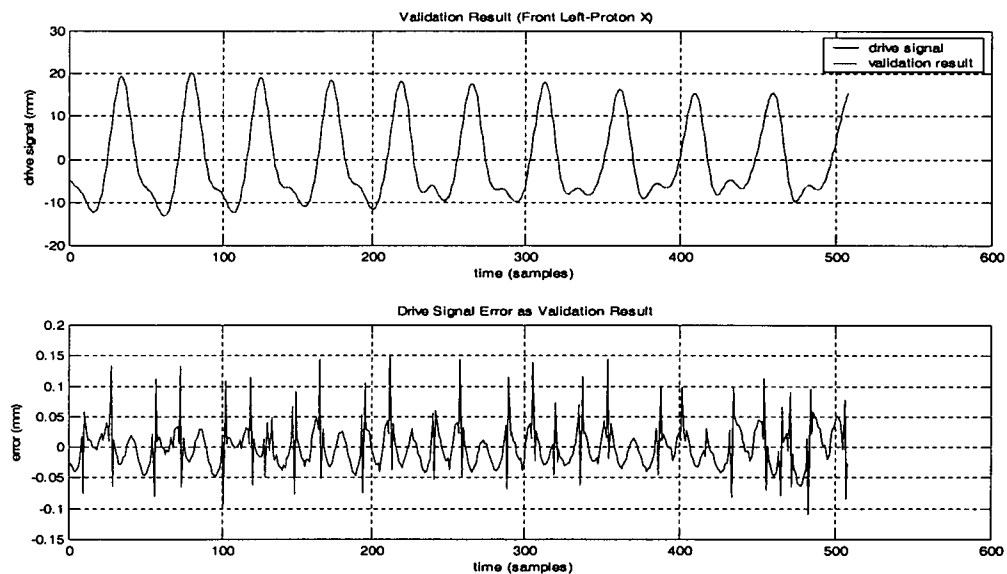


Figure 5.11 Validation result of ANN model.

Model Simulation Using China Road Data

Finally, simulation to the model was performed using China road data which has random profile characteristic. The simulated drive signal was obtained by using the weight parameters from test-track identification process and setting the body acceleration data as an input to the model. Figure 5.12 shows the simulation results of ANN model.

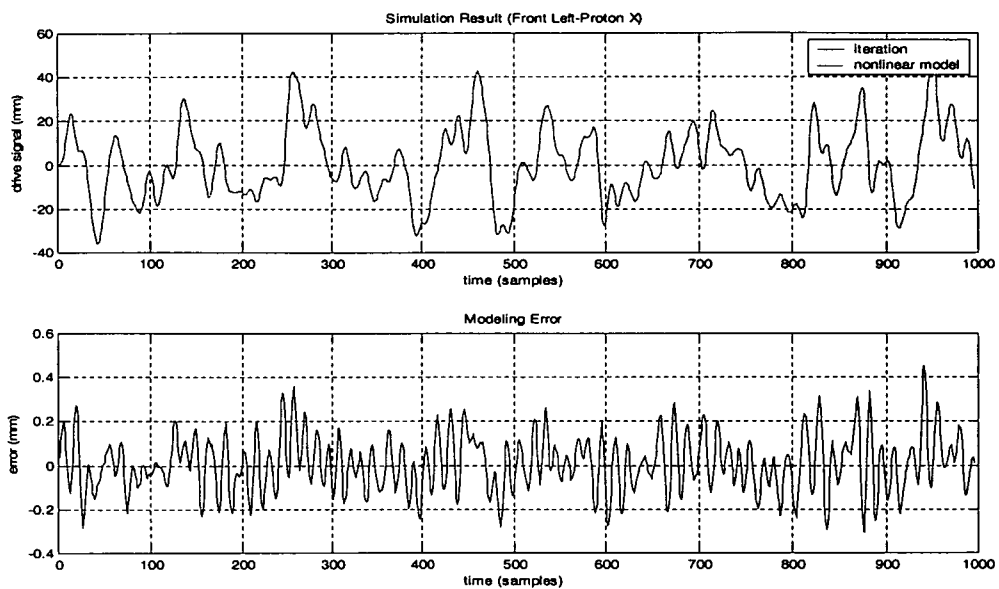


Figure 5.12 Simulation result of ANN model.

CHAPTER 6

DISCUSSION

This chapter briefly discusses the main issue in this research. The results of vehicle suspension system modeling for both linear and nonlinear modeling are the main topics briefed in this chapter.

6.1 Linear Modeling

The linear modeling of vehicle suspension is performed using quarter-car transfer function model. Since this model eliminates vehicle movements, such as yawing, rolling, pitching, and bouncing, the modeling results are not accurate. Better results will be obtained if the model is refined by including all factors which effect the vehicle movement.

The simulated drive signal is obtained by substituting car parameters, measured acceleration signal, integrated velocity and displacement signal into the model. For China road modeling, the simulated drive signal from modeling processes is compared with the iterated drive signal from the road simulator. While, for Proton test-track modeling, since the iterated drive signal was not provided, two simulated drive signal obtained from two models of cars which were driven over the same track are compared.

Modeling results on China road show that the simulated drive signal have similar profile trend with iterated drive signal even the two profiles are not exactly the same. This is due to nonlinearity of the suspension system, such as shock absorber parts, and inexact car parameters variable. The RMS Error for China road drive signal modeling for Proton X at front-left (FL) and rear-left (RL) wheel is tabulated in Table 6.1.

Table 6.1 RMS error for China road drive signal modeling.

	WHEEL POSITION	
	FL	FR
RMS Error	19.58%	9.49%

Different case occurred on Proton test-track modeling. Due to the poor quality of integrated signals indicated by the sine trend on velocity and displacement signal, filtering should be applied to the simulated drive signal to eliminate unwanted component in the data, as explained in Chapter 5. A high-pass filter was constructed to reject the low frequency noise below 5 Hz.

It is shown in Figure 5.6 and 5.8 that the filtered FFT amplitude is smaller than the unfiltered one. It eliminates the sine trend on the simulated drive signal by rejecting the low frequency sine wave which is contained in the signal.

Since two models of cars, i.e. Proton X and Proton Y, were driven over the same test track and the same vehicle speed, the simulated drive signal comparison can be made between the two. Modeling results, as shown in Figure 5.9 and 5.10, show that the two simulated drive signals are almost the same each other. Even the simulated drive signal cannot resemble the true profile, the profile trend is correct, indicated by a similar amount of curve peaks in simulated drive signal and bumps in test-track profile for certain period of time. The RMS Error for Proton test-track drive signal modeling at front-left and rear-left wheel position for Proton X is tabulated in table 6.2.

Table 6.2 RMS error for Proton test-track drive signal modeling

	WHEEL POSITION	
	FL	FR
RMS Error	0.22%	0.65%

It should be noted, that since the iterated drive signal was not made available by Proton, the validation process between simulated and iterated drive signal could not be performed.

6.2 Artificial Neural Network Model

On the second method, that is artificial neural network modeling (ANN), vehicle suspension is treated as a black box model and only considers on the input and output of suspension system. Therefore the car parameters and integration calculation are not required. The nonlinearity of suspension is also accommodated by nonlinear characteristic capability of ANN modeling.

The first step in ANN modeling is determination of model structure or identification. It means that the network architectures, activation functions, and the methods of setting the weights (training) must be first determined. Model identification was performed using Proton test-track data. As an input to the model is the first half data of sprung acceleration data, while the output is the first half data of simulated drive signal.

By substituting input-output data into predetermined network structure model and setting 500 times iteration, network parameters can be determined, as shown in Figure 3.11. Another result from this identification process is weight parameter for each connection link.

By using the identification-result weights, validation to the model can be performed afterwards. To validate the model, the second half data of body acceleration data is treated as an input, while the output is the second half data of simulated drive signal. Figure 5.9 shows that the validated drive signal almost coincides with the iterated drive signal, which is indicated by the small error difference (maximum error 0.2 mm).

Finally, simulation to the model is performed using China road data which has random profile characteristic. The simulated drive signal was obtained by using the weight parameters from test-track identification process and setting the body acceleration data as an input to the model. As shown in Figure 5.10, the simulated drive signal almost coincides with the iterated drive signal, which is indicated by the small error difference (maximum error 0.5 mm). The RMS Error for China road drive signal modeling for Proton X at front-left and rear-left wheel position using ANN modeling is tabulated in table 6.3.

Table 6.3 RMS error for China road drive signal modeling using ANN

	WHEEL POSITION	
	FL	FR
RMS Error	0.39%	4.34%

CHAPTER 7

CONCLUSION

Remote Parameter Control (RPC) is a simulation technique that is used to reproduce the vehicle motions recorded during previous test-drive using a four posters road simulator in a controlled laboratory environment. This technique involves an iterative, off-line procedure. By using a relatively broadband noise input and the inverse of system Frequency Response Function (FRF), this off-line refinement process iterates until sufficient tracking accuracy is obtained. The main weakness of this procedure is that the drive signal output is specific for certain model of car. It means that if another model of car is used, the drive signal will be different even if the cars are driven over the same track. This problem can be solved by constructing a model that represents the dynamic characteristic of vehicle. The objective is to find the vehicle suspension model and by using the model and model parameters, the drive signal can be determined.

There are two modeling approaches conducted in this research: transfer function modeling and neural network modeling. In the first approach, mathematical modeling was introduced to model two types of road profile input. For the first road profile, i.e. China road, modeling results show that the simulated drive signal which is derived from vehicle suspension transfer function has similar trend with iterated drive signal from road simulator even the two profiles are not exactly the same. For the second profile, i.e. Proton test-track, two models of cars, i.e. Proton X and Proton Y, were driven over the same test track and the same vehicle speed, therefore the simulated drive signal comparison can be made between the two. The modeling results show that the two simulated drive signals are nearly the same each other. Even the simulated drive signals cannot exactly resemble the true profile, the profile trend is correct, indicated by a similar amount of curve peaks in the simulated drive signals and bumps in the test-track profile for certain of time. In the second approach, nonlinear modeling using artificial neural network was applied to simulate the vehicle suspension system. Model identification and validation was performed using Proton test-track data, while simulation to the model was

carried out using China road data. Modeling result shows that the simulated drive signal is tally with the iterated drive signal, which is indicated by the small difference (error) between the two. The comparison of drive signals between the systems (iterated drive signal from road simulator) and modeling results (linear and nonlinear) at front left and rear left wheel position for Proton X are illustrated in Figure 7.1 and 7.2.

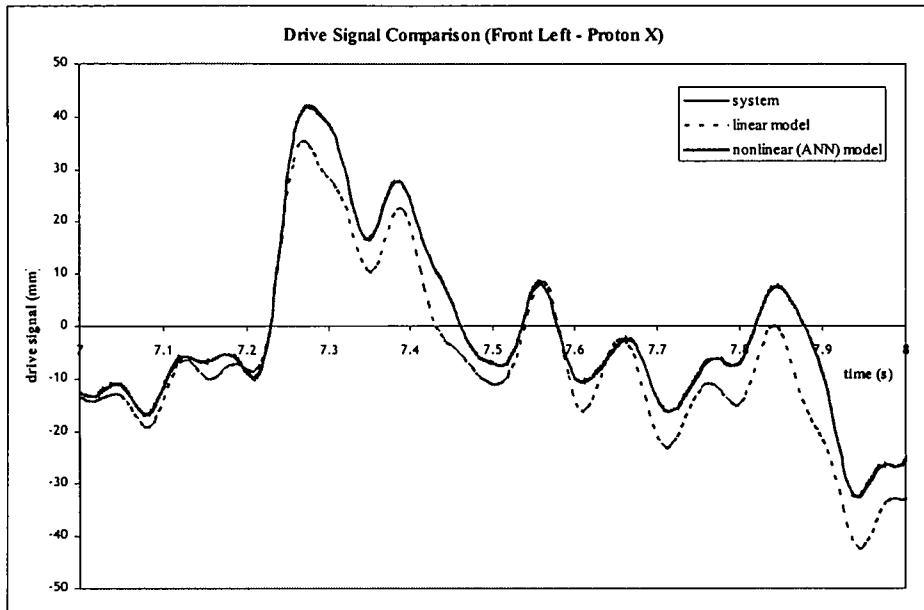


Figure 7.1 Drive signal comparison (front left-Proton X).

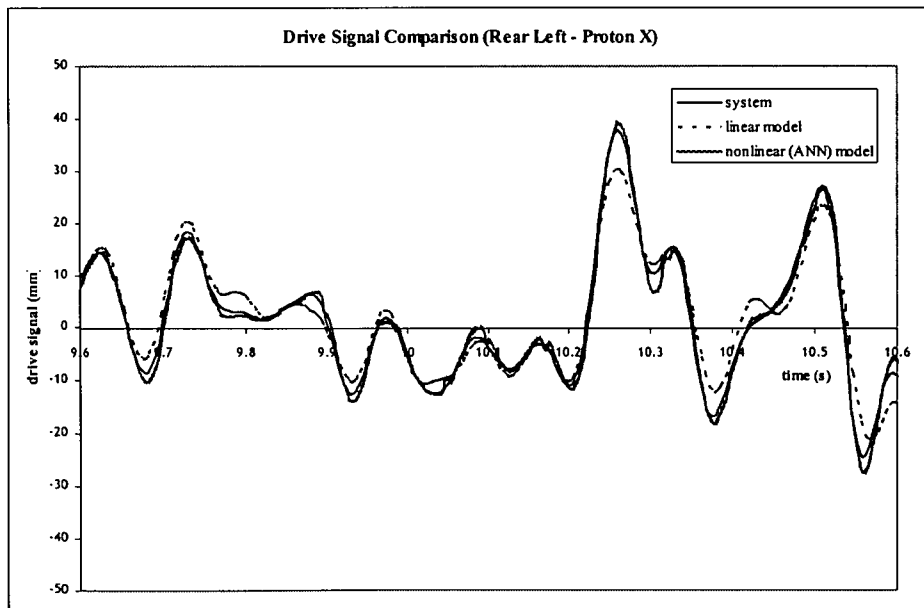


Figure 7.2 Drive signal comparison (rear left-Proton X).

Since the drive signal has been reproduced and simulated, the test drive for service loads measurement which is time-consuming and expensive can be avoided. The drive signal input is applied to the four hydraulic actuators of the road simulator with any model of car that needs to be tested. This will in turn give a lot of cost saving, instead of repeating data measurement on the same road surface or test-track using different model of cars, especially for overseas operations.

REFERENCES

- Arifin, A., Petrick, L., & Berling, P., Using Modal Parameters to Monitor Vehicle Changes during a Durability Test, *SAE, Inc.*, 2000.
- Dixon, J. C., *Tires, Suspension and Handling*, SAE, Inc., 2nd edition, 1996.
- ElBeheiry, E. M. and Karnopp, D. C., Optimal Control of Vehicle Random Vibration with Constrained Suspension Deflection, *Journal of Sound and Vibration* 189 (5), pp. 547-564, 1996.
- Fausett, L., *Fundamentals of Neural Networks*, Prentice Hall, Inc., 1994.
- Gillespie, T. D., *Fundamentals of Vehicle Dynamics*, SAE, Inc., 1992.
- Hines, J. W., *Fuzzy and Neural Approaches in Engineering*, John Wiley & Sons, Inc., 1997.
- Katech, *Development of a Dynamic Road Profile and Roughness Measuring System*, 2000.
- Lacombe, J., Tire Model for Simulations of Vehicle Motion on High and Low Friction Road Surfaces, *Proceedings of the 2000 Winter Simulation Conference*, 2000.
- Mohd Ihsan, A. K. A. and Mohd Noor, M. J., *Matlab: Aplikasi dalam Kejuruteraan*, ACE, 2002.
- Rao, M. D. and Gruenberg, S., Measurement of Equivalent Stiffness and Damping of Shock Absorbers, *Michigan Technological University*, 1997.
- Renner, T.E., Empirical Dynamics Models for Nonlinear Suspension Components, *MTS Systems*, 2000.

Ruihong, Z. and Runhua, T., The Application of Modern Robust Optimal Design Method to Shock Absorber, *Hebei University of Technology*, 1999.

Santosa, I.B., *Penerapan Jaringan Syaraf Tiruan sebagai Pengendali pada Sistem Tak Linier Variabel Jamak*, ITB, 1998.

Sayers, M. W. and Karamihas, S. M., *The Little Book of Profiling*, University of Michigan, 1998.

Storer, D., Gatti, S., & Pisino, E., Characterizing the Transfer of Road-Surface Excited Vibrations through Vehicle Suspension Systems, *European Conference on Vehicle Noise and Vibration*, 1998.

Takahashi et al., The Modeling of Tire Overturning Moment Characteristics and Its Influence on Vehicle Behavior, *Toyota Motor Corporation*, 2000.

Tao, J. J., Modeling Suspension Damper Modules using LS-DYNA, *7th International LS-DYNA Users Conference*, 2000.

Westwick, D. T., George, K., & Verhaegen, M., Nonlinear Identification of Automobile Vibration Dynamics, *Proceedings of the 7th Mediterranean Conference on Control and Automation (MED99) Haifa, Israel*, 1999.

APPENDICES***RANDOM INPUT***

- A1 PROTON X – FRONT LEFT – ACCELERATION SIGNAL
- A2 PROTON X – FRONT LEFT – INTEGRATION SIGNAL
- A3 PROTON X – FRONT LEFT – SIMULATION RESULT
- B1 PROTON X – FRONT RIGHT – ACCELERATION SIGNAL
- B2 PROTON X – FRONT RIGHT – INTEGRATION SIGNAL
- B3 PROTON X – FRONT RIGHT – SIMULATION RESULT
- C1 PROTON X – REAR LEFT – ACCELERATION SIGNAL
- C2 PROTON X – REAR LEFT – INTEGRATION SIGNAL
- C3 PROTON X – REAR LEFT – SIMULATION RESULT
- D1 PROTON X – REAR RIGHT – ACCELERATION SIGNAL
- D2 PROTON X – REAR RIGHT – INTEGRATION SIGNAL
- D3 PROTON X – REAR RIGHT – SIMULATION RESULT

DETERMINISTIC INPUT

- E1 PROTON Y – FRONT LEFT – ACCELERATION SIGNAL
- E2 PROTON Y – FRONT LEFT – INTEGRATION SIGNAL
- E3 PROTON Y – FRONT LEFT – SIMULATION RESULT
- F1 PROTON X – FRONT LEFT – ACCELERATION SIGNAL
- F2 PROTON X – FRONT LEFT – INTEGRATION SIGNAL
- F3 PROTON X – FRONT LEFT – SIMULATION RESULT
- G PROTON X-PROTON Y – FRONT LEFT – SIMULATION RESULT
- H1 PROTON Y – REAR LEFT – ACCELERATION SIGNAL
- H2 PROTON Y – REAR LEFT – INTEGRATION SIGNAL
- H3 PROTON Y – REAR LEFT – SIMULATION RESULT

- I1 PROTON X – REAR LEFT – ACCELERATION SIGNAL
- I2 PROTON X – REAR LEFT – INTEGRATION SIGNAL
- I3 PROTON X – REAR LEFT – SIMULATION RESULT
- J PROTON X-PROTON Y – REAR LEFT – SIMULATION RESULT

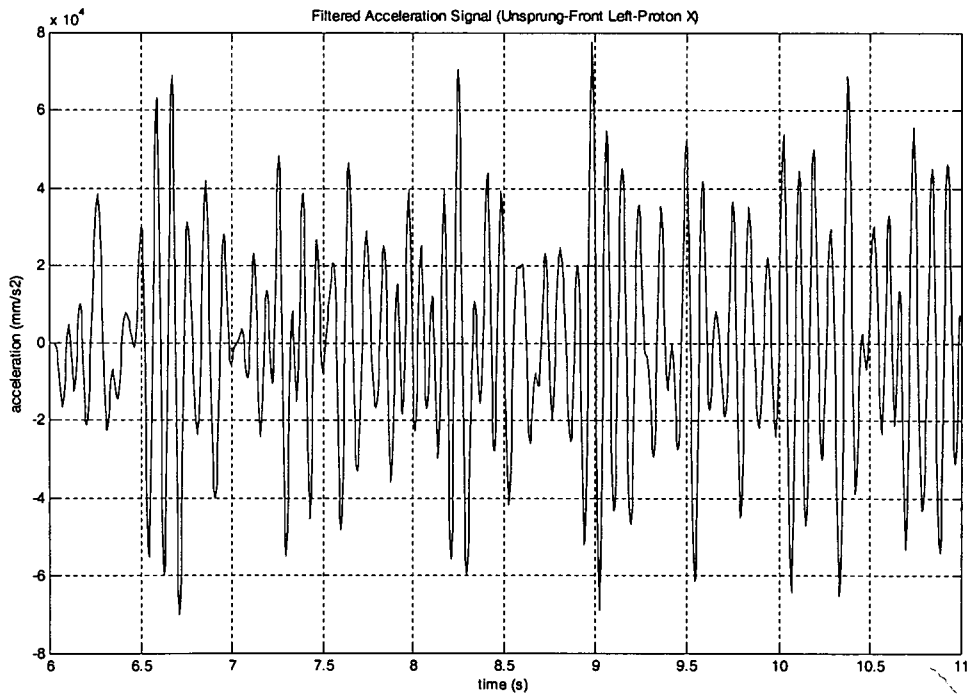
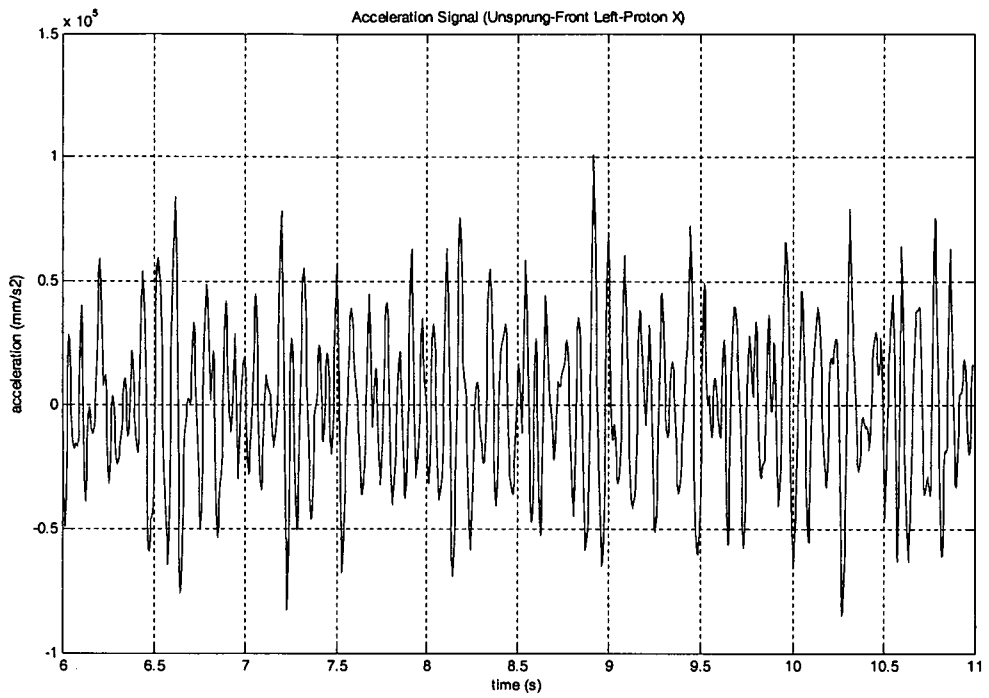
ARTIFICIAL NEURAL NETWORK

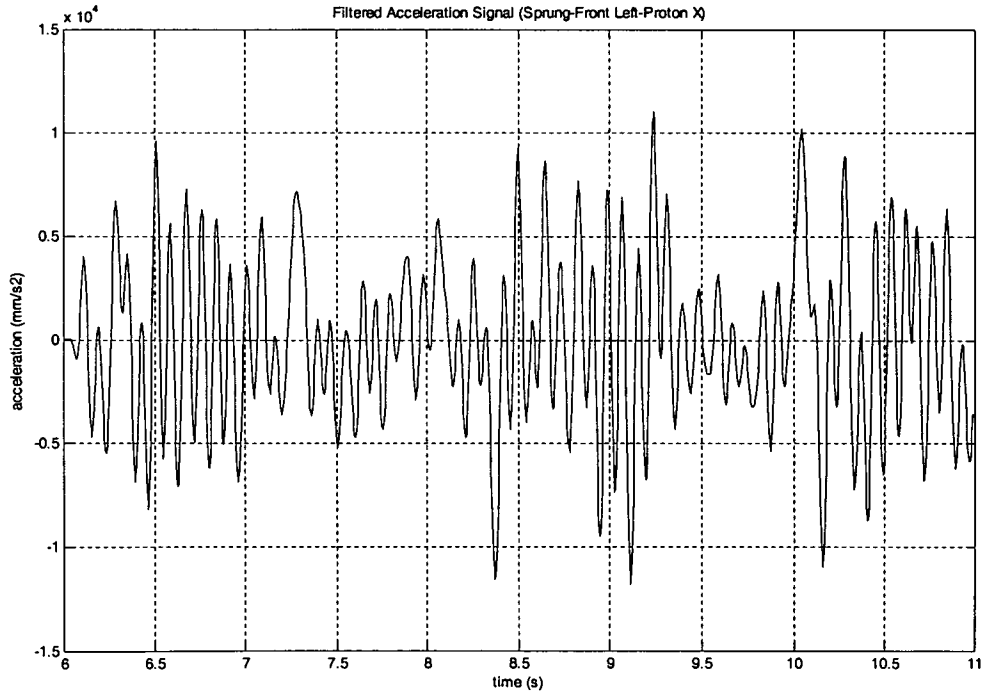
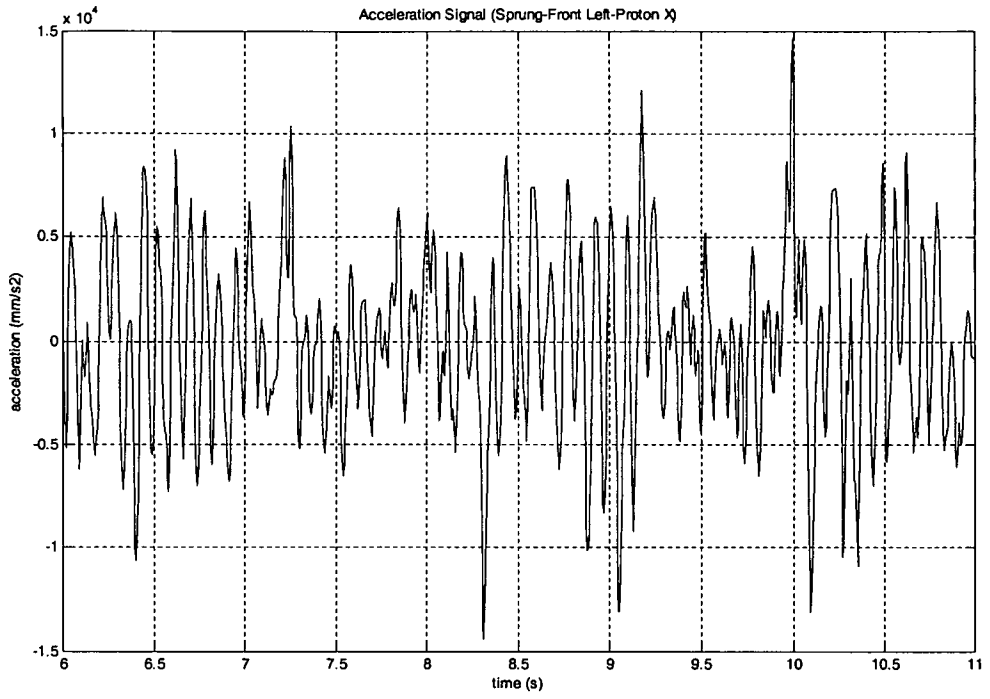
- K1 PROTON X – FRONT LEFT – VALIDATION & SIMULATION RESULT
- K2 PROTON X – REAR LEFT – VALIDATION & SIMULATION RESULT

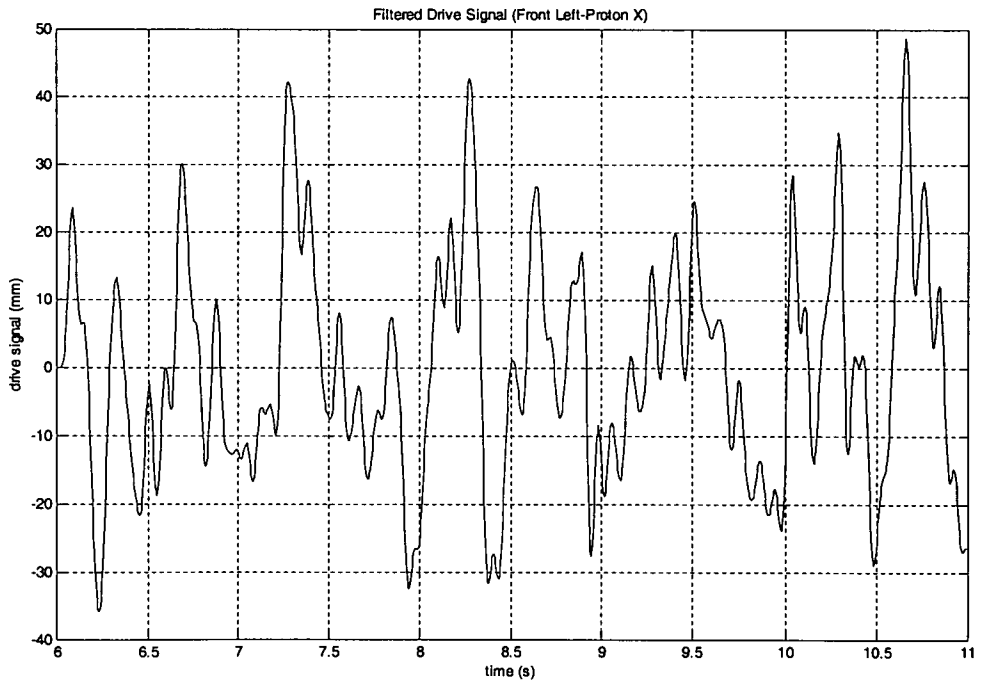
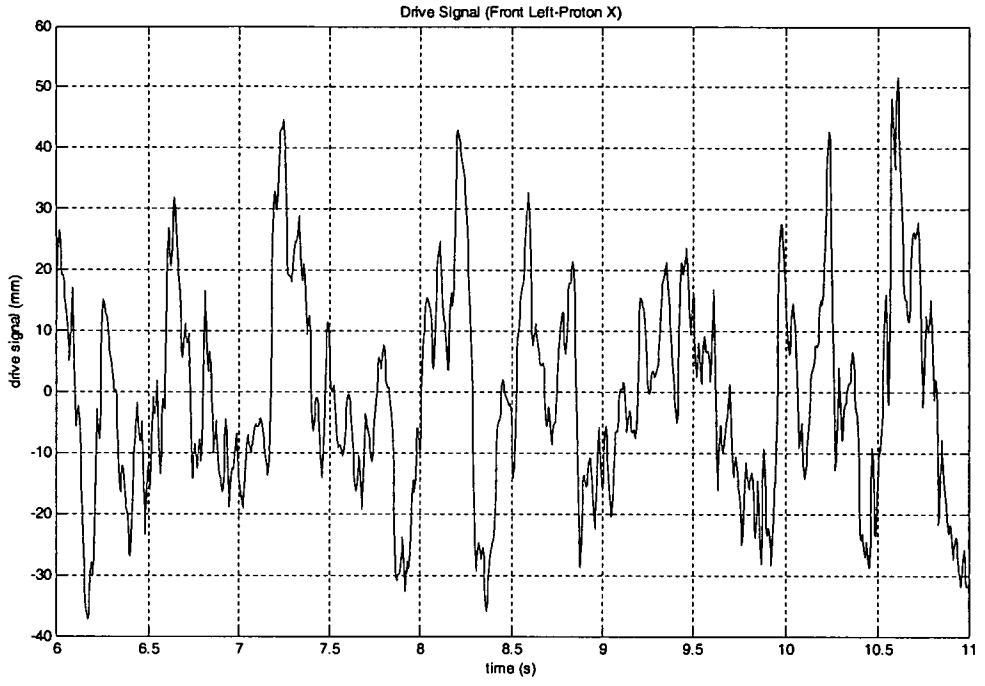
MATLAB PROGRAMMING

- L RAW DATA FILTERING (PROTON X – FRONT LEFT)
- M INTEGRATION AND DIFFERENTIATION (PROTON X – FRONT LEFT)
- N LINEAR SIMULATION

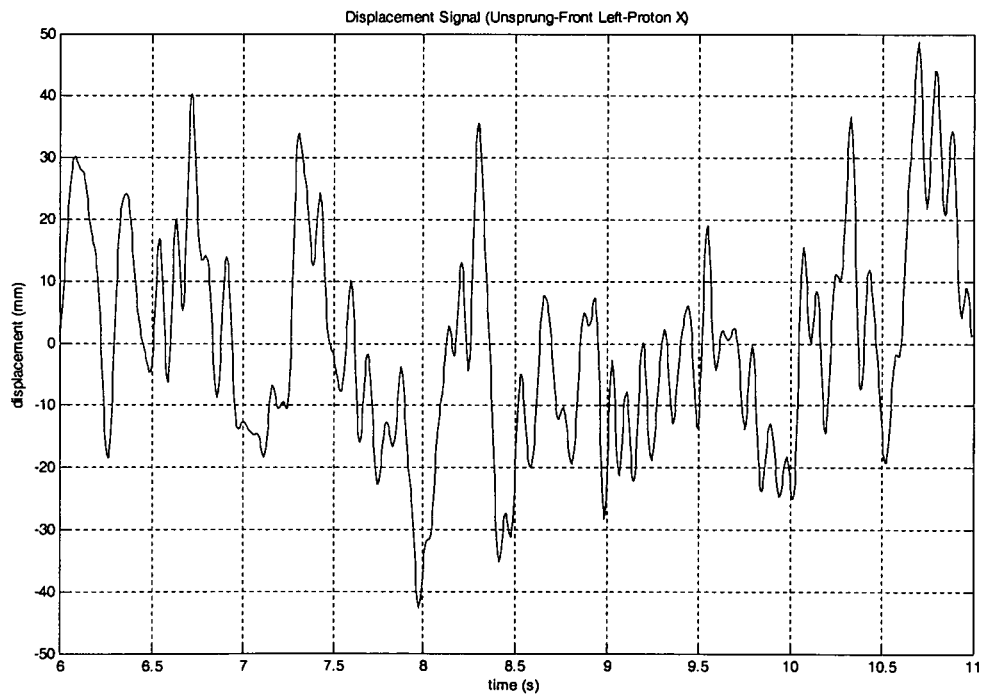
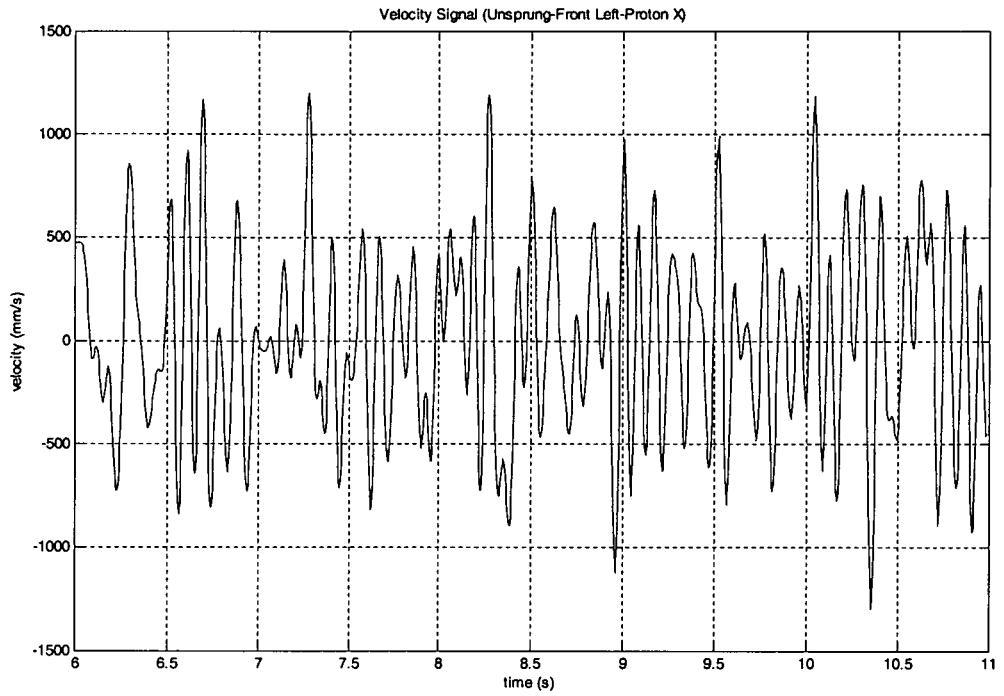
APPENDIX A1

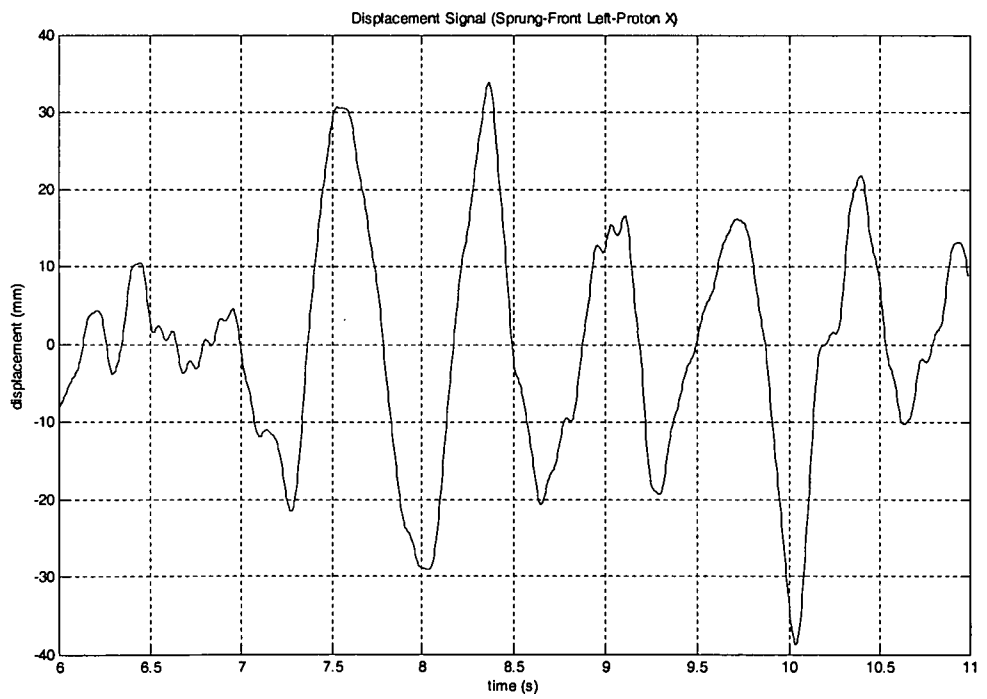
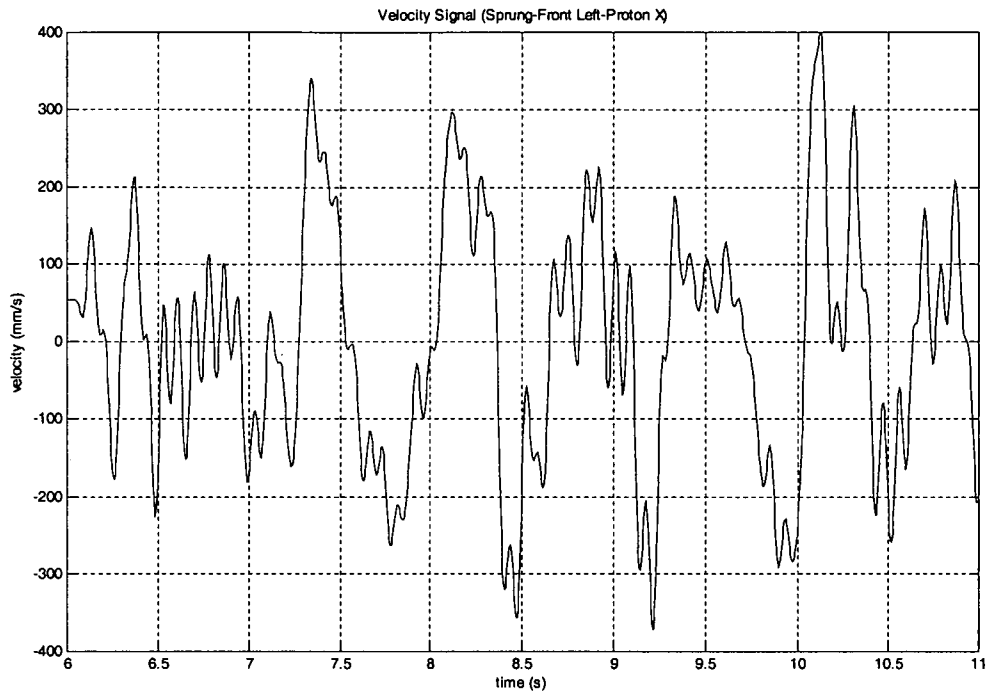




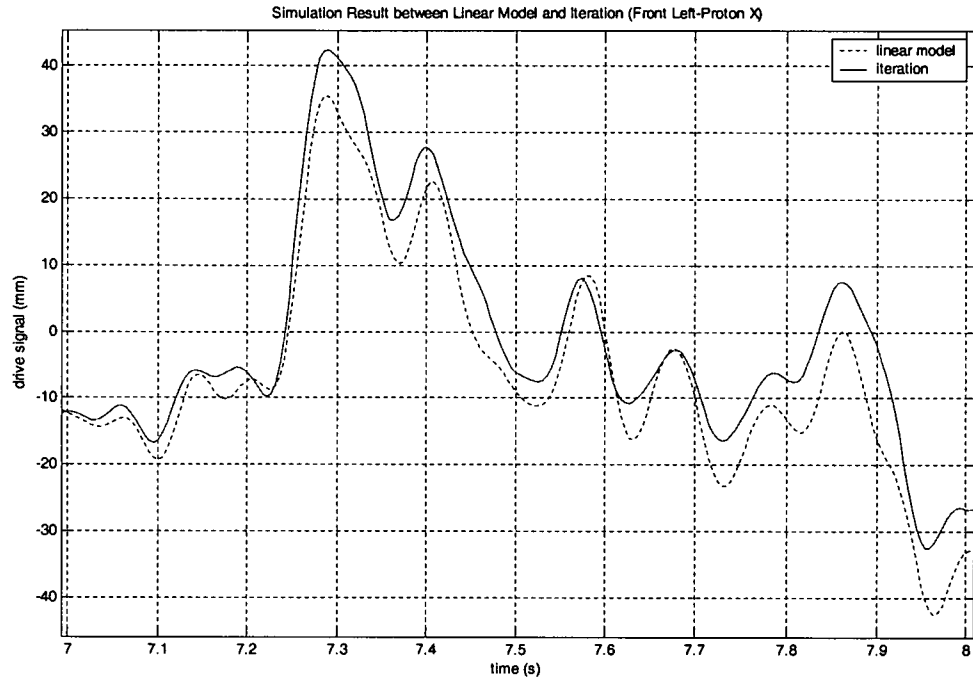


APPENDIX A2

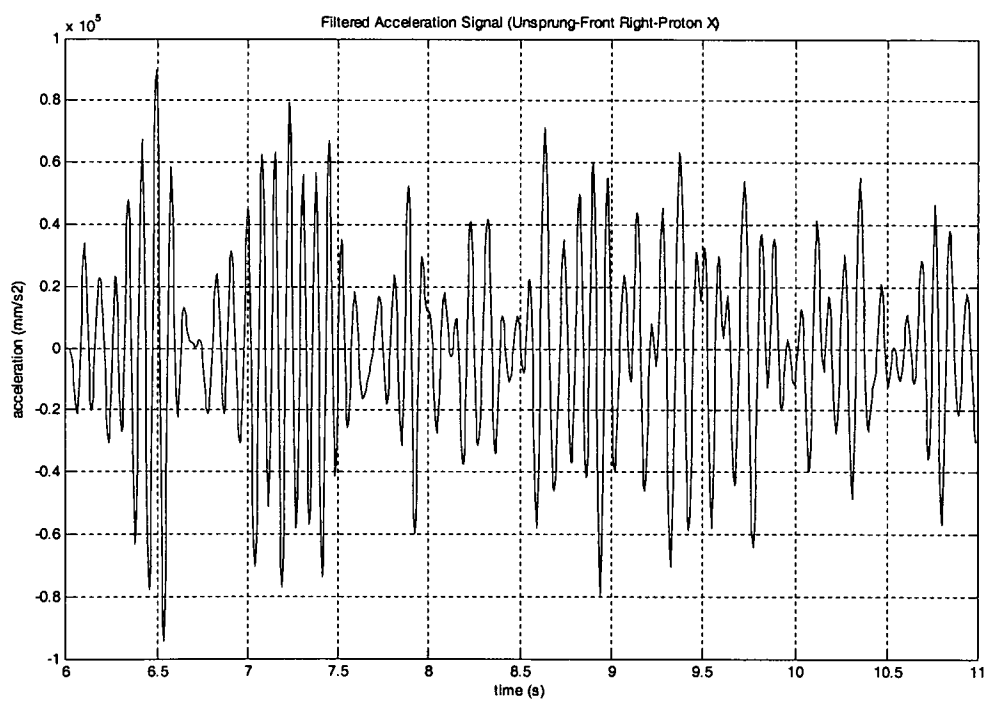
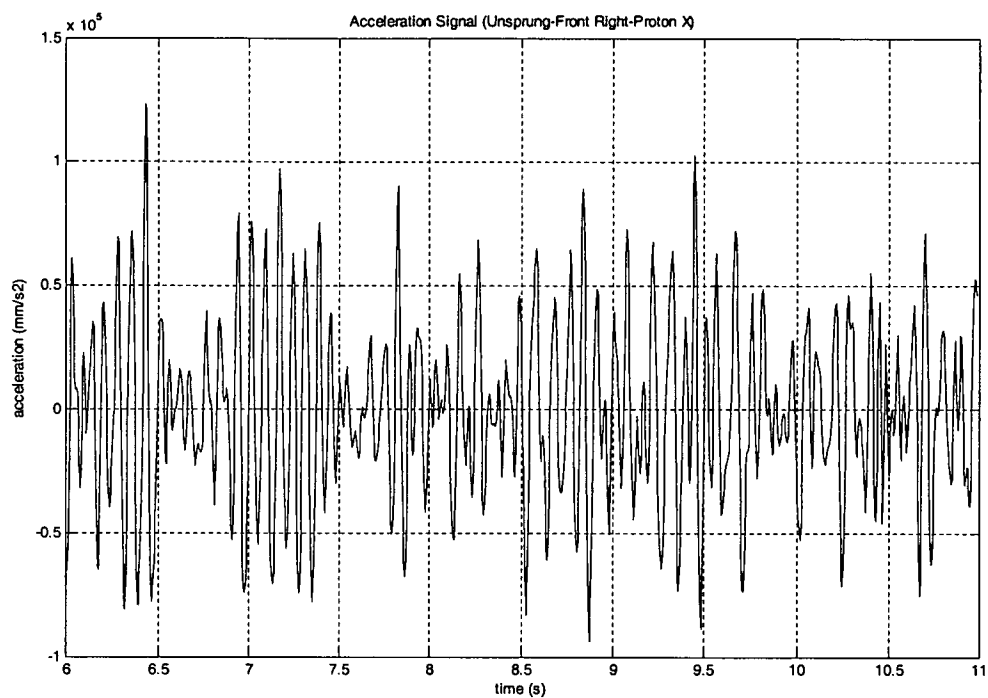


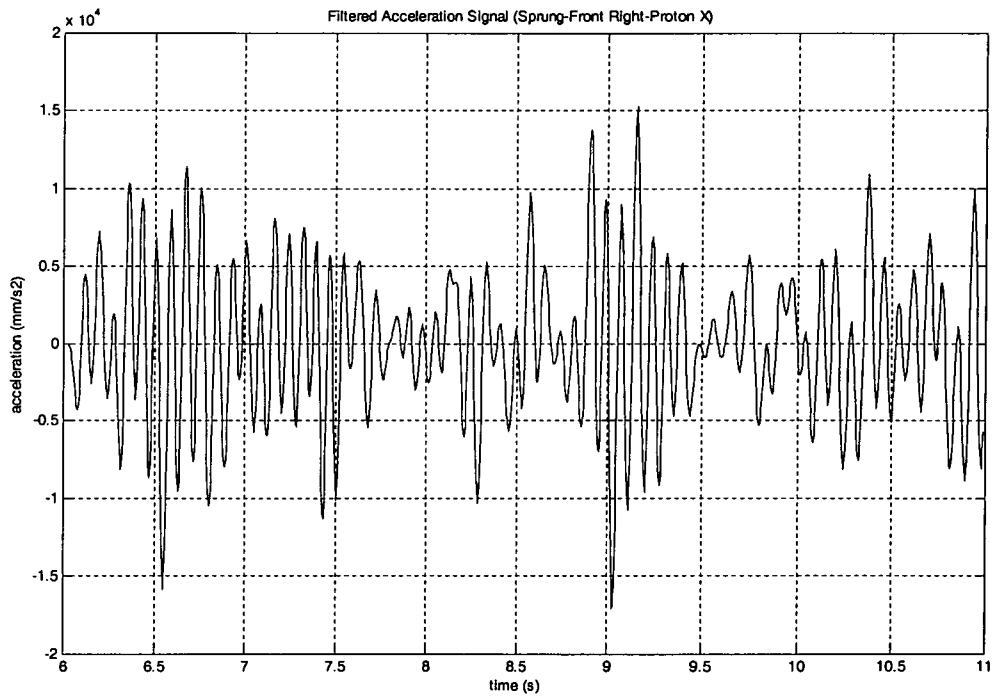
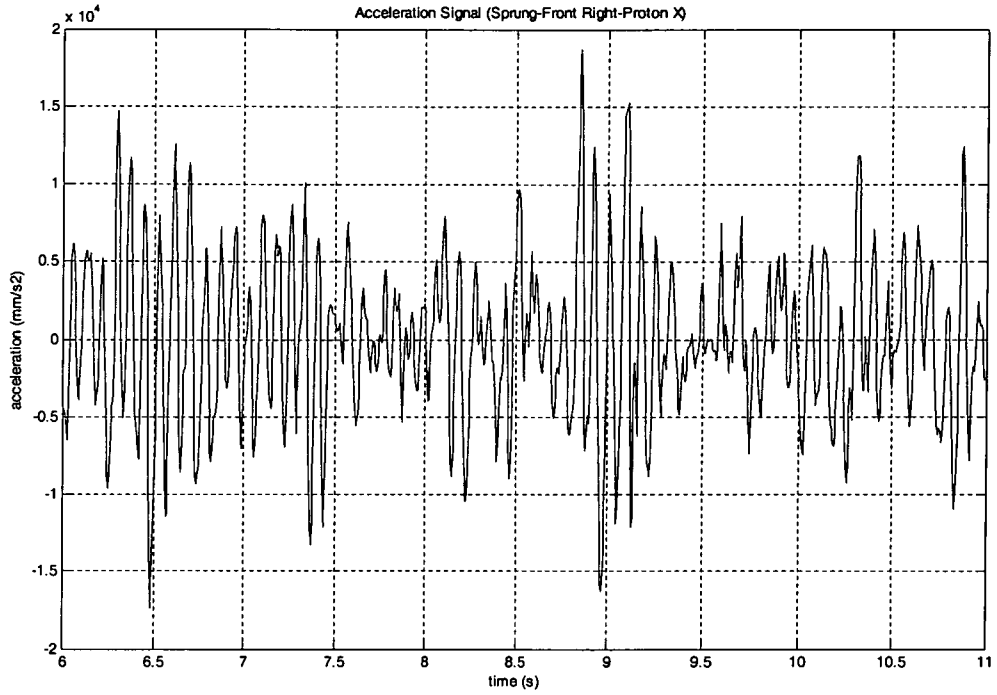


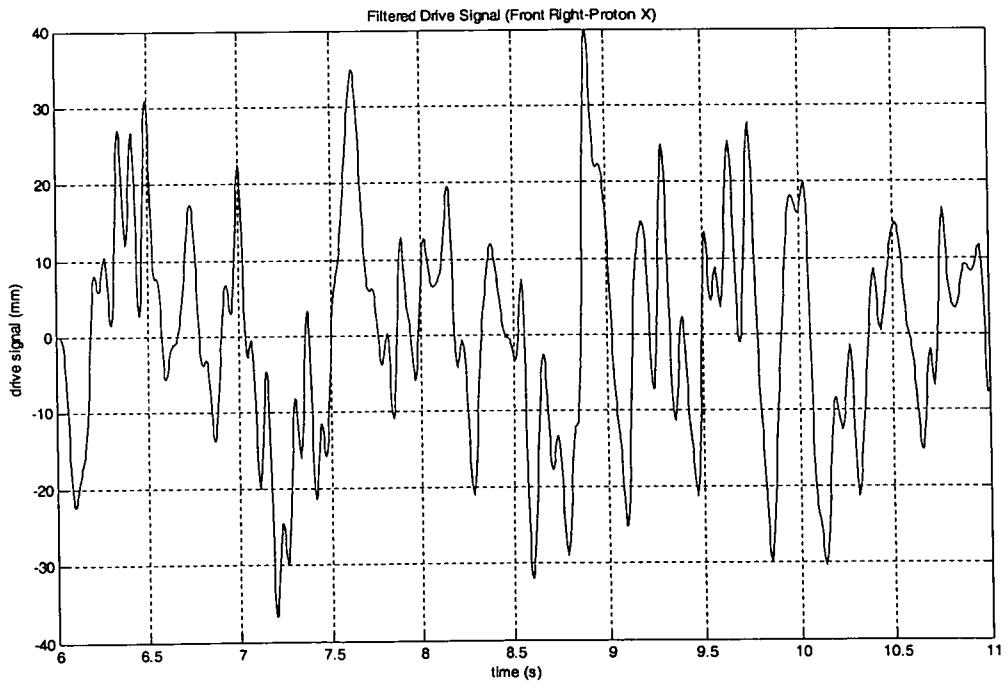
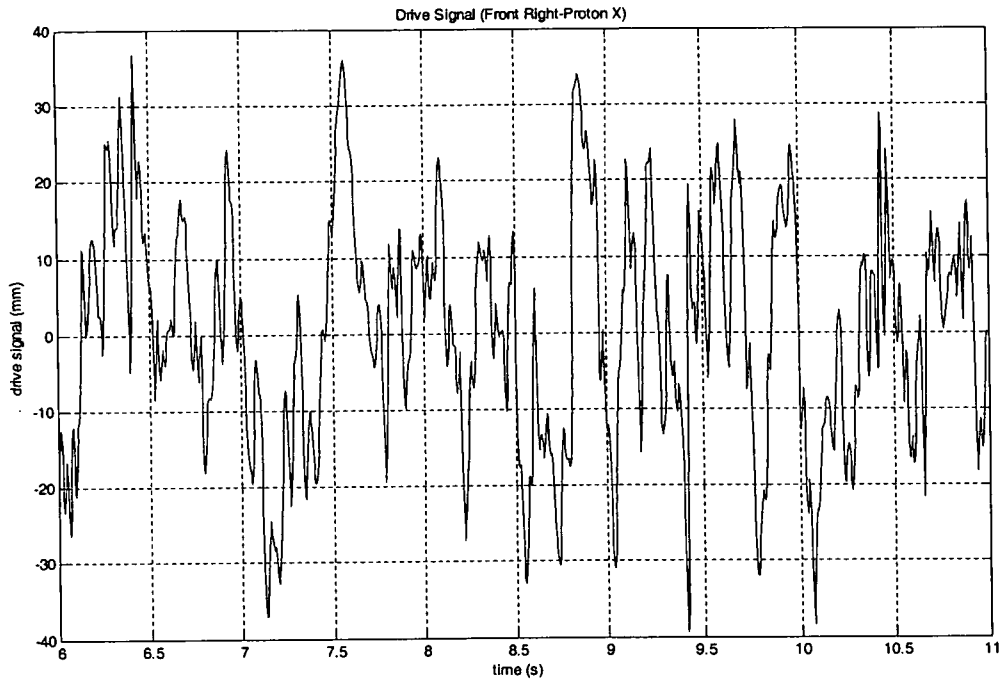
APPENDIX A3



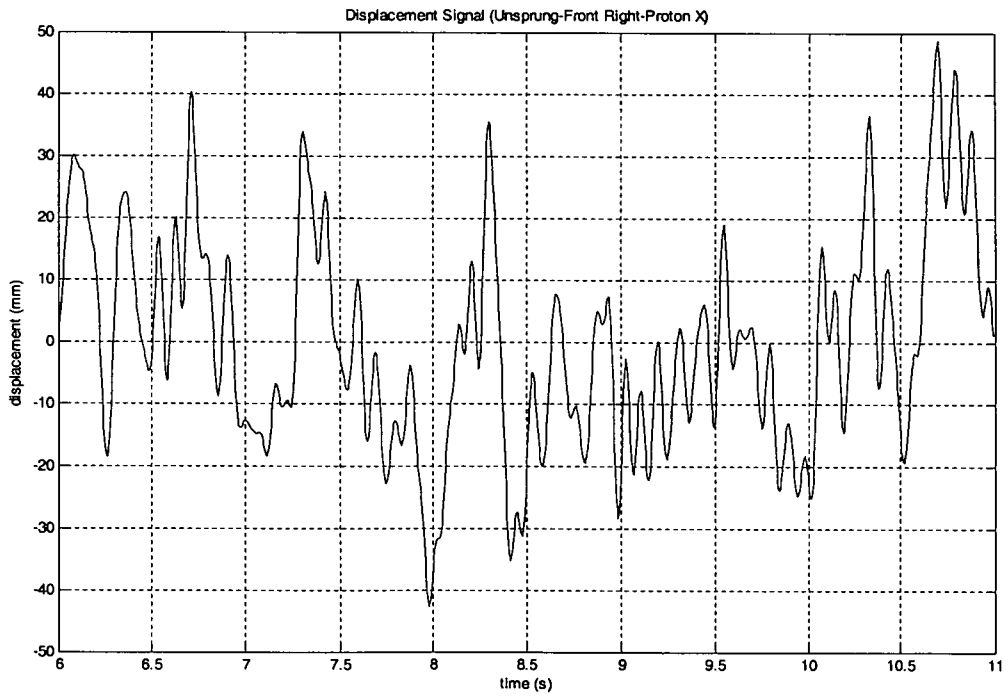
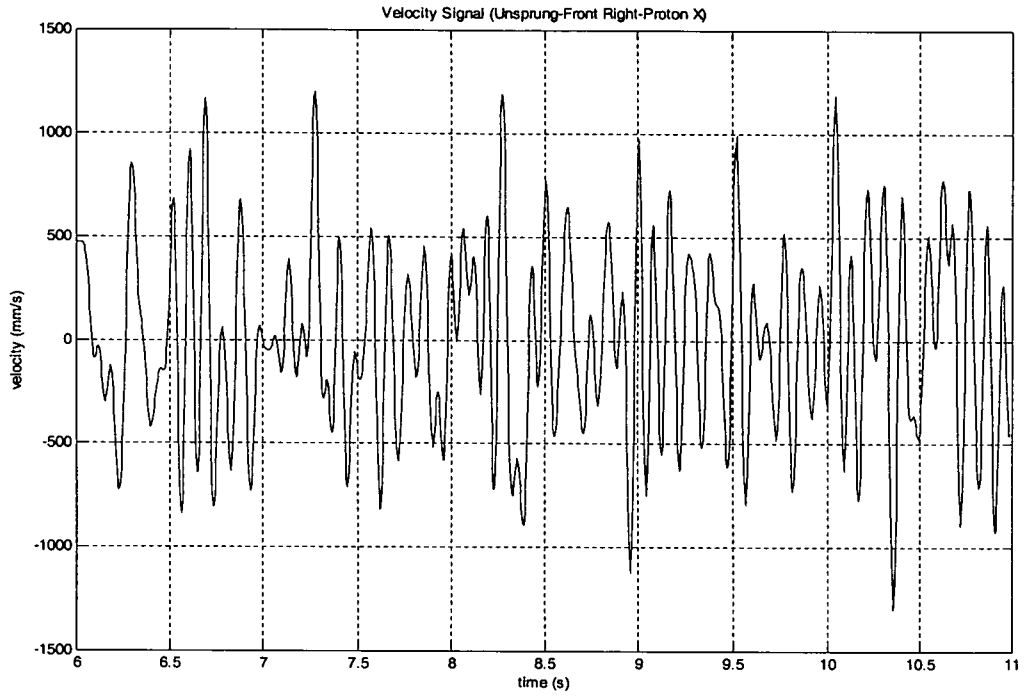
APPENDIX B1



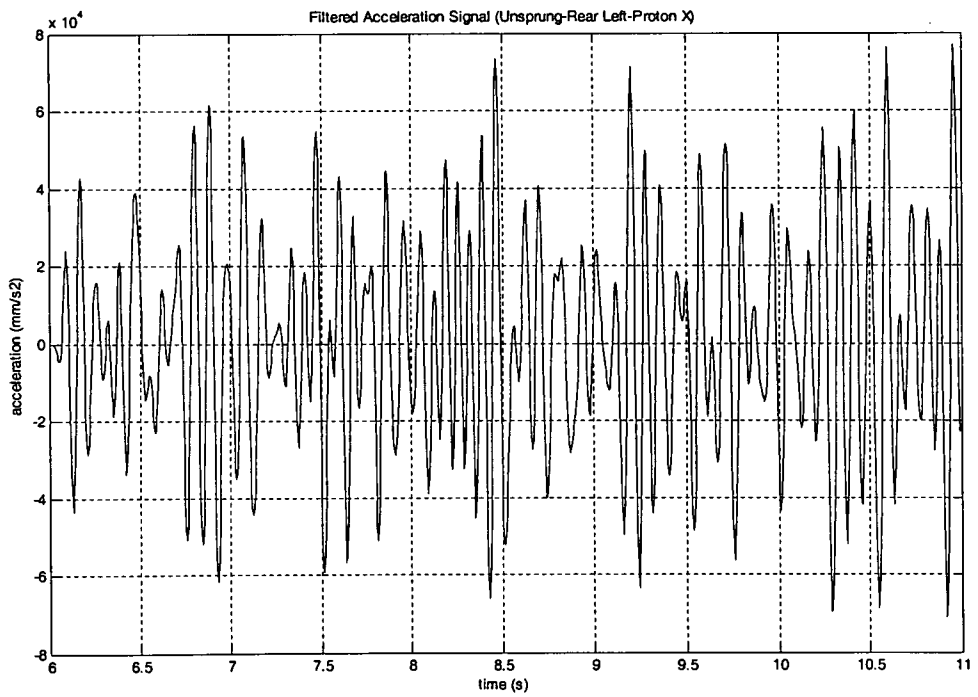
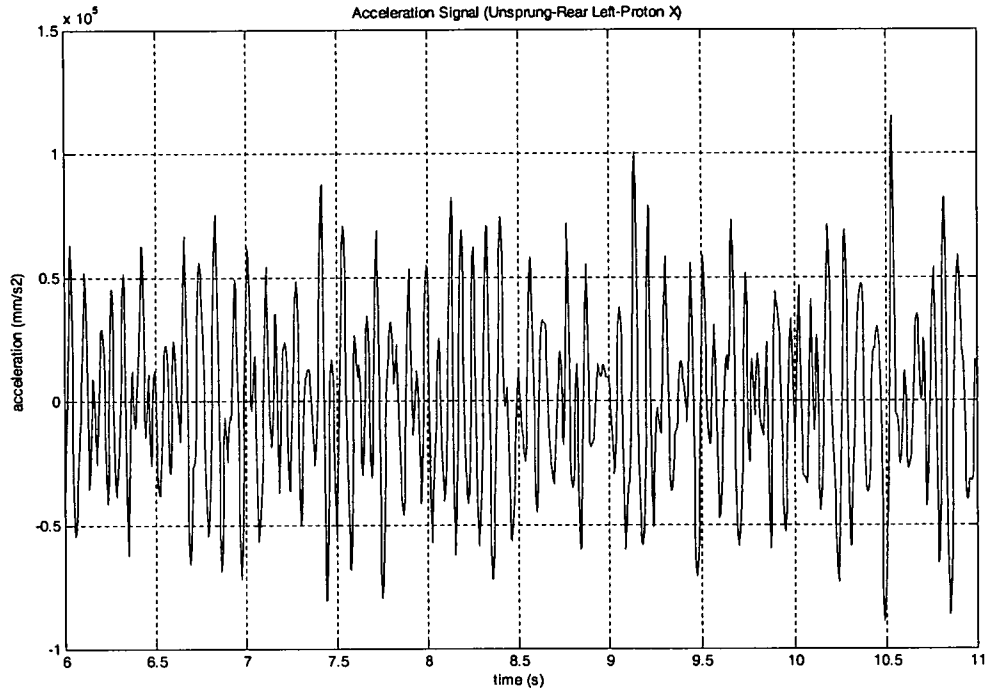


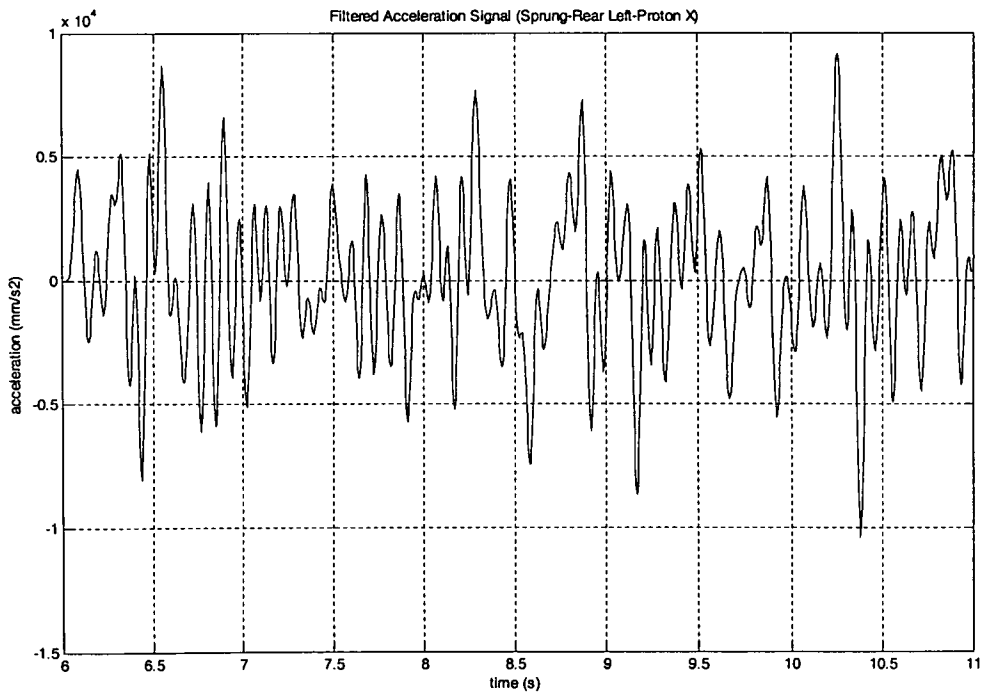
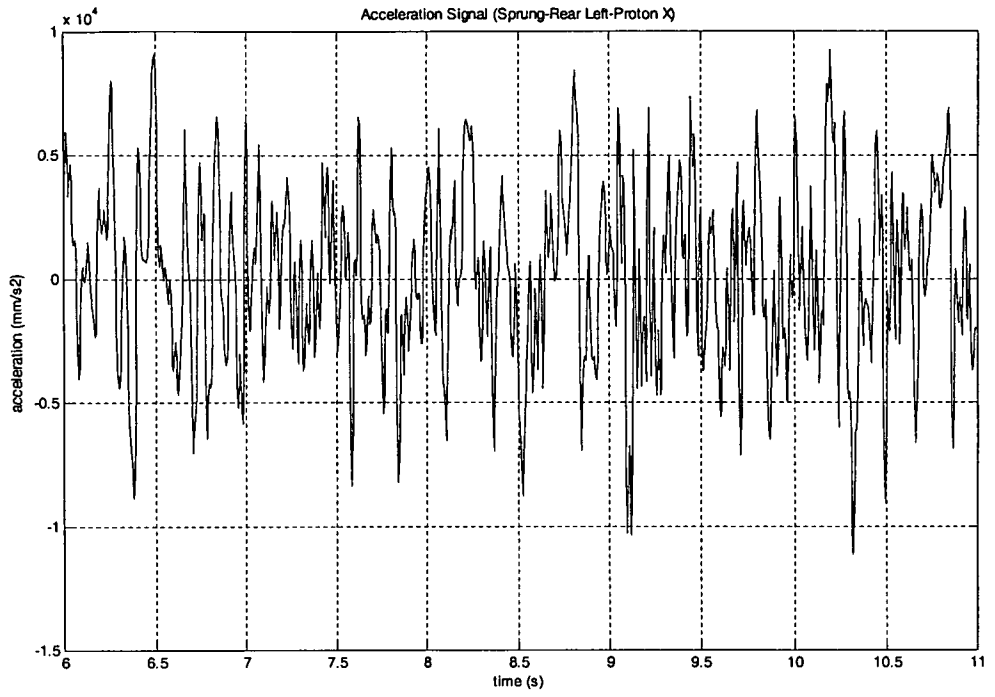


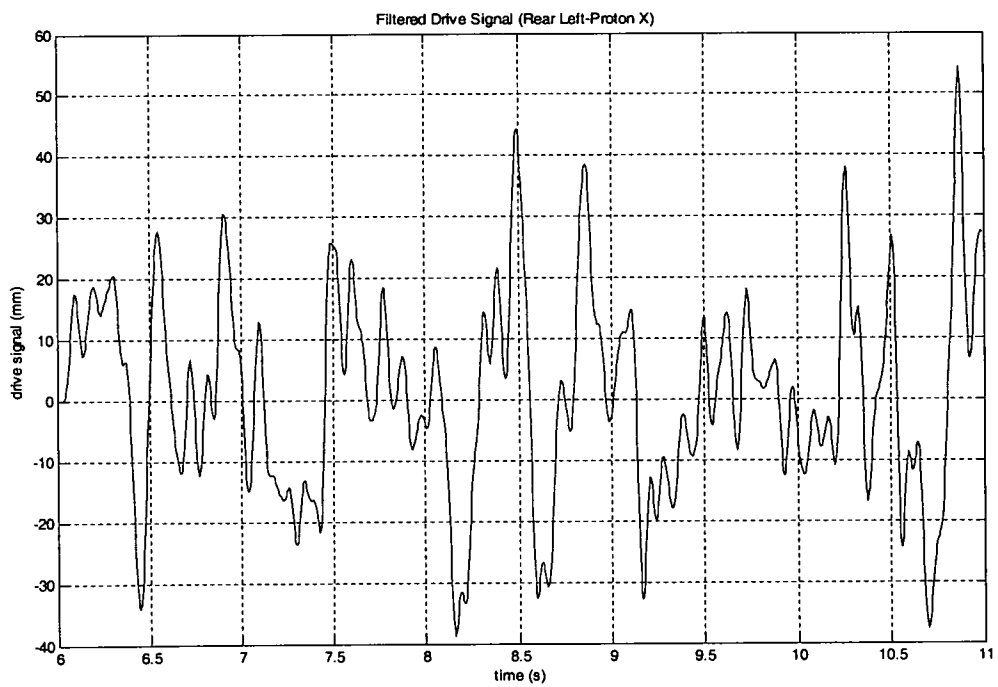
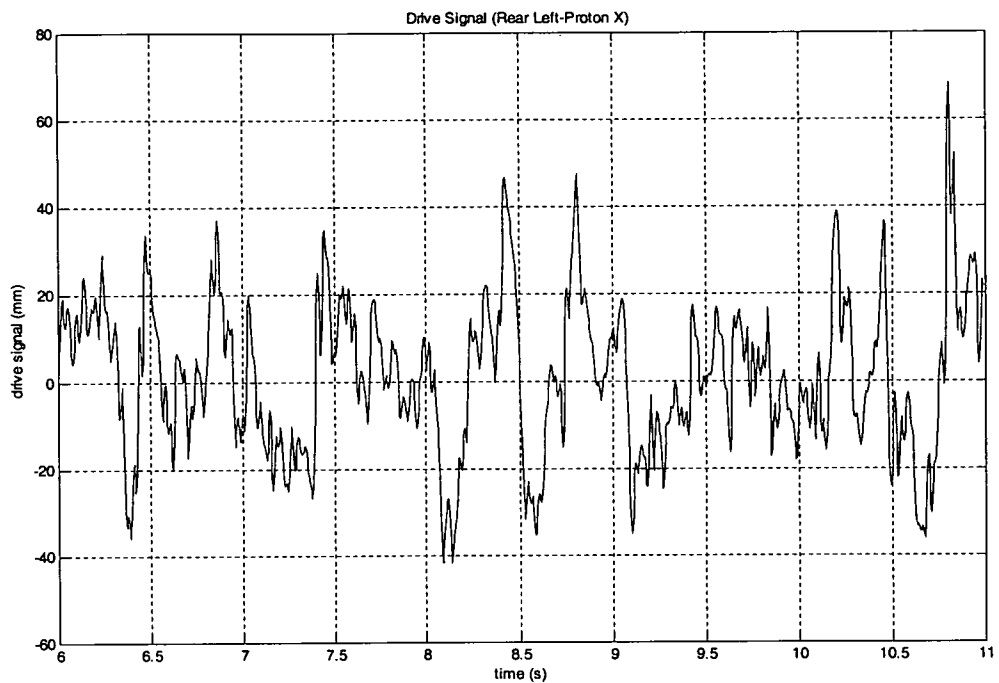
APPENDIX B2



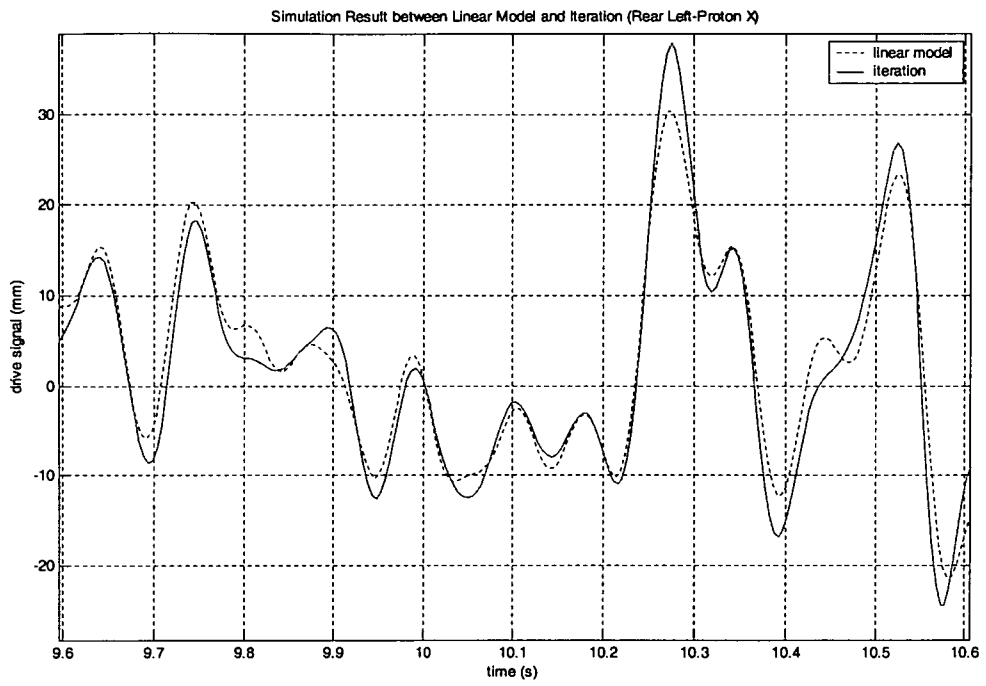
APPENDIX C1



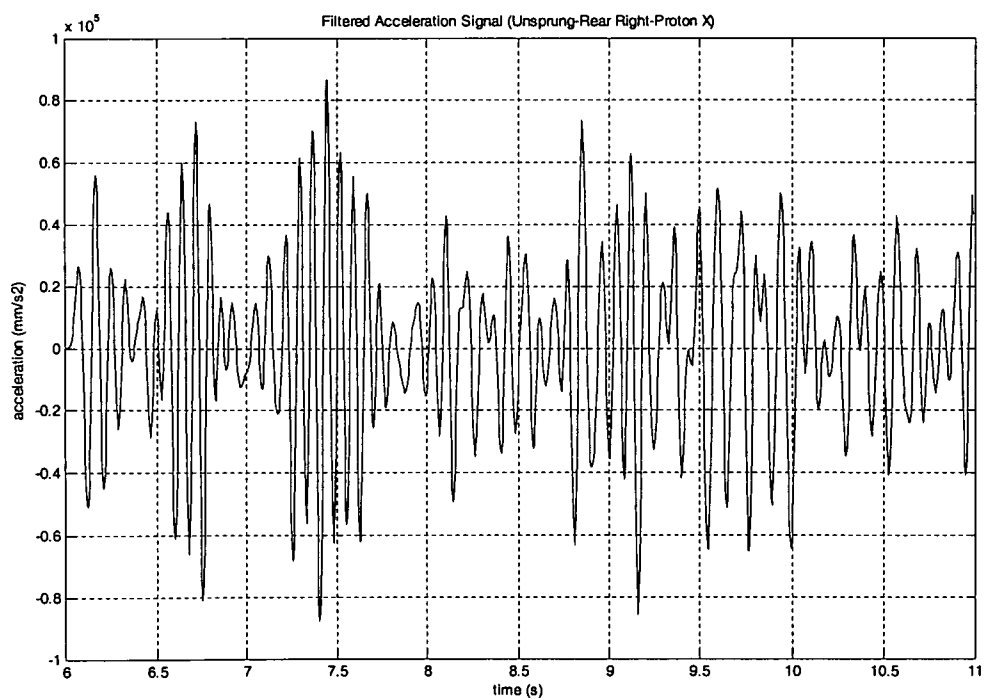
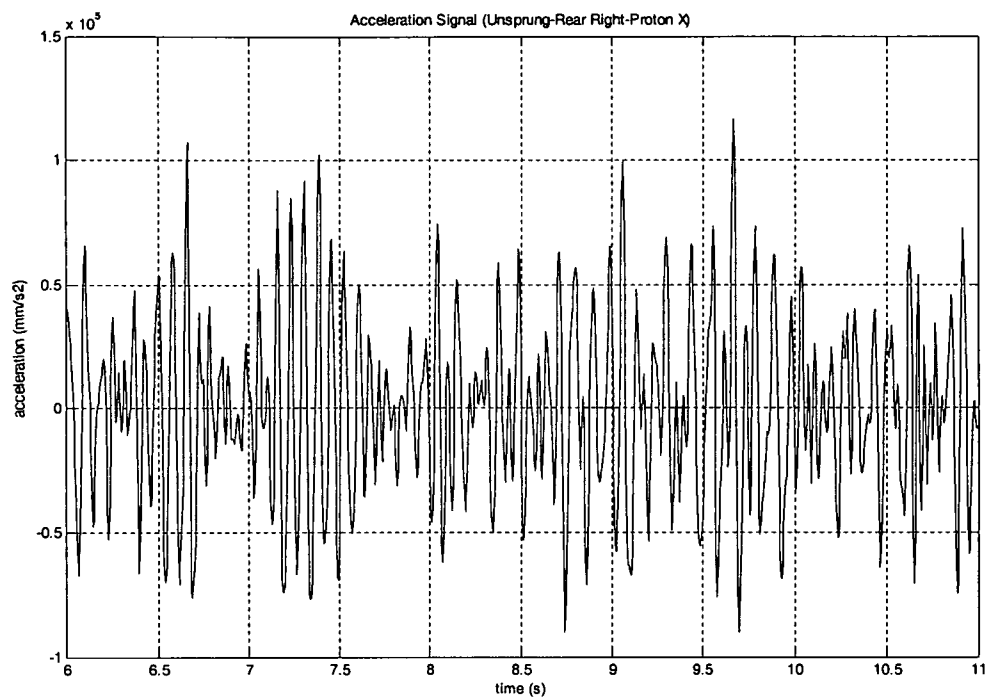


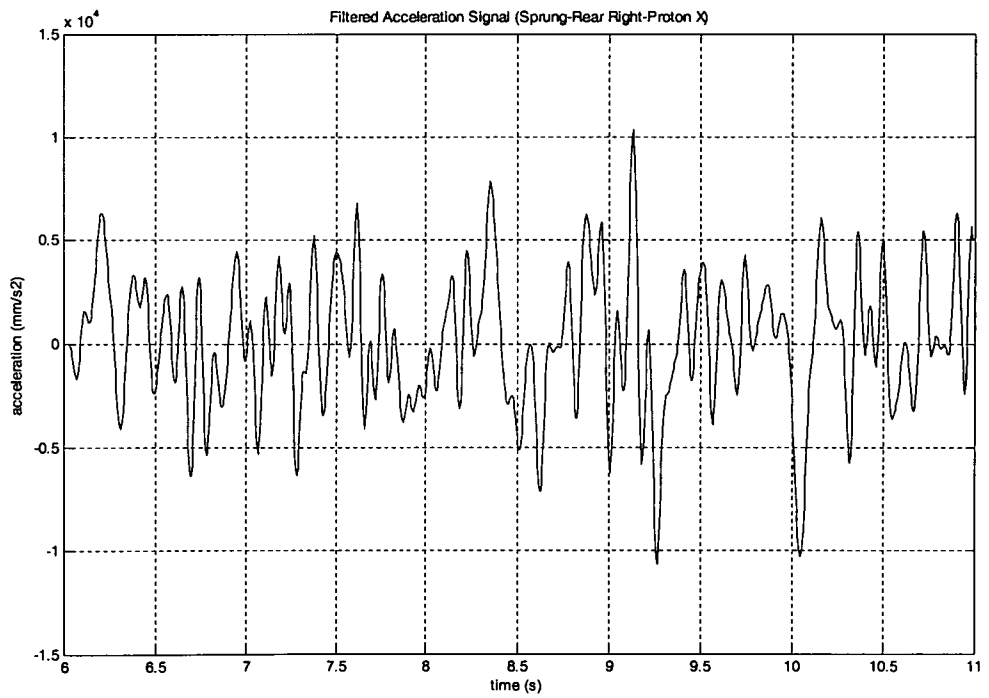
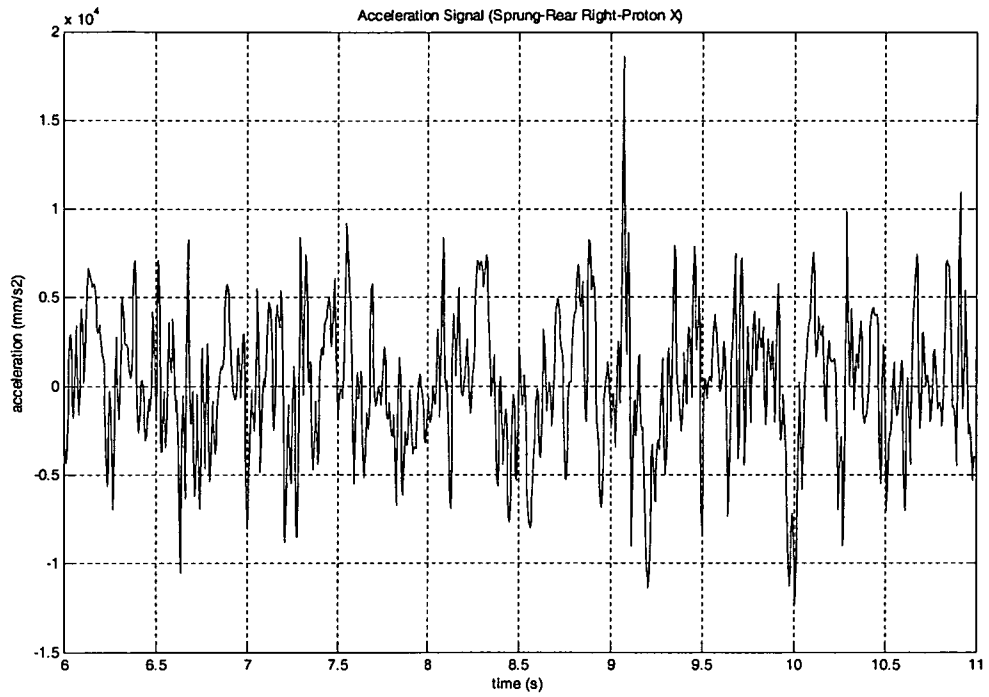


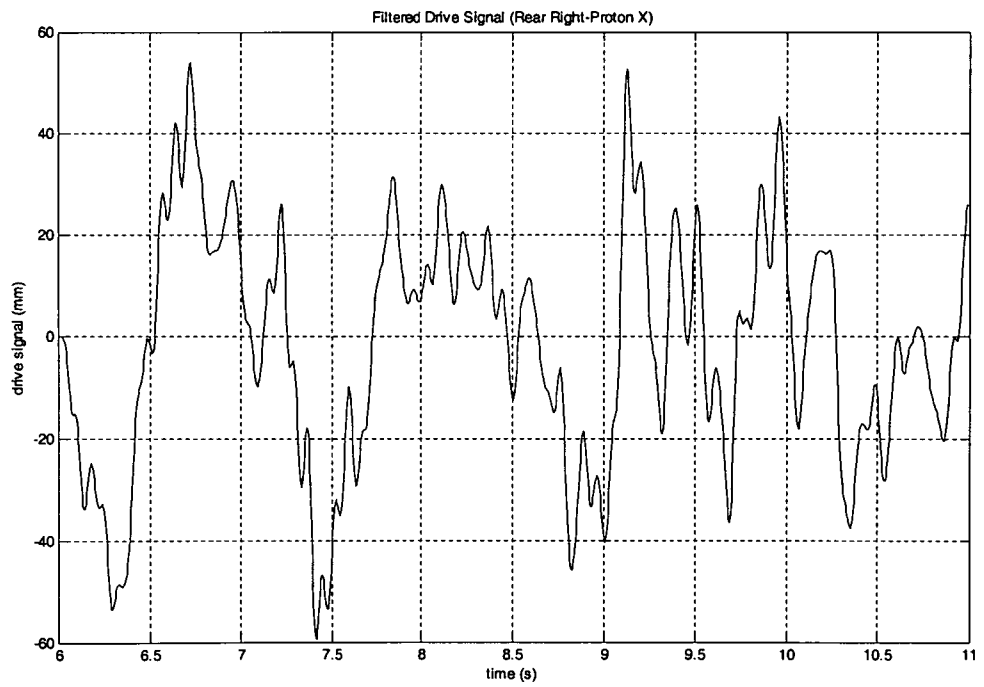
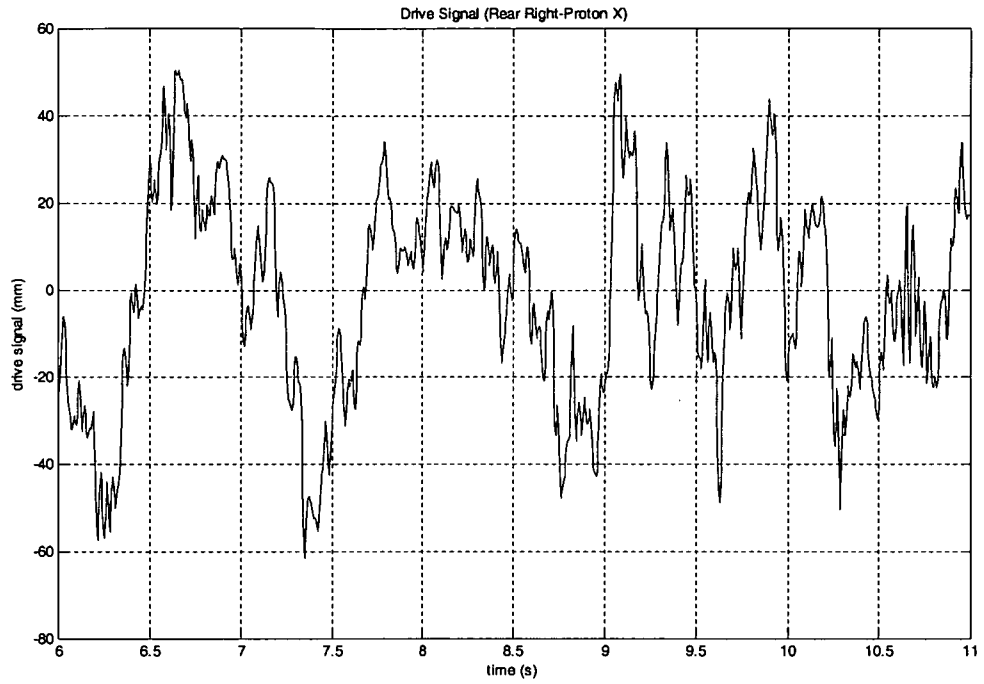
APPENDIX C3



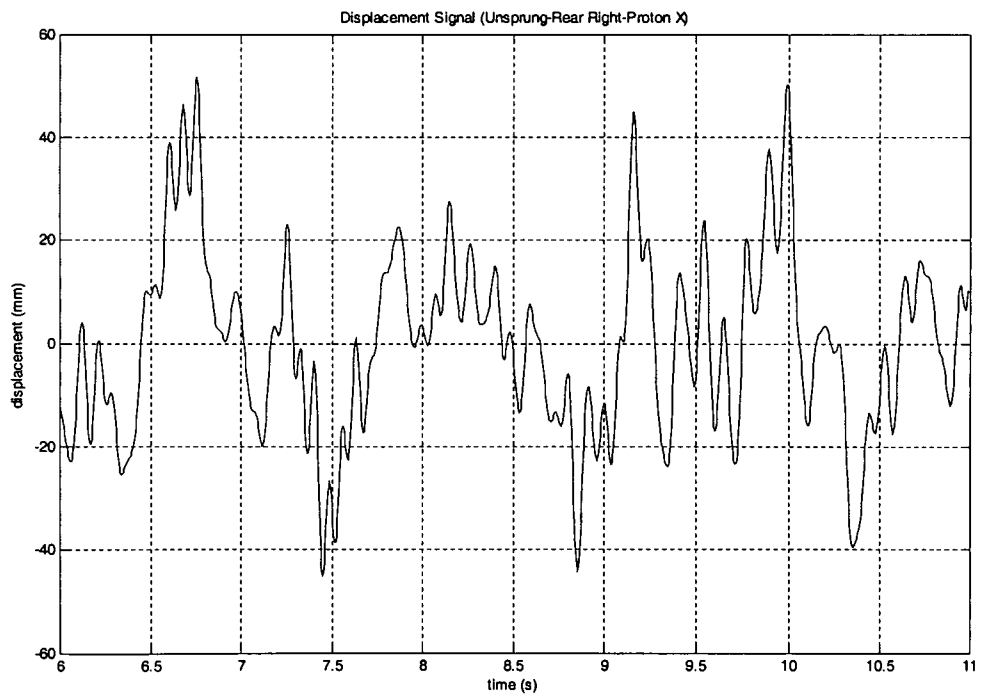
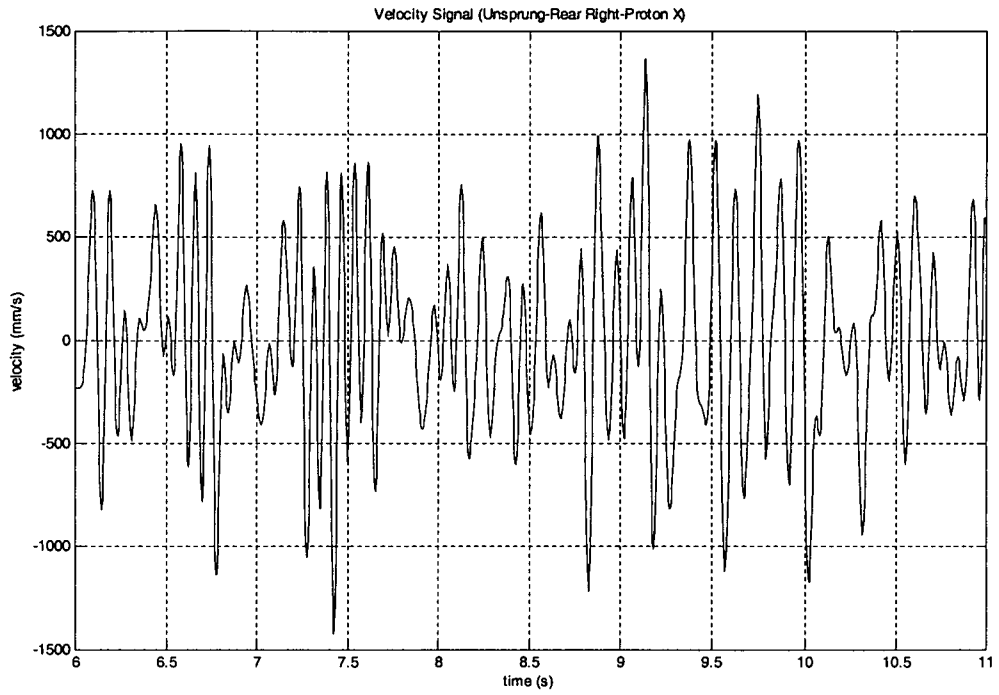
APPENDIX D1

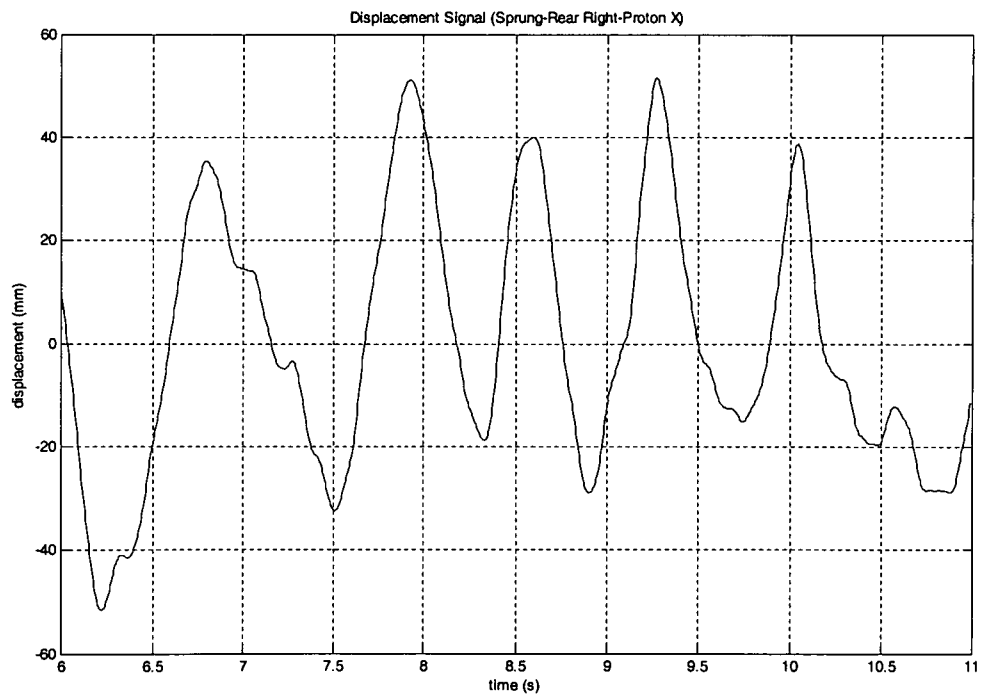
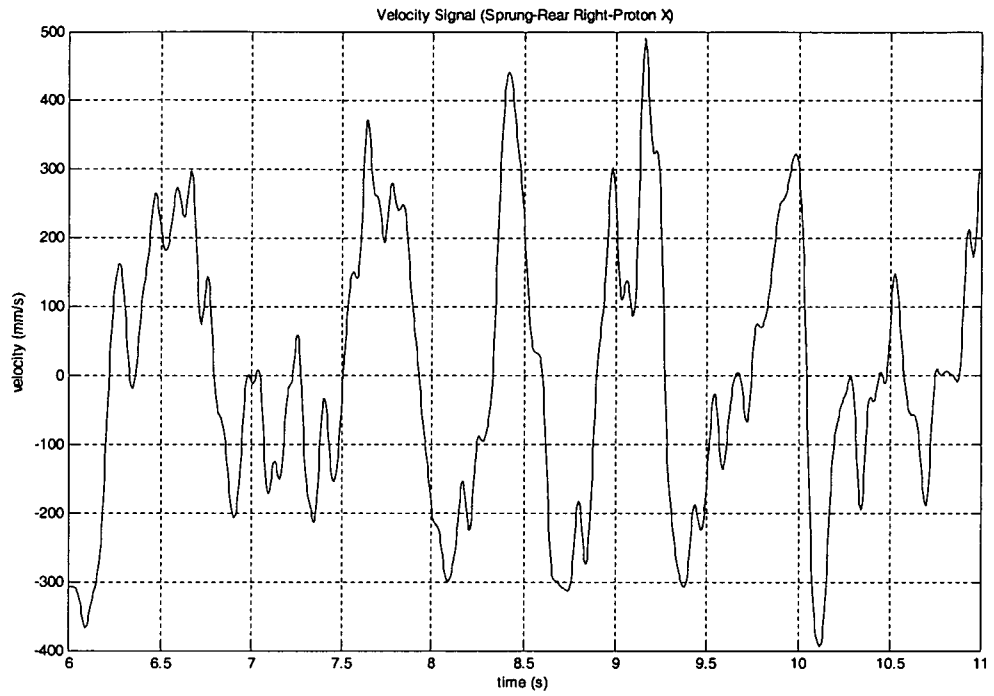




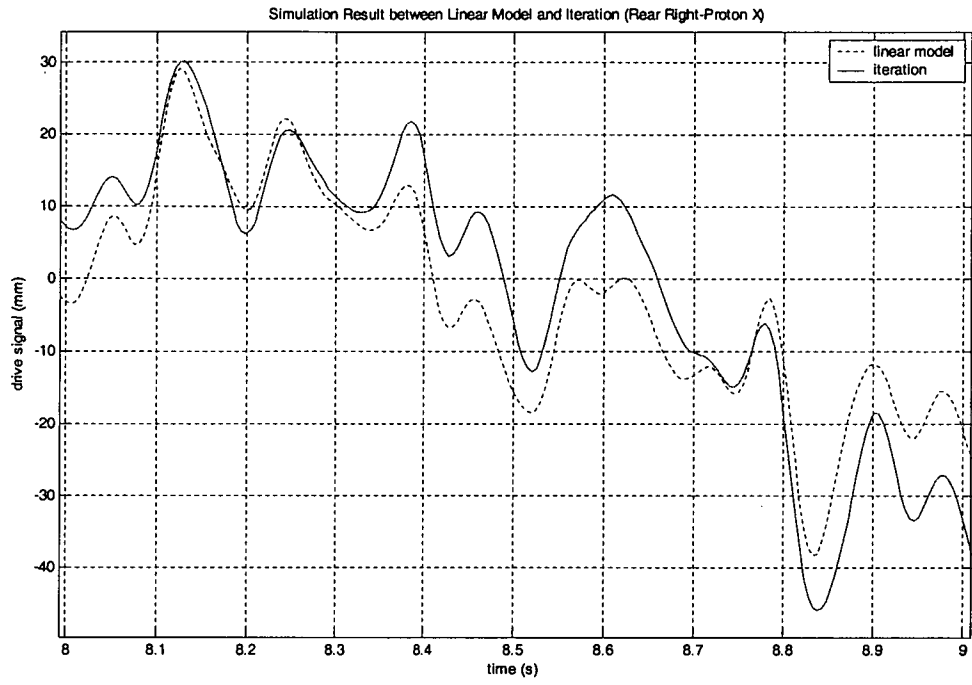


APPENDIX D2

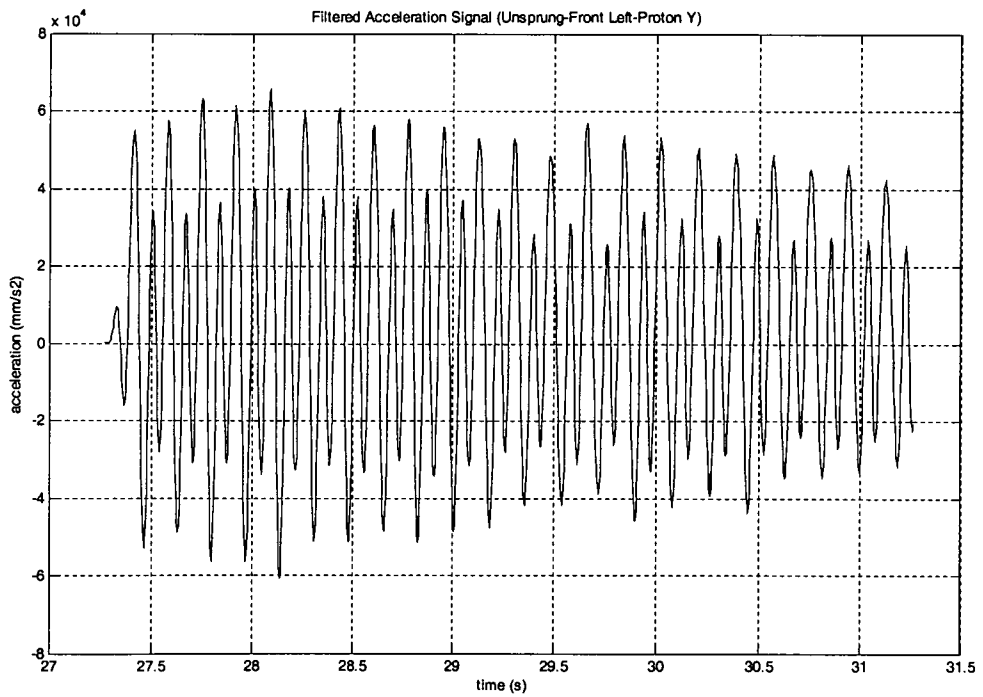
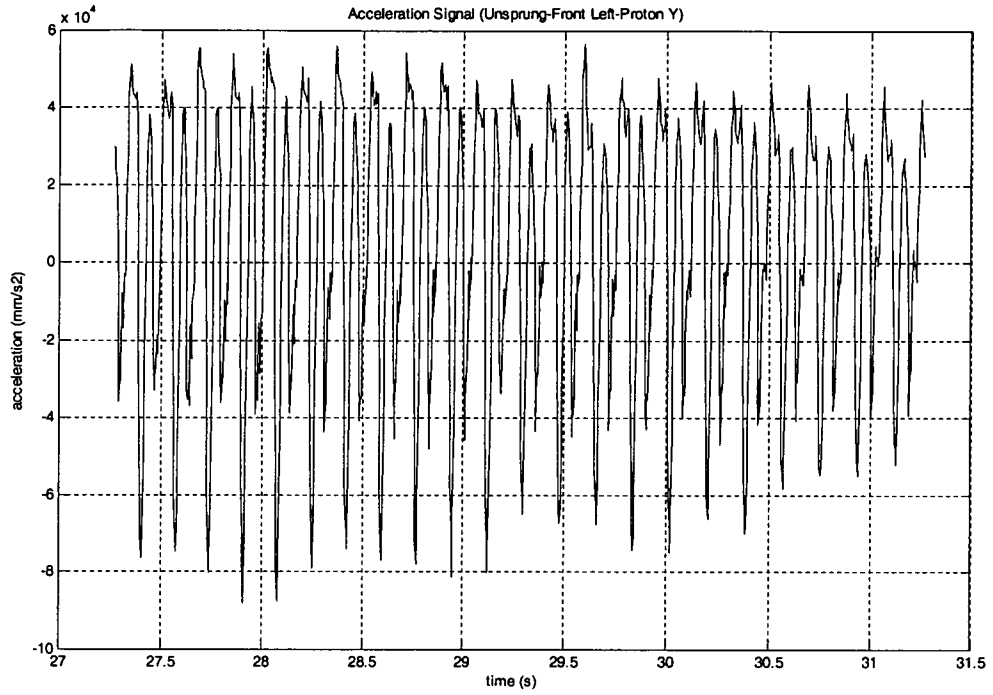


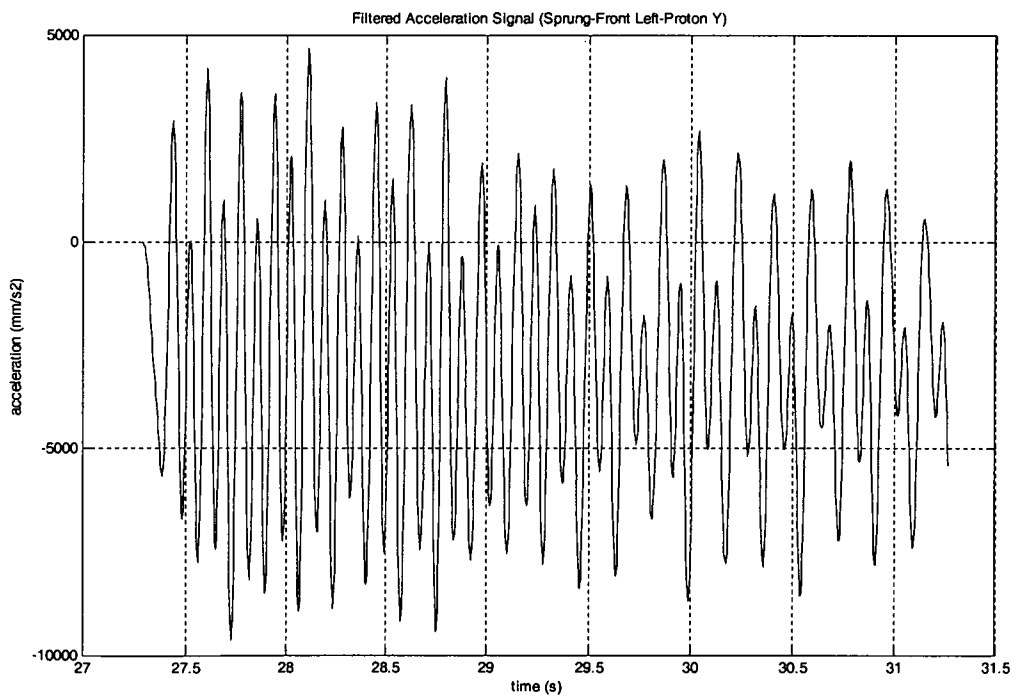
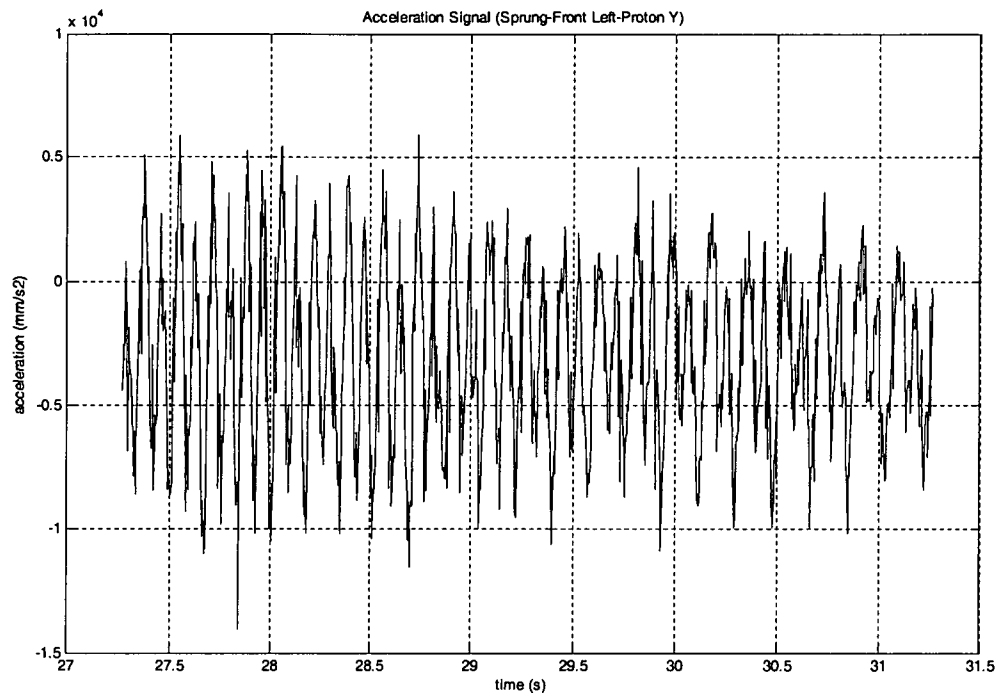


APPENDIX D3

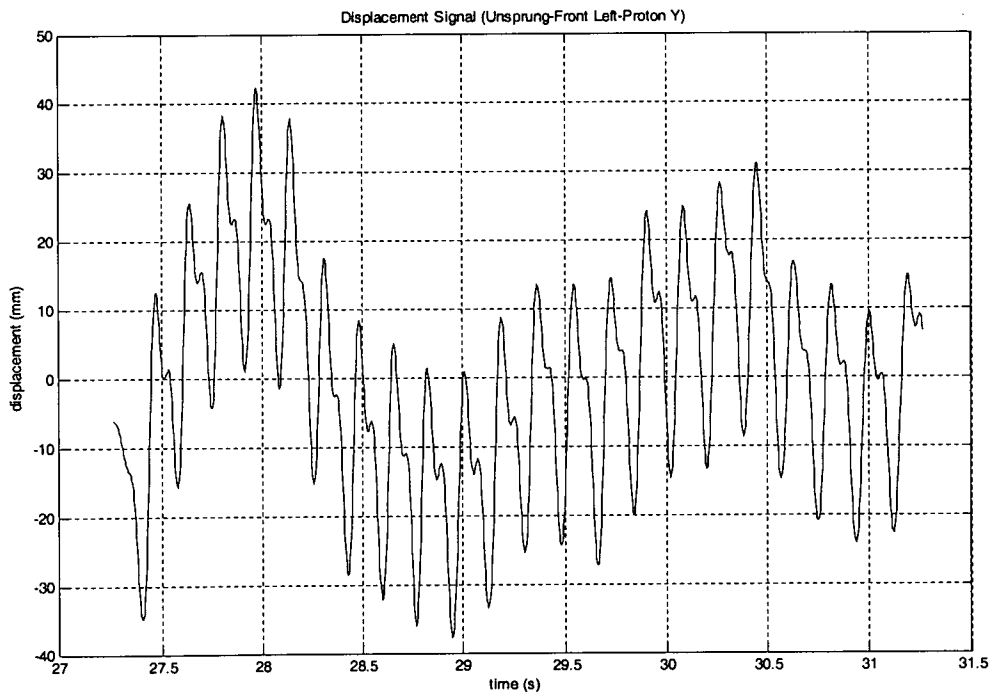
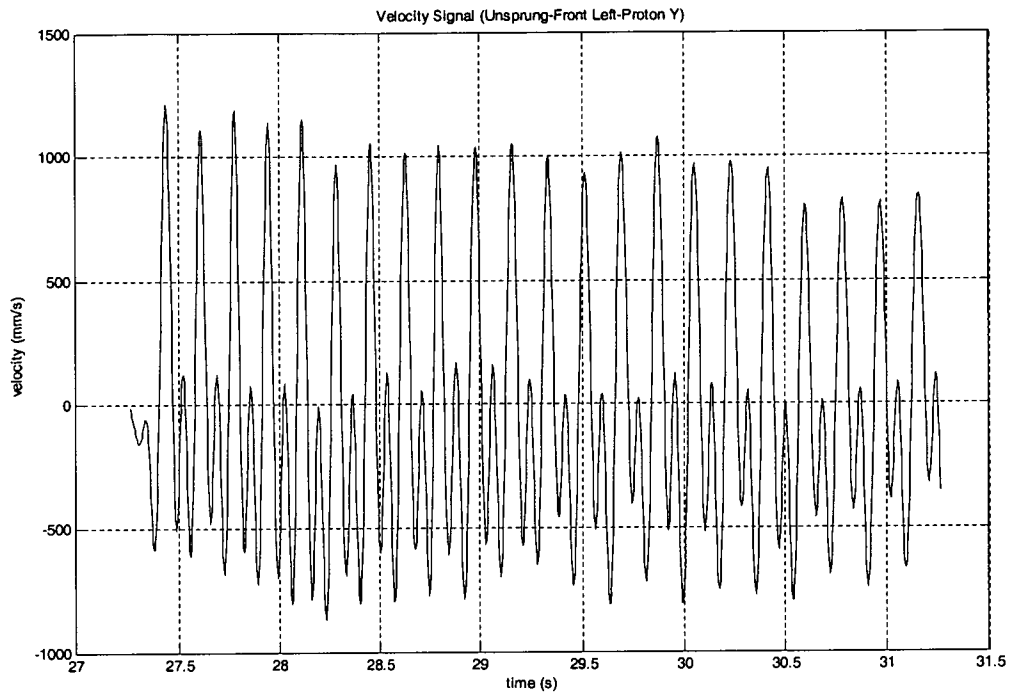


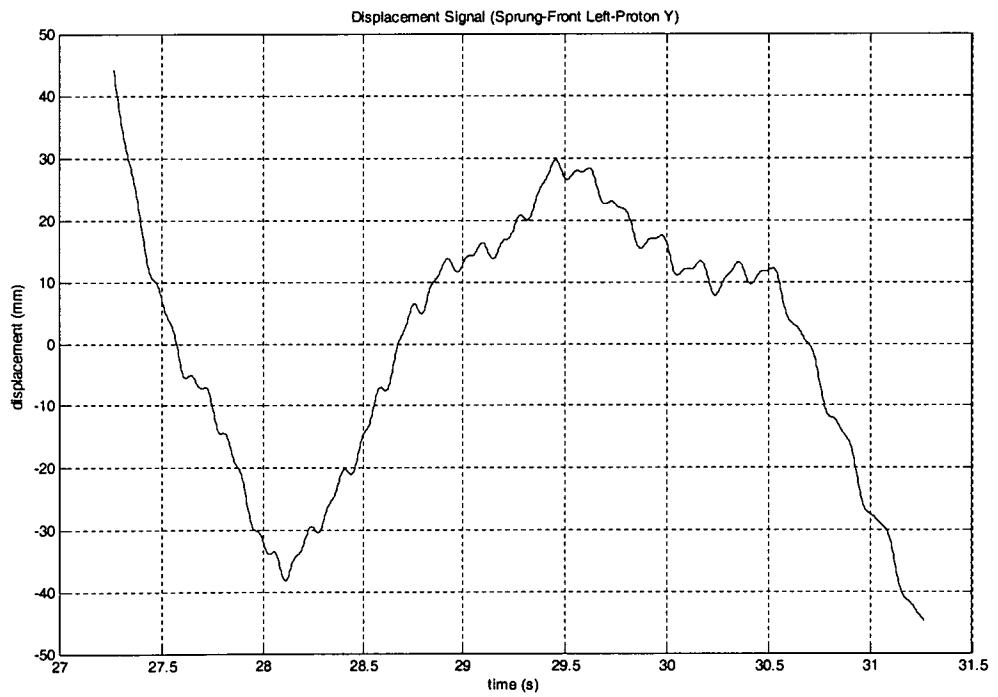
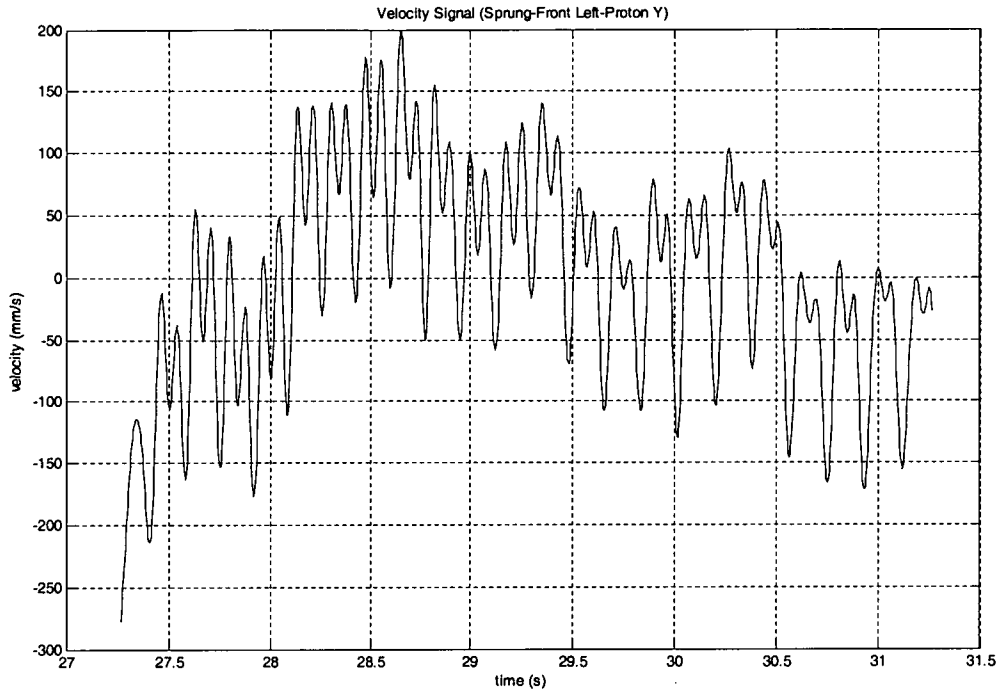
APPENDIX E1



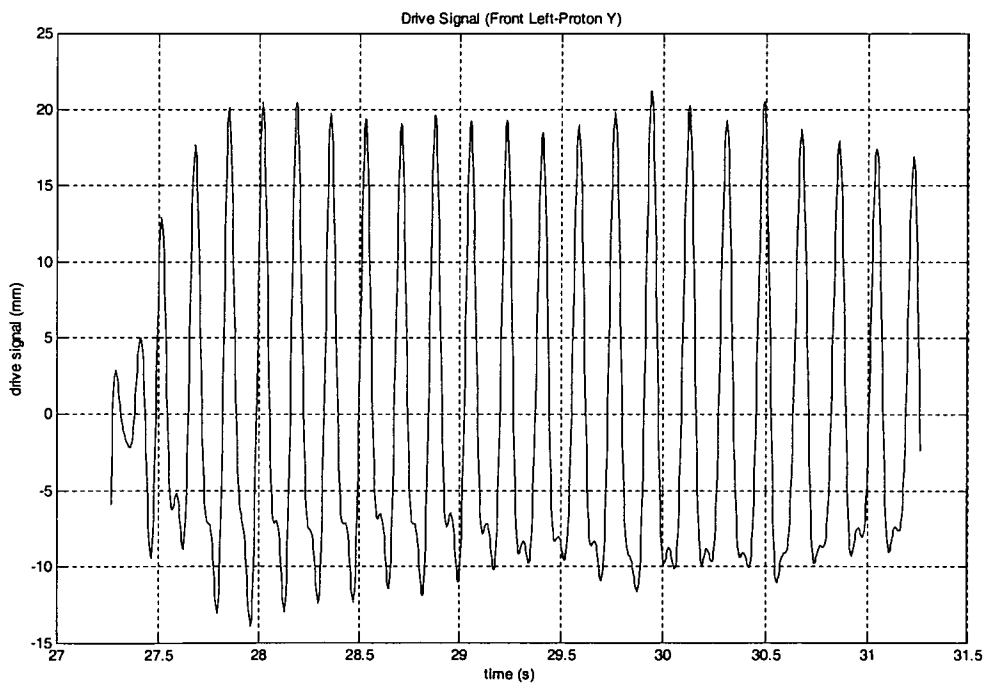
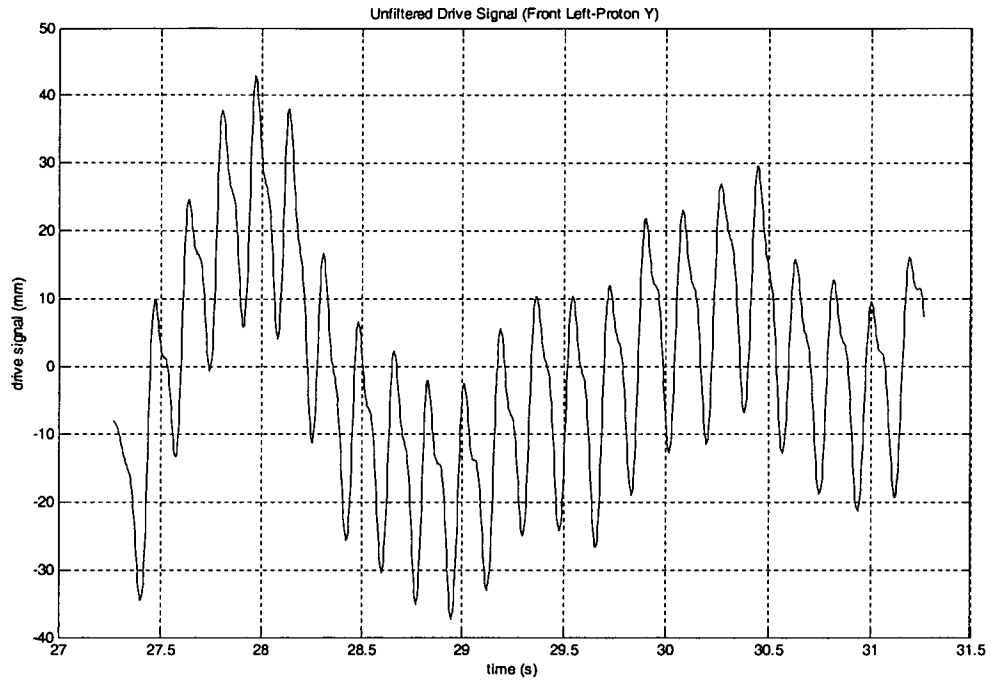


APPENDIX E2

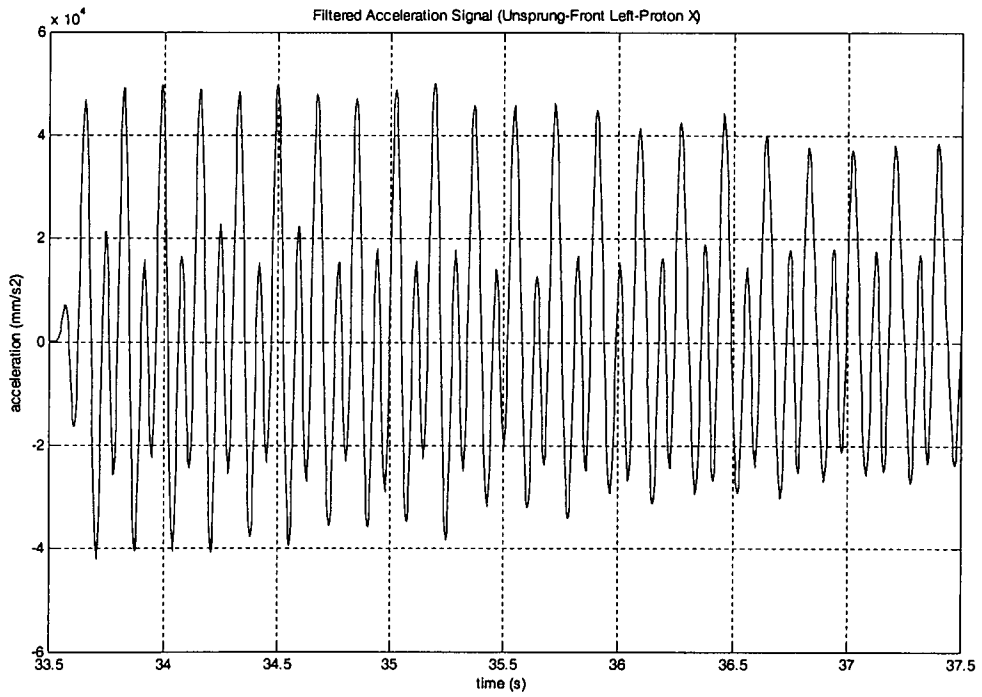
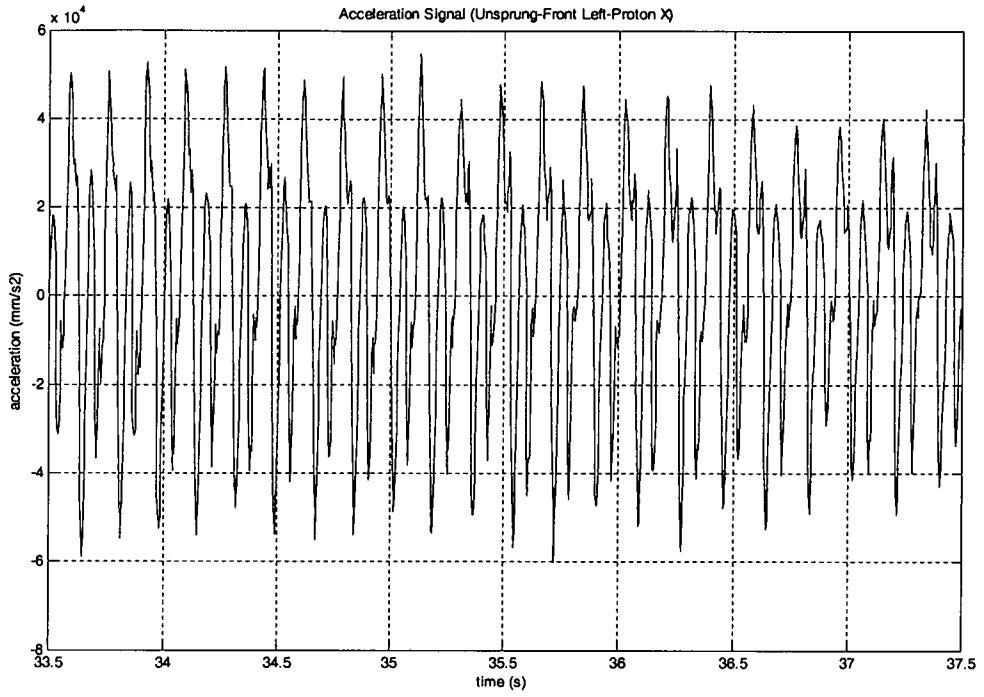


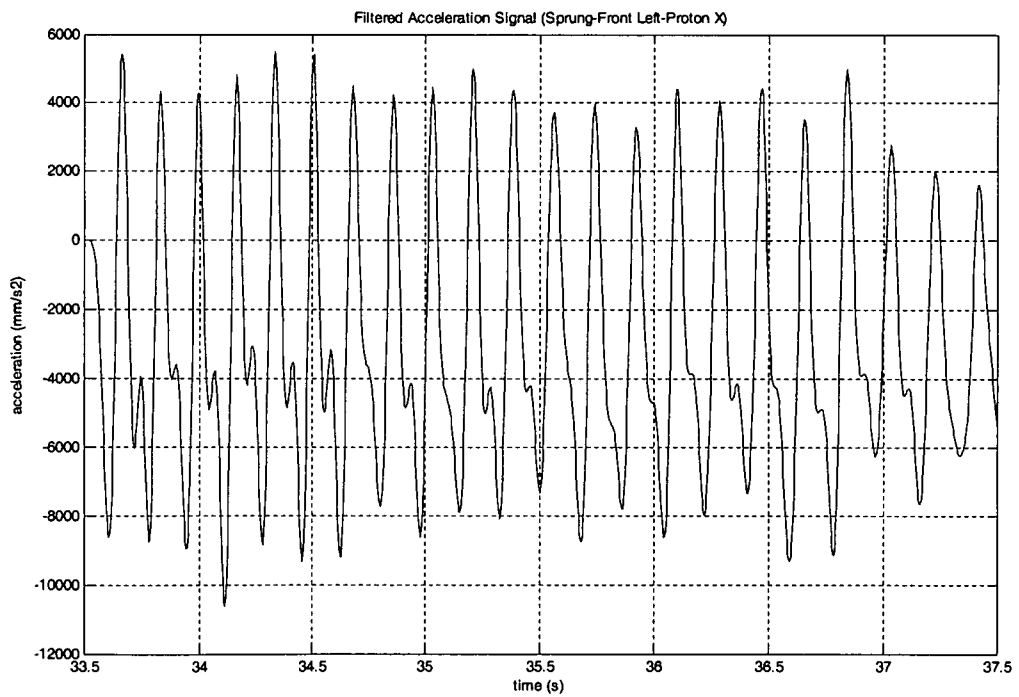
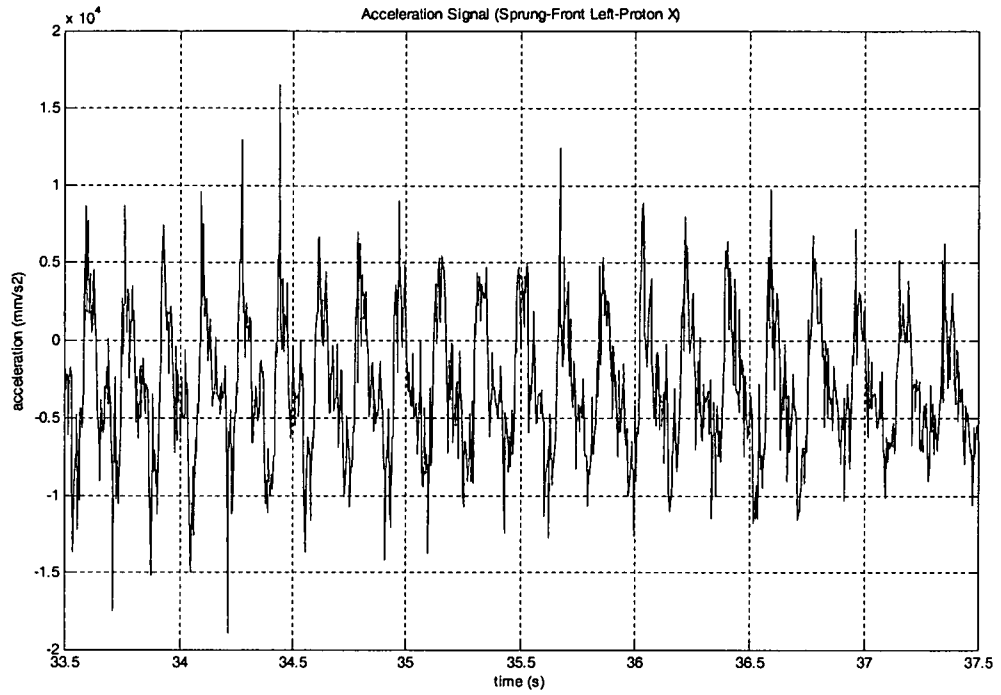


APPENDIX E3

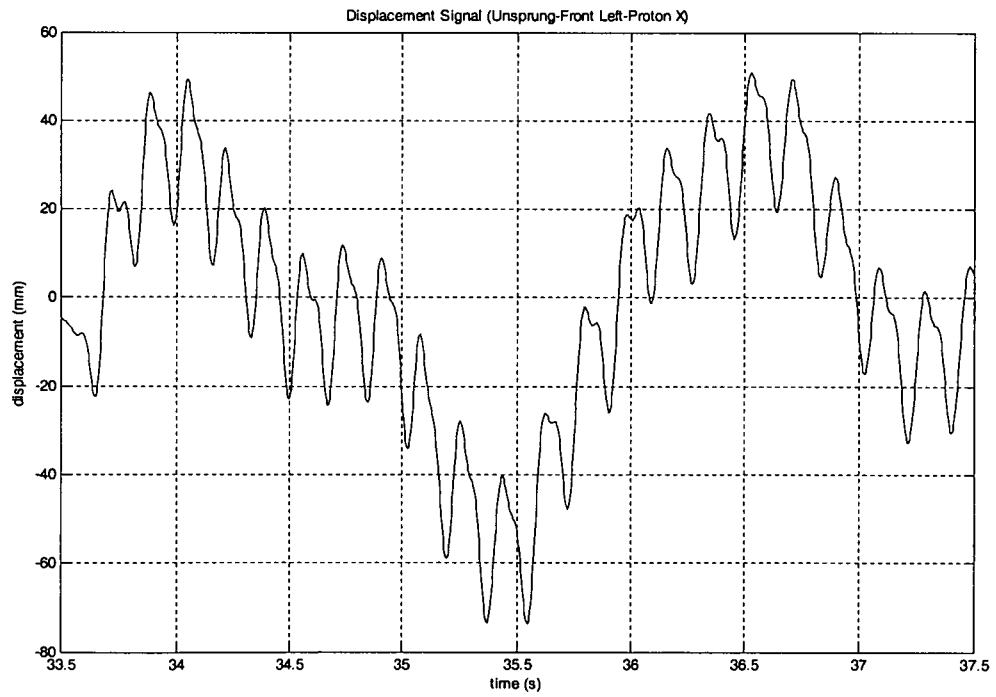
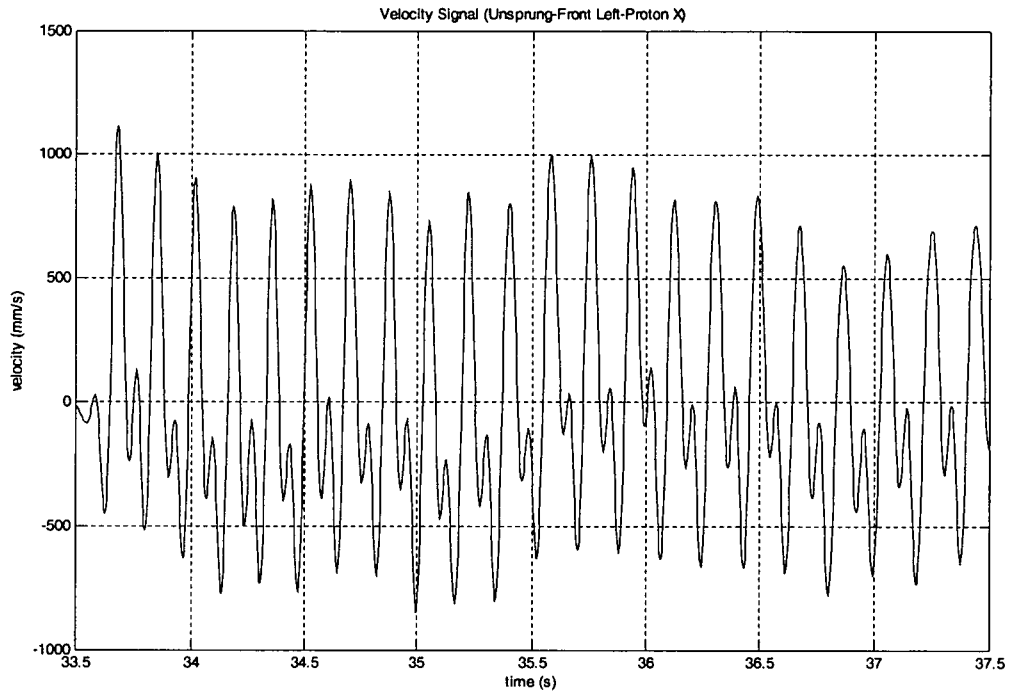


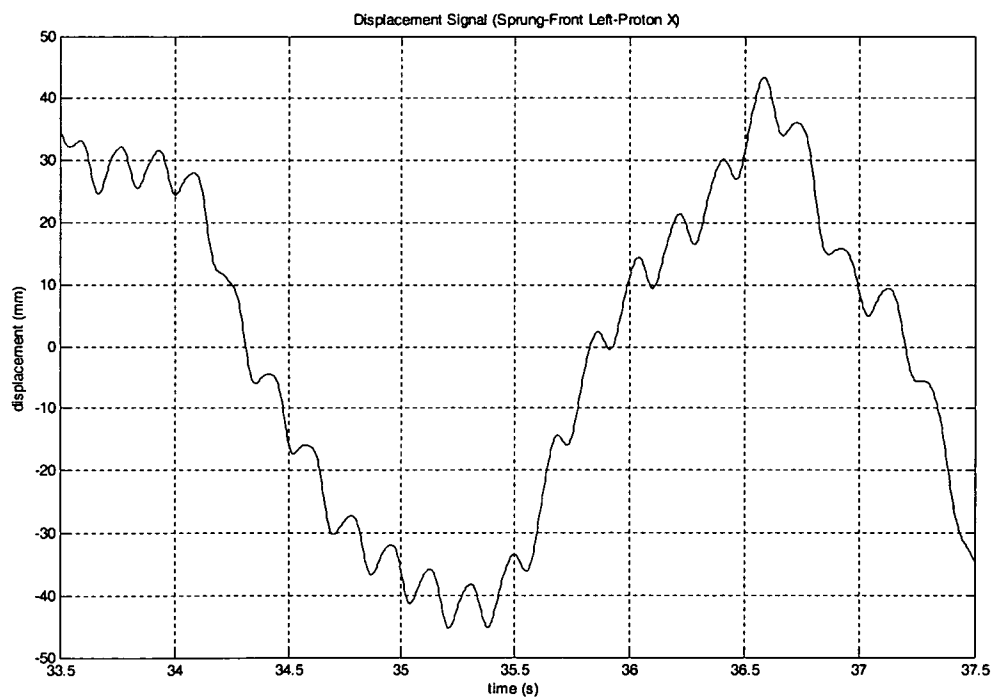
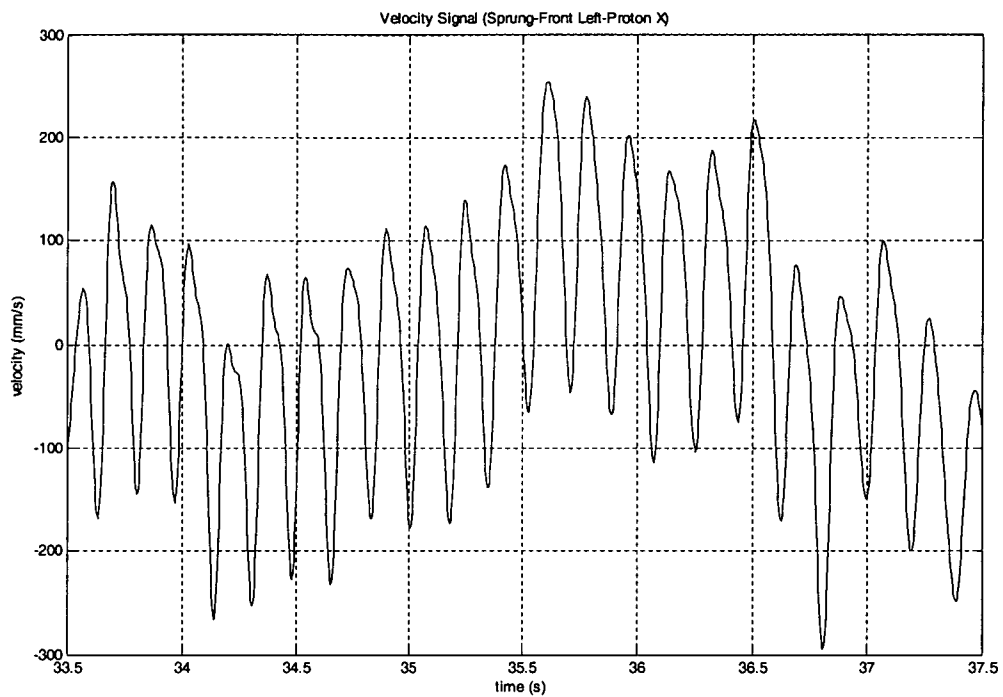
APPENDIX F1



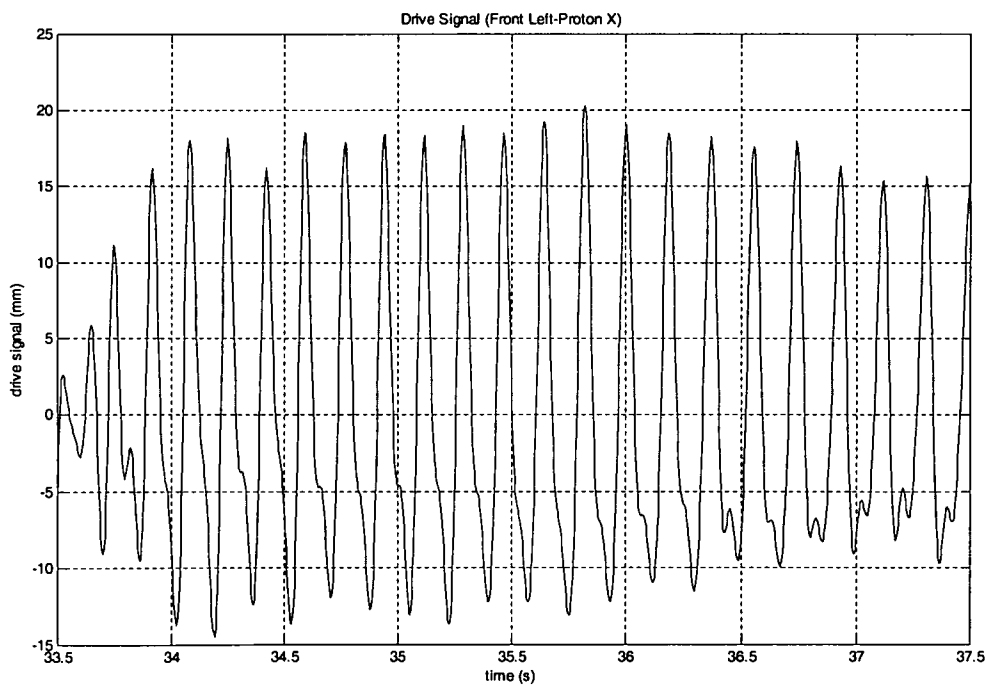
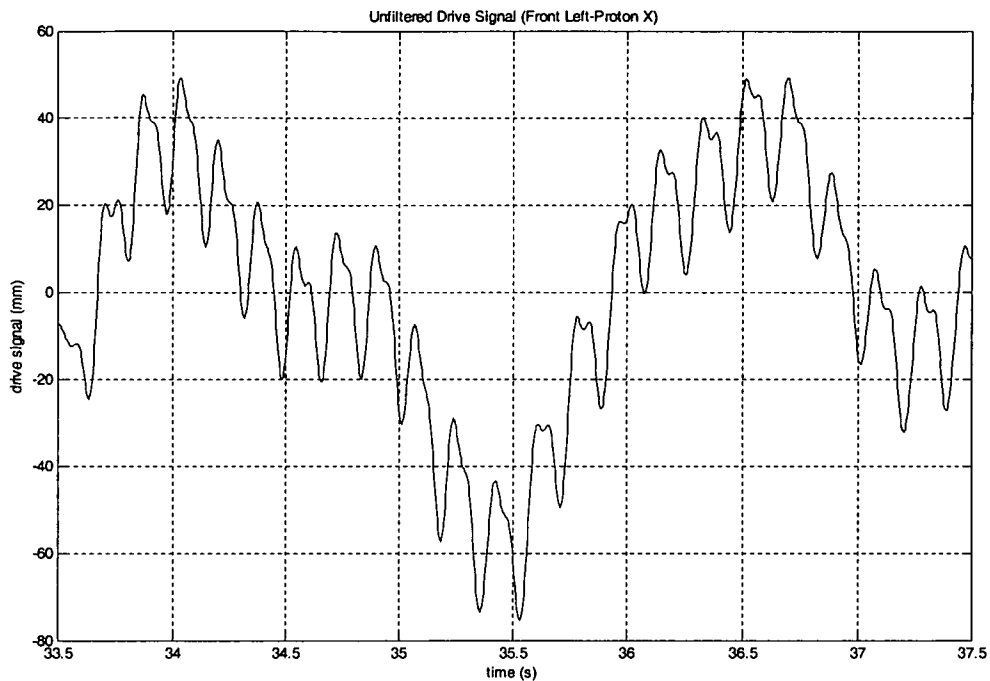


APPENDIX F2

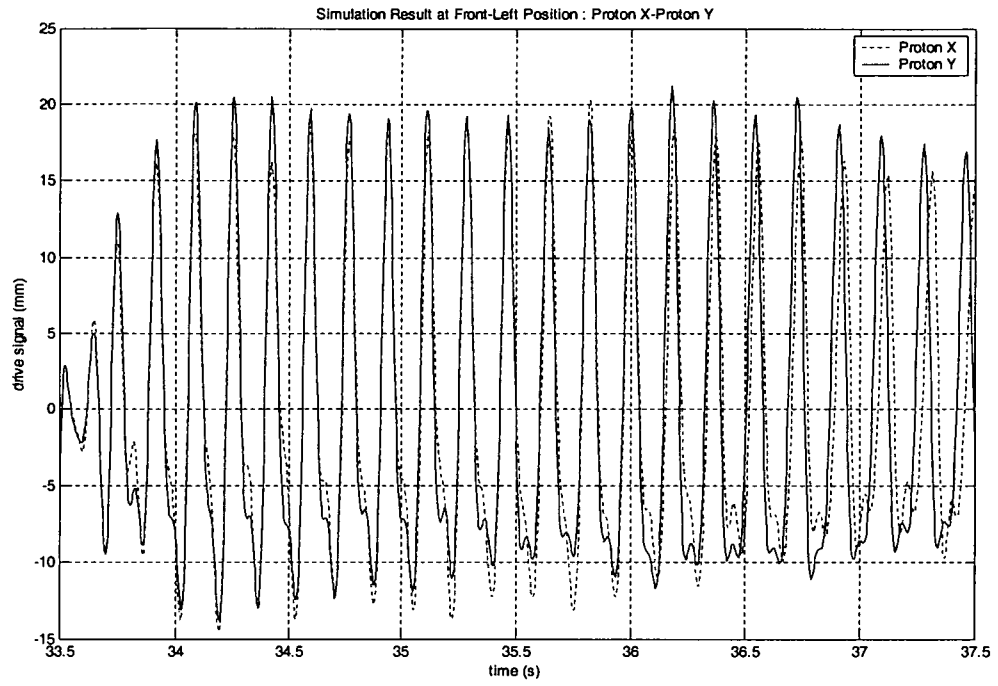




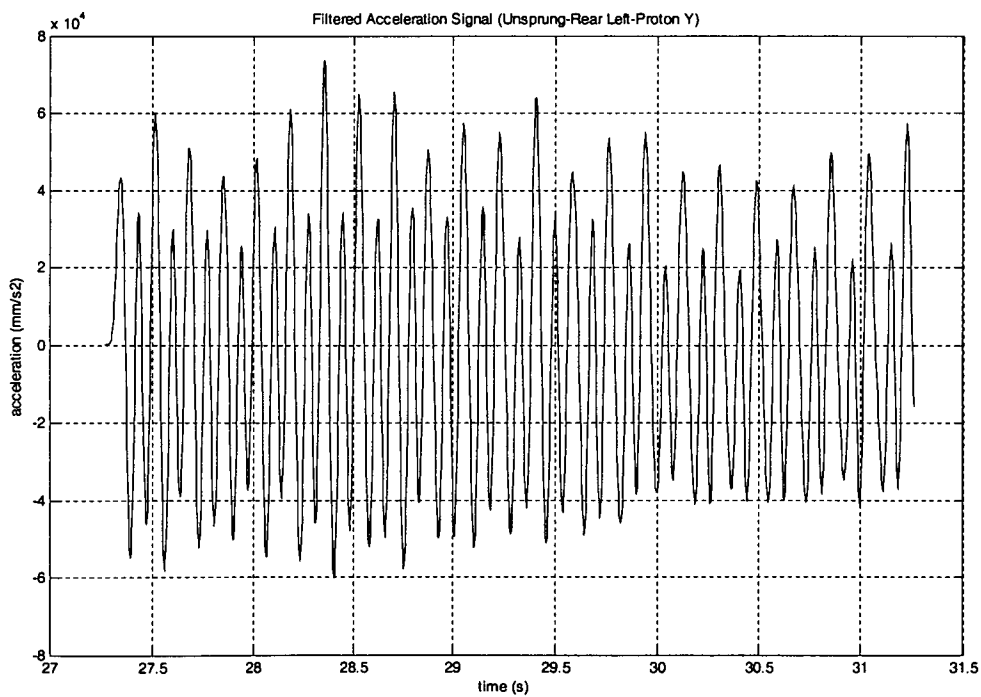
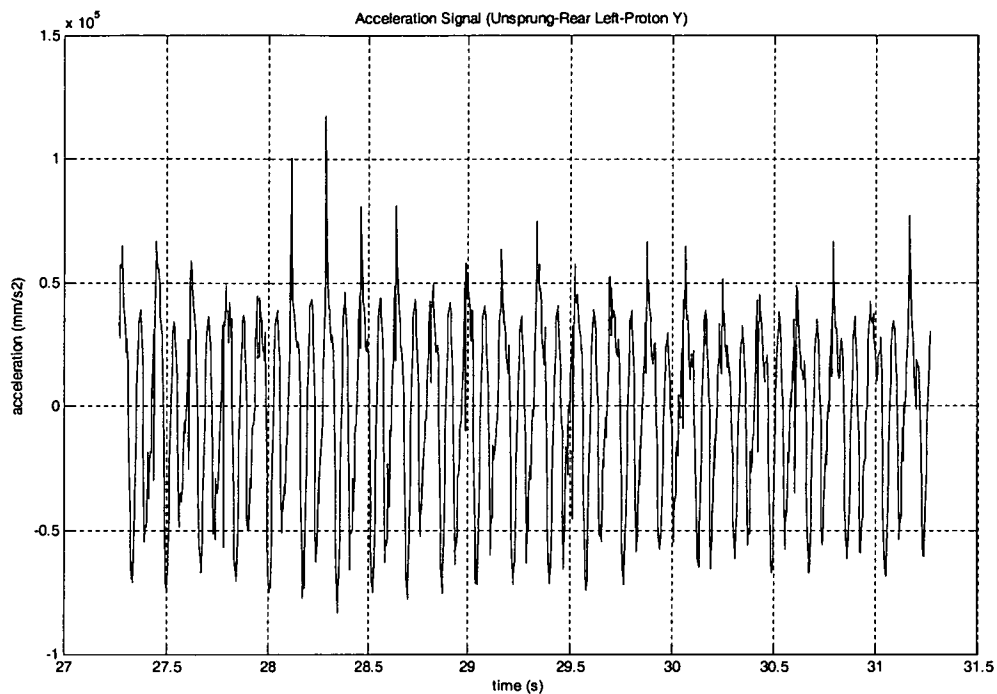
APPENDIX F3

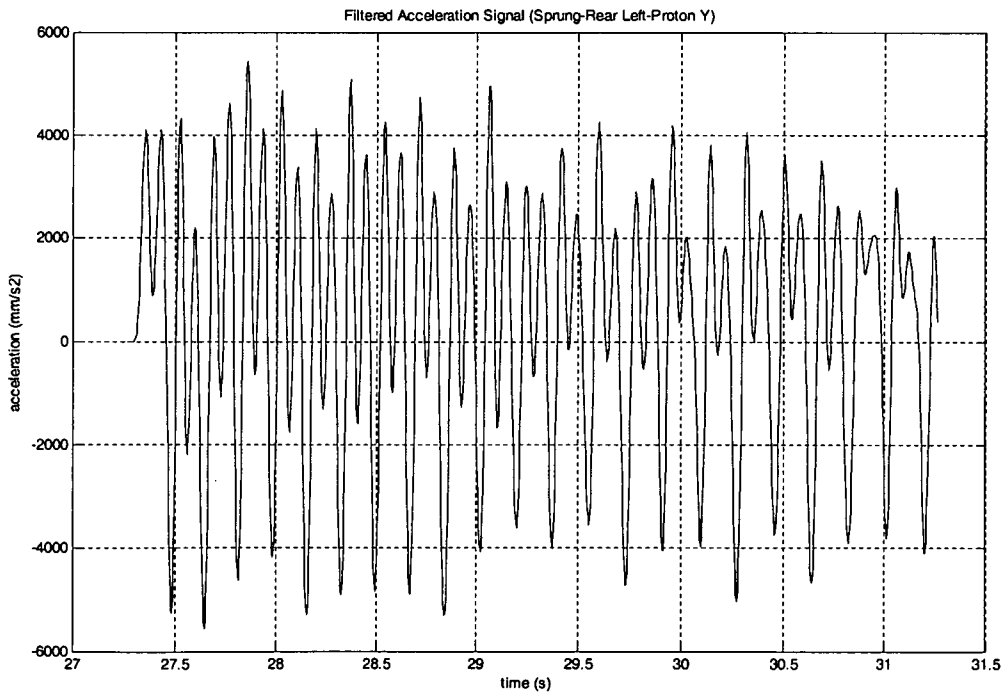
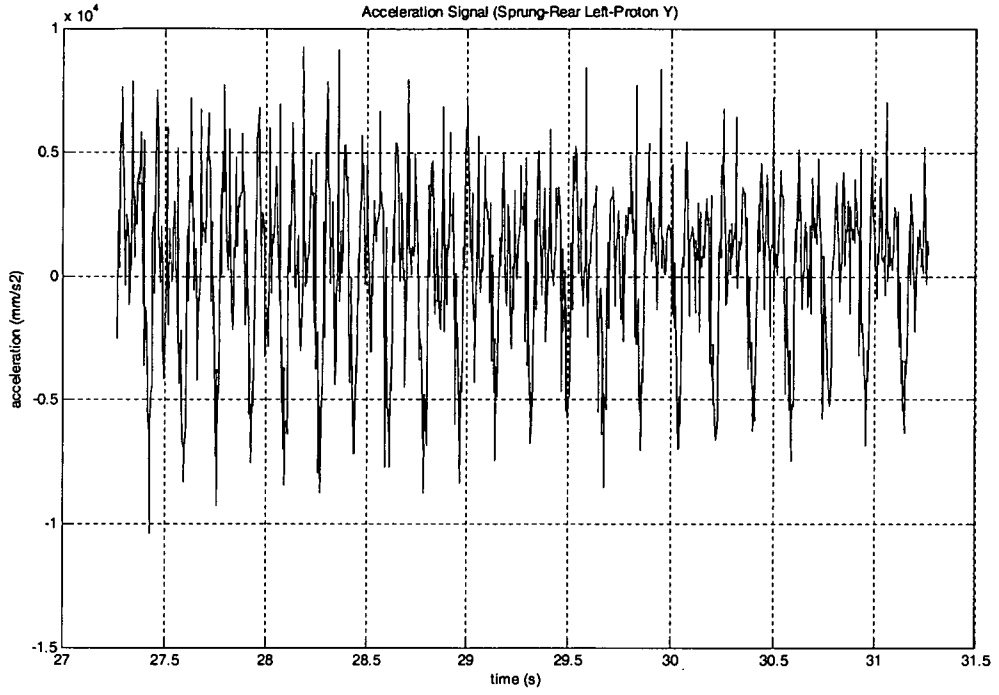


APPENDIX G

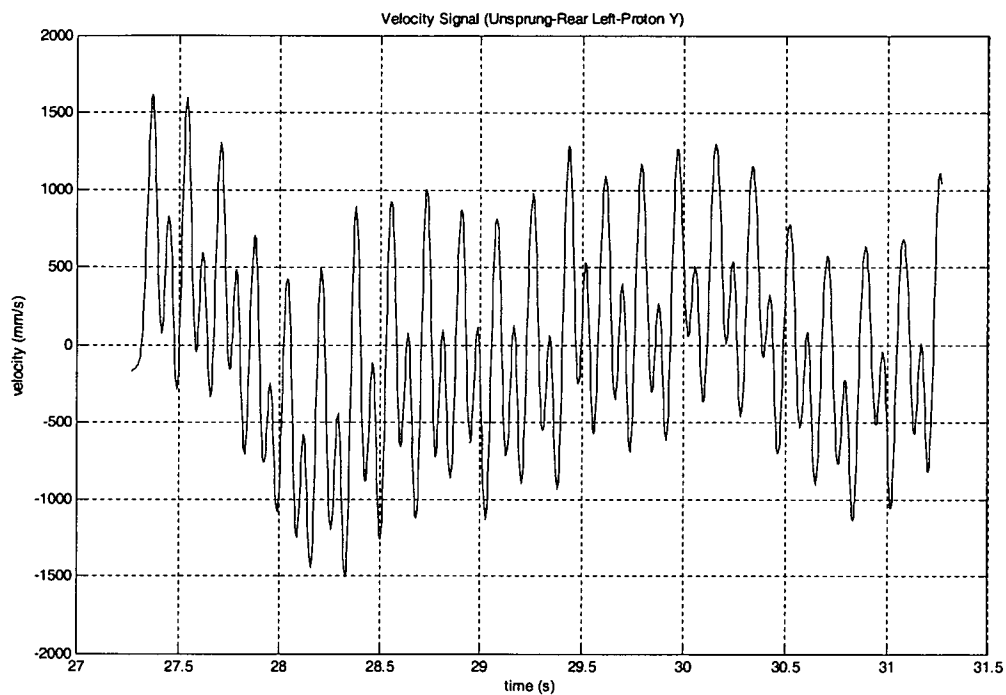


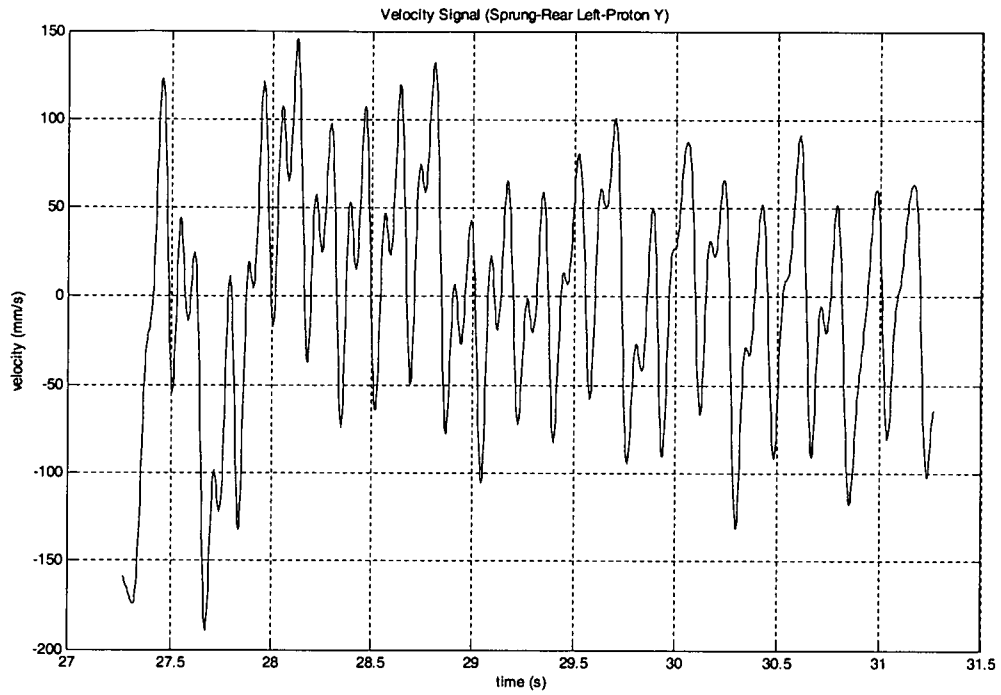
APPENDIX H1



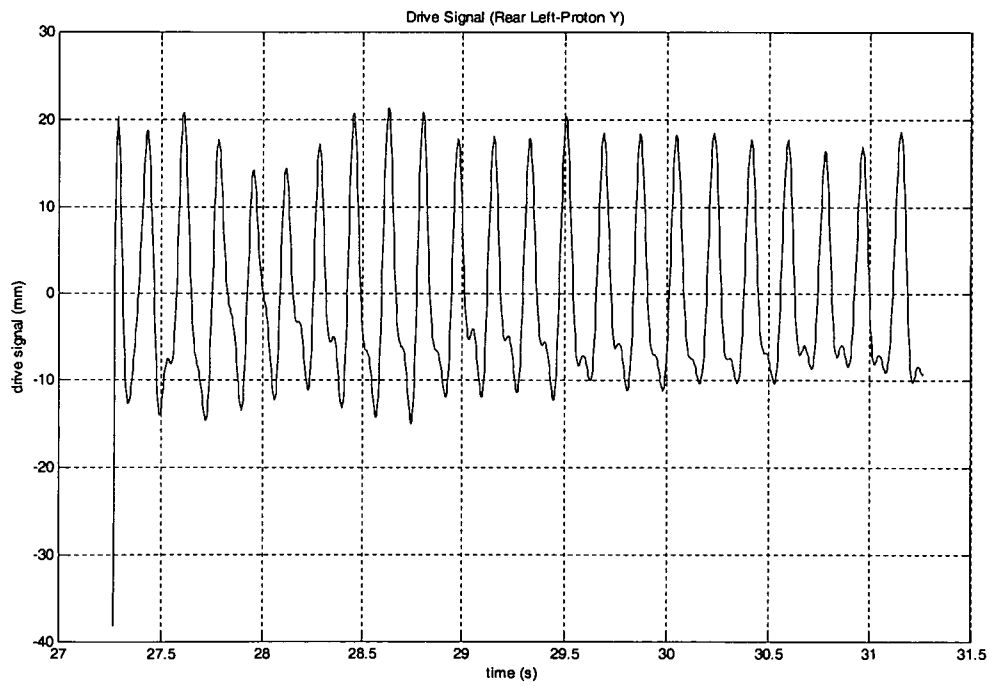
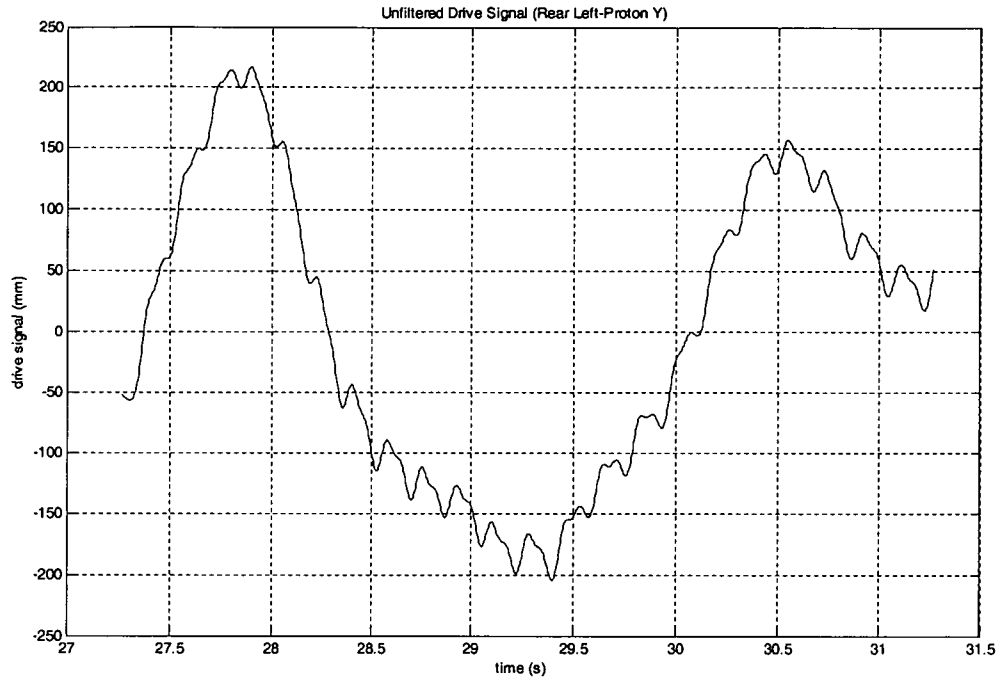


APPENDIX H2

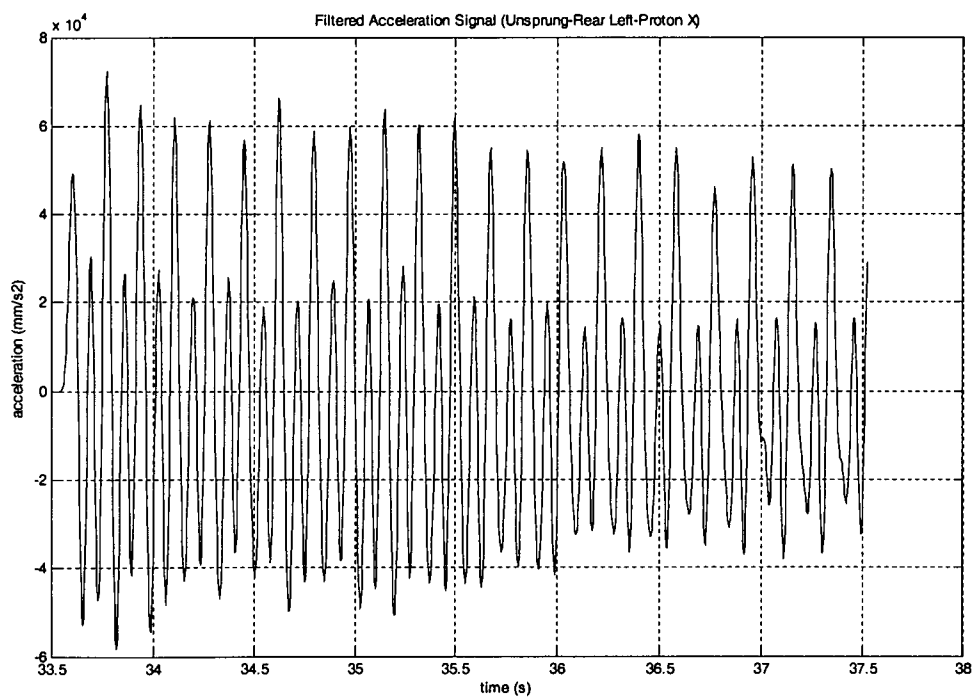
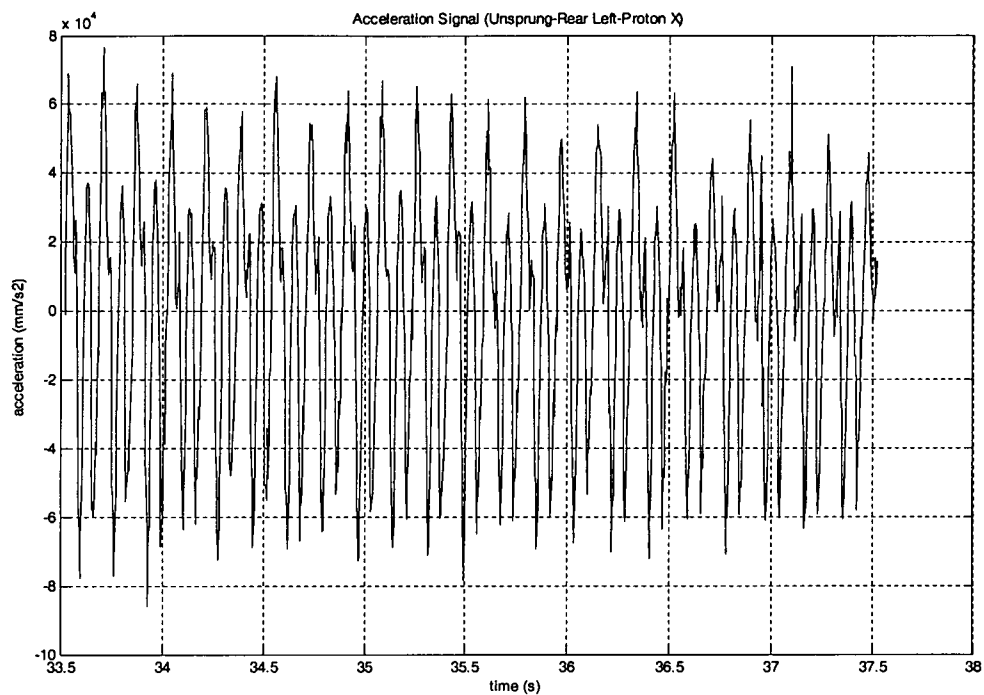


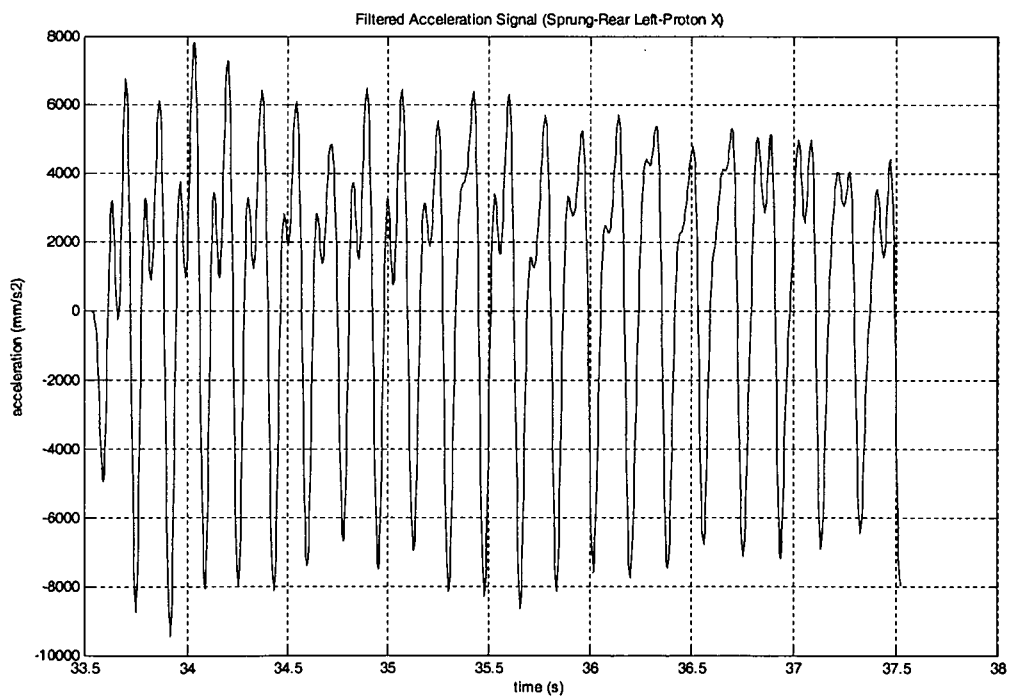
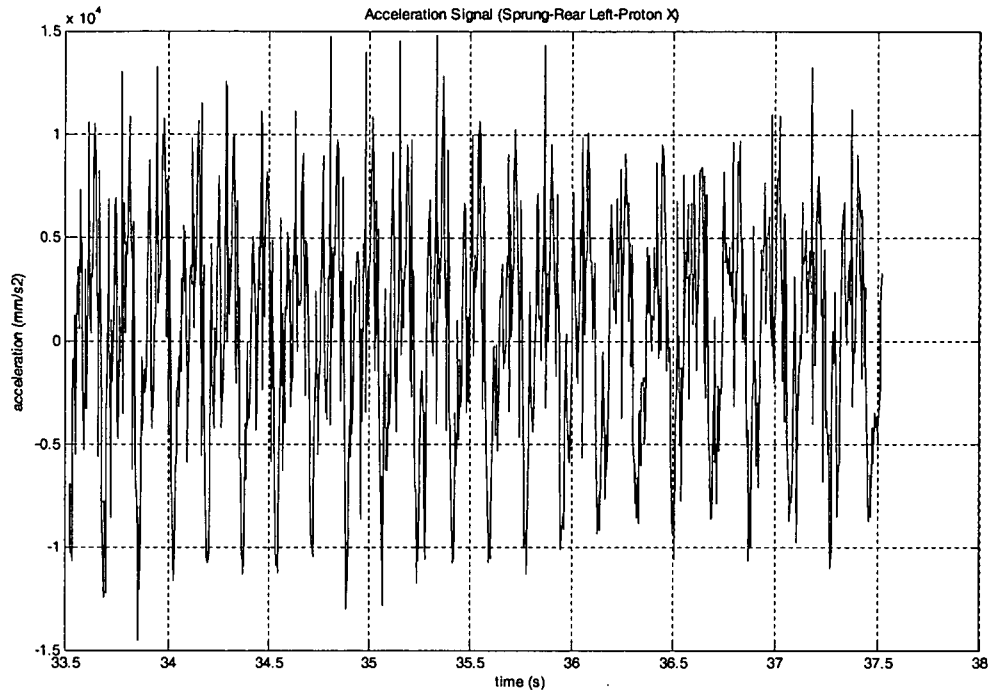


APPENDIX H3

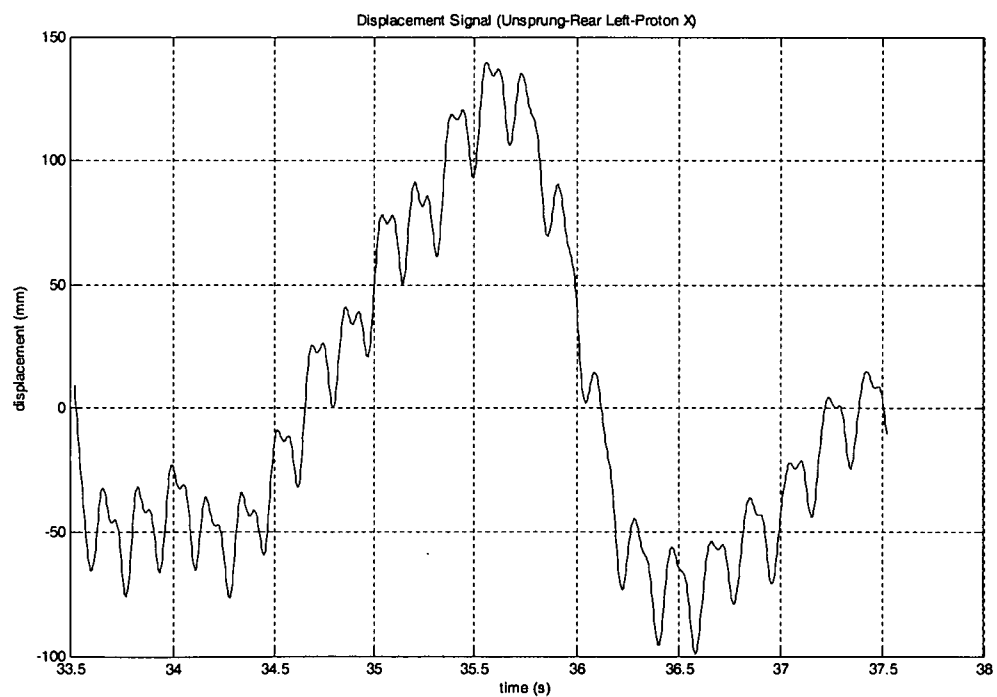
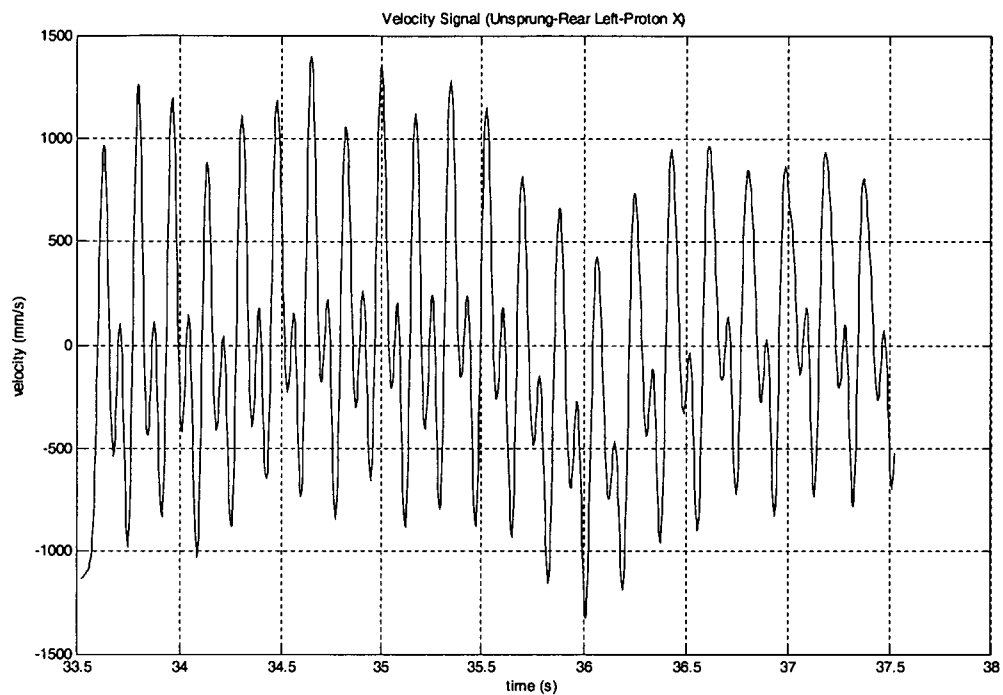


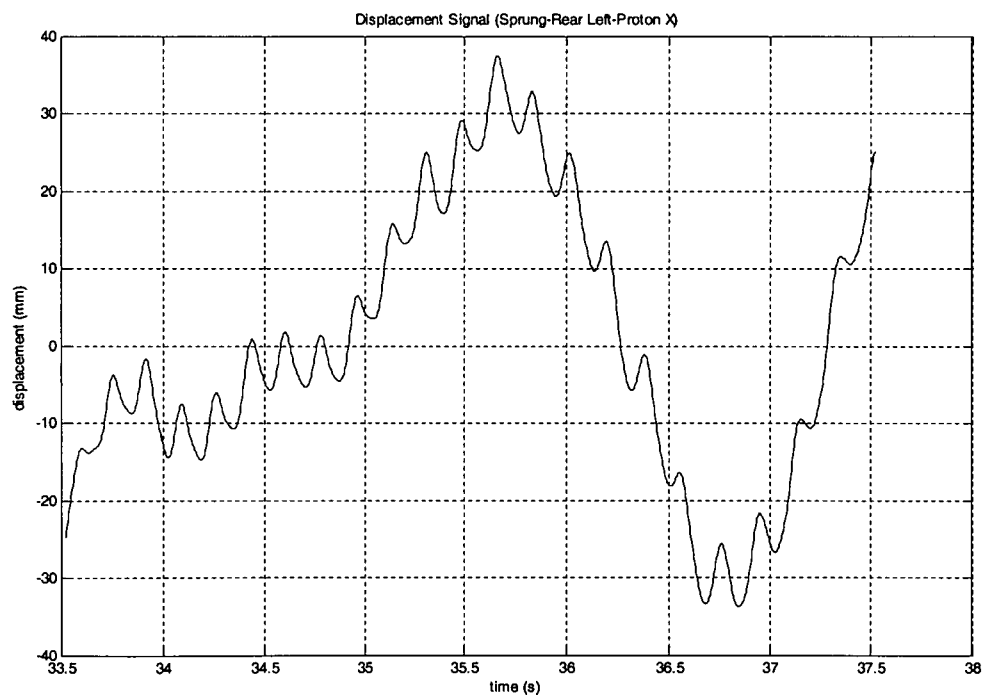
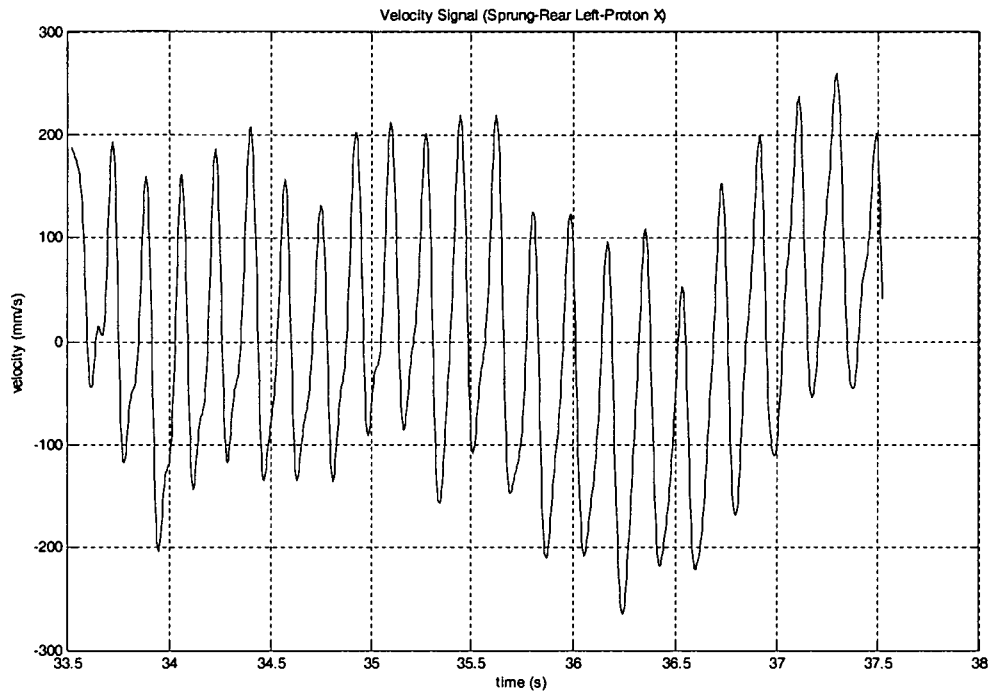
APPENDIX I1



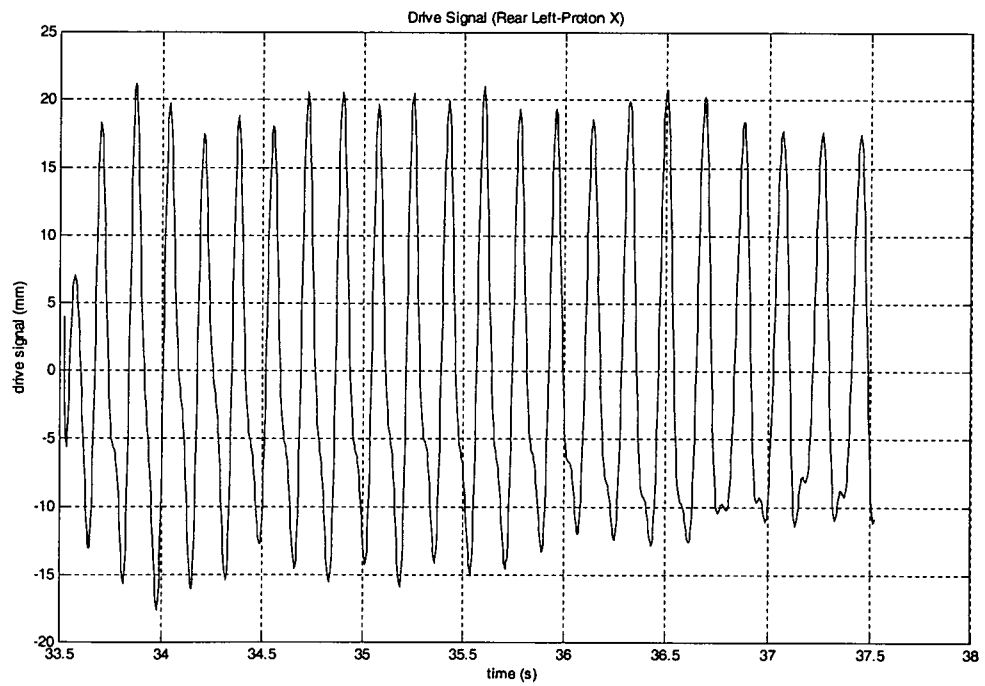
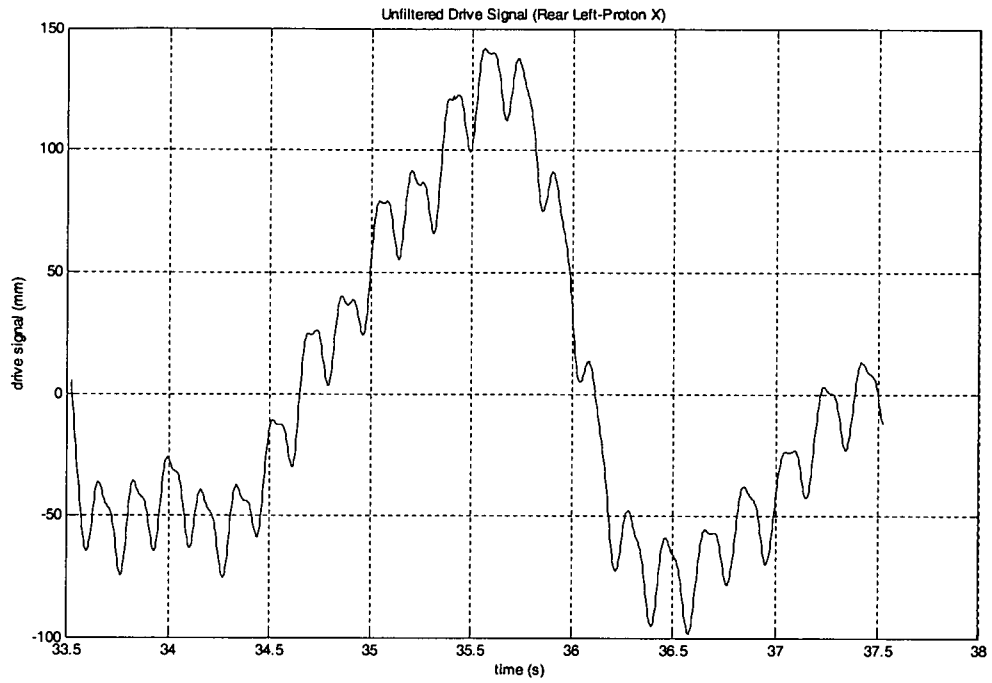


APPENDIX I2

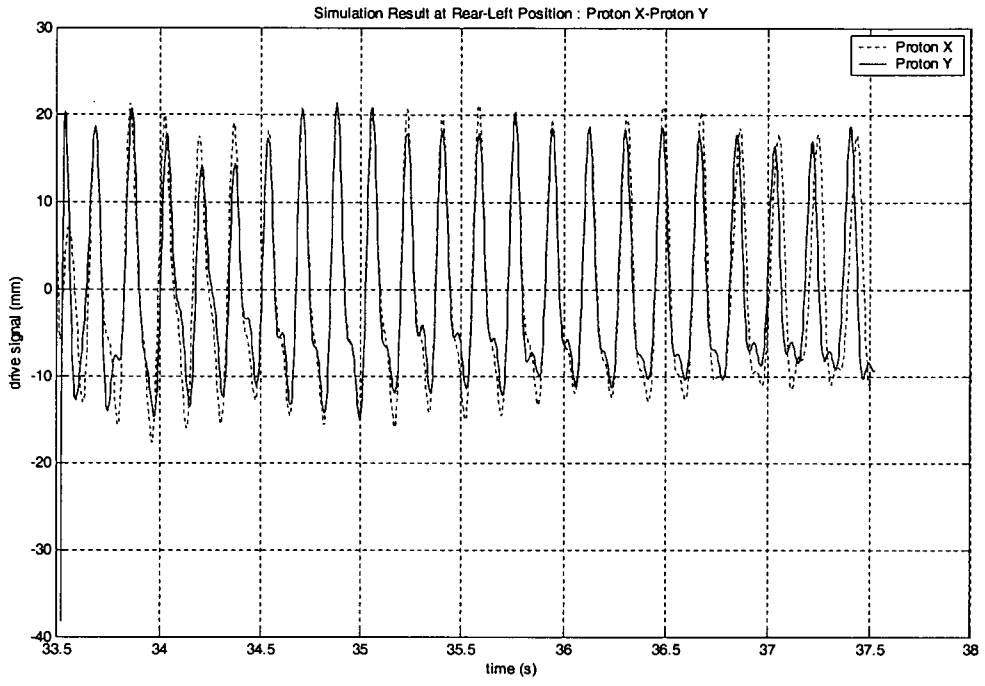




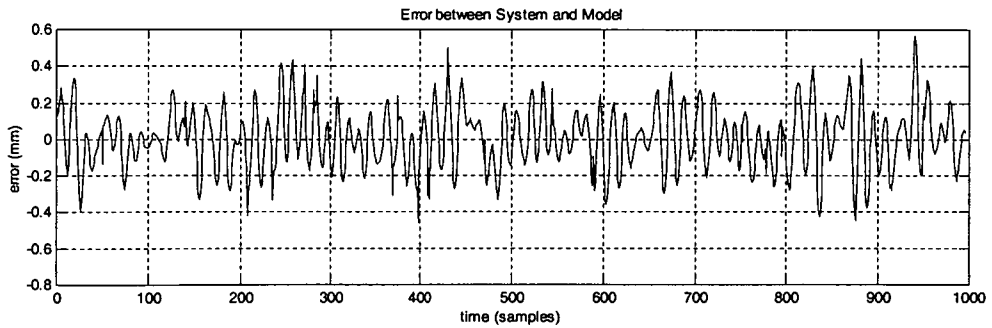
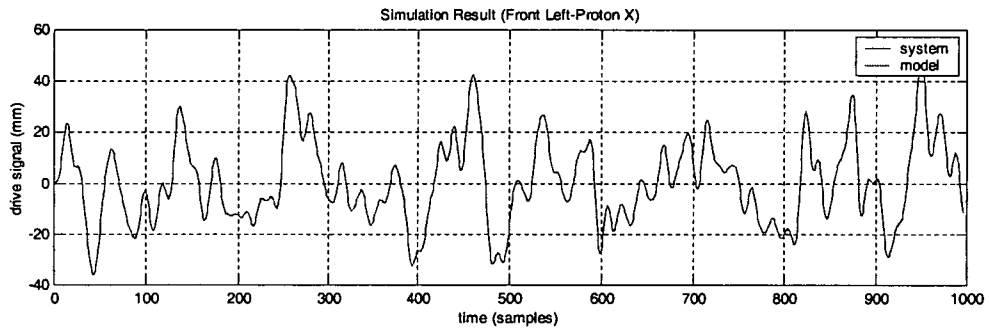
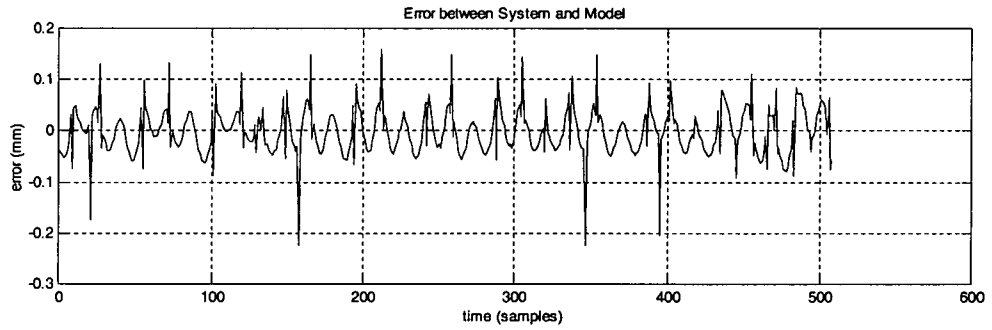
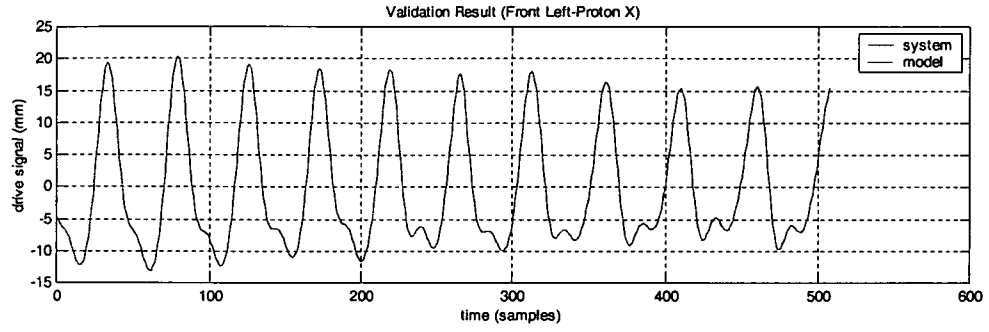
APPENDIX I3



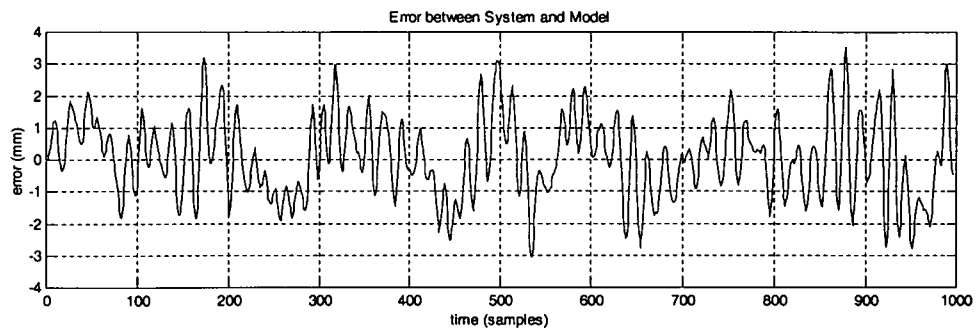
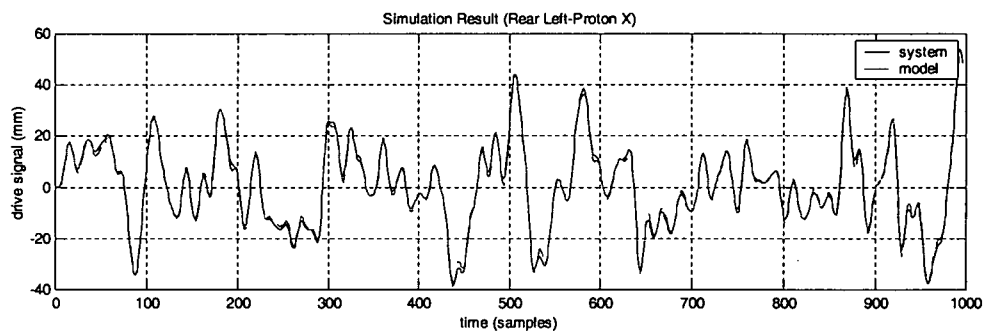
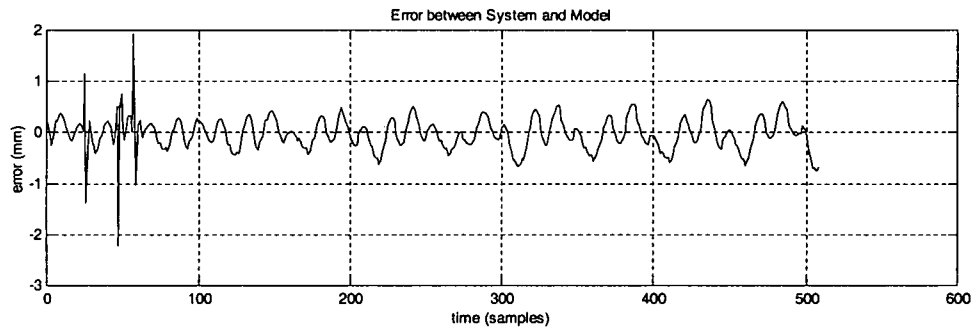
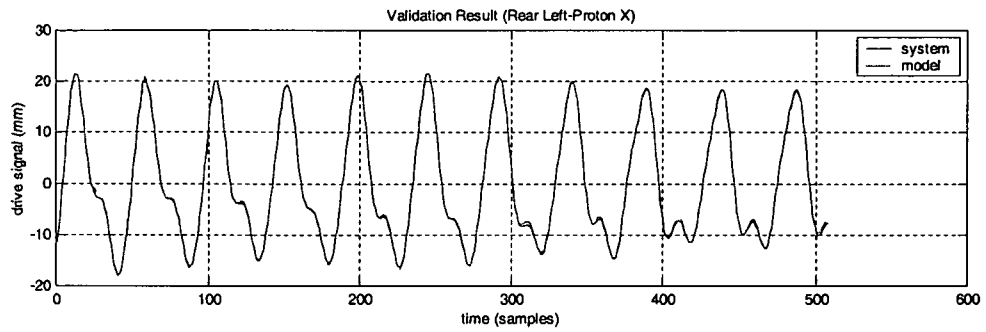
APPENDIX J



APPENDIX K1



APPENDIX K2



APPENDIX L

```

clear all

cd c:\research\wajaf1
load flx.txt
x=flx(:,1);
y1=flx(:,2);
y2=flx(:,3);
y3=flx(:,4);
n1=length(y1);
n2=length(y2);

%=====
% unsprung mass

q=y1*9800; %convert unit from g to mm/s2

plot(x,q)
title('Acceleration Signal (Unsprung-Front Left-Proton X)')
ylabel('acceleration (mm/s2)')
xlabel('time (s)')
grid

Q=fft(q,512);
Pq=Q.*conj(Q)/512;
ff=204.8*(0:127)/512;
plot(ff,Pq(1:128))
title('FFT Acceleration Signal (Unsprung-Front Left-Proton X)')
ylabel('amplitude (mm/s2)')
xlabel('frequency (Hz)')
grid

[b,a]=butter(8,15/102.4);
w=filter(b,a,q);
plot(x,w)
title('Filtered Acceleration Signal (Unsprung-Front Left-Proton X)')
ylabel('acceleration (mm/s2)')
xlabel('time (s)')
grid

W=fft(w,512);
Pw=W.*conj(W)/512;
ff=204.8*(0:127)/512;
plot(ff,Pw(1:128))
title('FFT - Filtered Acceleration Signal (Unsprung-Front Left-Proton X)')
ylabel('amplitude (mm/s2)')
xlabel('frequency (Hz)')
grid

```

```

plot(ff,Pq(1:128),'m',ff,Pw(1:128),'b')
title('Filtered & Unfiltered FFT Signal (Unsprung-Front Left-Proton X)')
ylabel('amplitude (mm/s2)')
xlabel('frequency (Hz)')
legend('unfiltered','filtered')
grid

% sprung

z=y2*9800; %convert unit from g to mm/s2

plot(x,z)
title('Acceleration Signal (Sprung-Front Left-Proton X)')
ylabel('acceleration (mm/s2)')
xlabel('time (s)')
grid

Z=fft(z,512);
Pz=Z.*conj(Z)/512;
ff=204.8*(0:127)/512;
plot(ff,Pz(1:128))
title('FFT Acceleration Signal (Sprung-Front Left-Proton X)')
ylabel('amplitude (mm/s2)')
xlabel('frequency (Hz)')
grid

[b,a]=butter(8,15/102.4);
s=filter(b,a,z);
plot(x,s)
title('Filtered Acceleration Signal (Sprung-Front Left-Proton X)')
ylabel('acceleration (mm/s2)')
xlabel('time (s)')
grid

S=fft(s,512);
Ps=S.*conj(S)/512;
ff=204.8*(0:127)/512;
plot(ff,Ps(1:128))
title('FFT - Filtered Acceleration Signal (Sprung-Front Left-Proton X)')
ylabel('amplitude (mm/s2)')
xlabel('frequency (Hz)')
grid

plot(ff,Pz(1:128),'m',ff,Ps(1:128),'b')
title('Filtered & Unfiltered FFT Signal (sprung-Front Left-Proton X)')
ylabel('amplitude')
xlabel('frequency (Hz)')
legend('unfiltered','filtered')
grid

```

```

% input (road)

plot(x,y3)
title('Drive Signal (Front Left-Proton X)')
ylabel('drive signal (mm)')
xlabel('time (s)')
grid

Y3=fft(y3,512);
Py3=Y3.*conj(Y3)/512;
ff=204.8*(0:127)/512;
plot(ff,Py3(1:128))
title('FFT Iterated Drive Signal (Front Left-Proton X)')
ylabel('amplitude (mm)')
xlabel('frequency (Hz)')
grid

[b,a]=butter(8,15/102.4);
m1=filter(b,a,y3);
plot(x,m1)
title('Filtered Drive Signal (Front Left-Proton X)')
ylabel('drive signal (mm)')
xlabel('time (s)')
grid

M=fft(m1,512);
Pm=M.*conj(M)/512;
ff=204.8*(0:127)/512;
plot(ff,Pm(1:128))
title('FFT - Filtered Iterated Drive Signal (Front Left-Proton X)')
ylabel('amplitude (mm)')
xlabel('frequency (Hz)')
grid

plot(ff,Py3(1:128),'m',ff,Pm(1:128),'b')
title('Filtered & Unfiltered FFT Signal (sprung-FL-Proton X)')
ylabel('amplitude')
xlabel('frequency (Hz)')
legend('unfiltered','filtered')
grid

% ===== %

```

APPENDIX M

```

clear all

cd c:\research\wajaf1
load flxf.txt
x=flxf(:,1); % time
y1=flxf(:,2); % acceleration,unsprung,front-left
y2=flxf(:,3); % acceleration,sprung,front-left
n1=length(y1);
n2=length(y2);

%=====

% unsprung mass

q=y1

plot(x,q)
title('Acceleration Signal')
ylabel('acceleration (mm/s2)')
xlabel('time (s)')
grid

w=cumtrapz(q)*0.00488281; %sampling time=0.00488281 sec
detrend_w=detrend(w) %remove DC offset

plot(x,w)
title('Velocity Signal (Unsprung-Front Left-Proton X)')
ylabel('velocity (mm/s)')
xlabel('time (s)')
grid

plot(x,detrend_w)
title('Detrend velocity data to remove DC offset in original data (Unsprung-Front Left-Proton X)')
ylabel('velocity (mm/s)')
xlabel('time (s)')
grid

plot(x,detrend_w)
title('Velocity Signal (Unsprung-Front Left-Proton X)')
ylabel('velocity (mm/s)')
xlabel('time (s)')
grid

```

```

e=cumtrapz(detrend_w)*0.00488281;%sampling time=0.00488281 sec
detrend_e=detrend(e) %remove DC offset

plot(x,detrend_e)
title('Displacement Signal (Unsprung-Front Left-Proton X)')
ylabel('displacement (mm)')
xlabel('time (s)')
grid

%check reliability of integration by double differentiation the final result
for i=1:n1
h=0.00488281;
if i>2
    a1(i)=(3*detrend_e(i)-4*detrend_e(i-1)+detrend_e(i-2))/(2*h)
end
end

for i=1:n1
h=0.00488281;
if i>2
    b1(i)=(3*a1(i)-4*a1(i-1)+a1(i-2))/(2*h)
end
end

plot(x(6:1017),y1(6:1017),'b',x(6:1017),b1(6:1017),'r')
title('Acceleration Data Comparison (original-calculation) Unsprung-Front Left-Proton X')
ylabel('acceleration (mm/s2)')
xlabel('time (s)')
legend('original data','after-calculation data')
grid

%=====

% sprung mass

a=y2

plot(x,a)
title('Acceleration Signal')
ylabel('acceleration (mm/s2)')
xlabel('time (s)')
grid

s=cumtrapz(a)*0.00488281;%sampling time=0.00488281 sec
detrend_s=detrend(s) %remove DC offset

plot(x,s)
title('Velocity Signal (Sprung-Front Left-Proton X)')
ylabel('velocity (mm/s)')
xlabel('time (s)')
grid

```



```

plot(x,detrend_s)
title('Detrend velocity data to remove DC offset in original data (Sprung-Front Left-Proton X)')
ylabel('velocity (mm/s)')
xlabel('time (s)')
grid

```

```

plot(x,detrend_s)
title('Velocity Signal (Sprung-Front Left-Proton X)')
ylabel('velocity (mm/s)')
xlabel('time (s)')
grid

```

```

d=cumtrapz(detrend_s)*0.00488281; %sampling time=0.00488281 sec
detrend_d=detrend(d) %remove DC offset

```

```

plot(x,detrend_d)
title('Displacement Signal (Sprung-Front Left-Proton X)')
ylabel('displacement (mm)')
xlabel('time (s)')
grid

```

```

%check reliability of integration by double differentiate the final result

```

```

for i=1:n2
h=0.00488281;
if i>2
    a2(i)=(3*detrend_d(i)-4*detrend_d(i-1)+detrend_d(i-2))/(2*h)
end
end

```

```

for i=1:n2
h=0.00488281;
if i>2
    b2(i)=(3*a2(i)-4*a2(i-1)+a2(i-2))/(2*h)
end
end

```

```

plot(x(6:1017),y2(6:1017),'b',x(6:1017),b2(6:1017),'r')
title('Acceleration Data Comparison (original-calculation) Sprung-Front Left-Proton X')
ylabel('acceleration (mm/s2)')
xlabel('time (s)')
legend('original data','after-calculation data')
grid

```

APPENDIX N

```

clear all

cd c:\research\wajaf1
load xusflxf.txt % displacement,unsprung,front-left
load vusflxf.txt % velocity,unsprung,front-left
load ausflxf.txt % acceleration,unsprung,front-left
load xsflxf.txt % displacement,sprung,front-left
load vsflxf.txt % velocity,sprung,front-left
load asflxf.txt % acceleration,sprung,front-left
load xdflex.txt % displacement,drive,front-left
load flxf.txt % time

% define variables
k=flxf(:,1);
k1=k+0.015;
x1=xusflxf';
x2=xsflxf';
x3=vusflxf';
x4=vsflxf';
x5=ausflxf';
x6=asflxf';
x7=xdflex';
n=length(x7);

% car parameters
mt=35.19;
mb=355.31;
ks=23000;
kp=6000;
bs=3959;
bsn=1751;
kt=322192.2;

%linear formula

g=(mt/kt)*x5+(bs/kt)*x3-(bs/kt)*x4+((kp+ks+kt)/kt)*x1-((kp+ks)/kt)*x2;

plot(k,g,'b:',k1,x7,'r-')
title('Simulation Result between Linear Model and Iteration (Front Left-Proton X)')
ylabel('drive signal (mm)')
xlabel('time (s)')
legend('linear model','iteration')
grid

```

```
% rms error  
m=g(:,206:410)-x7(:,206:410);  
m1=m.^2;  
m2=sum(m1);  
m3=m2/205;  
m4=0.001.*m3.^0.5
```